MECHANISMS OF SUBSTRATE SELECTION BY THE SIGNAL RECOGNITION PARTICLE

Thesis by

Aileen Renia Ariosa

In Partial Fulfillment of the Requirements

For the Degree of

Doctor of Philosophy

California Institute of Technology

Pasadena, California

2014

(Defended May 28, 2014)

DEDICATION

To my grandparents;

Vicente and Adelaida Renia

Cosme and Abundia Ariosa

ACKNOWLEDGEMENTS

This journey hasn't been an easy one. However, despite all of the stress-filled days, late night experiments, and anxiety-ridden moments, it has been fun, awesome and worthwhile – all because of the people who have helped it become less complicated, more memorable, and full of cherished life lessons. With these people, the past six years have made me become, not only a better scientist, but also a better person.

First of many thanks go out to my thesis adviser, Dr. Shu-ou Shan. Shu-ou sets the bar really high for anyone who joins her lab and I am very grateful for that because it helped me grow and evolve as a biochemist. Her love and passion for science is quite infectious, you can't help but be inspired. Thanks for the patience and understanding. Next, I'd like to thank the members of my thesis committee: Dr. Douglas Rees, Dr. Carl Parker and Dr. Tom Miller. Thank you for the many concrete advice, scientific input and the willingness to motivate and push.

I am extremely thankful to have joined a lab that is full of AWESOME people. Props go out to Sowmya Chandrasekar, Xin Zhang, Peera Jaru-Ampornpan, Rumana Rashid, Vinh Lam, Kuang Shen, Thang Nguyen, Ishu Saraogi, Nathan Pierce, David Akopian, Michael Rome, Meera Rao, George Liang, Yu Hsien Hwang Fu, Un Seng Chio, Camille McAvoy and Jae Ho Lee. Thank your for making the lab not only a world-class place for scientific research but also for making the daily grind less complicated and enjoyable. Special thanks go out to Sowmya and Meera for being my caffeine buddies. Thank you for always being around to discuss not only matters of science but also matters of life and love. To Peera, thank you for being a calm and steady force in the lab. To Xin and Kuang, many thanks for teaching me the ropes and for continuing to give

advice and share ideas even after you've graduated. To David, Mike and Ishu, thank you for being always available to talk to and for the help with troubleshooting experiments. To Thang, thanks for bringing cheer to any situation unaffectedly and for being my lab bestie.

I would also like to acknowledge the hard work done by those behind the scenes – Margot Hoyt, Alison Ross, Blanca Ortega, Manuel Lagang and Santiago Laparra – thank you for making things easier for everyone in the lab. I would also like to thank Divina Bautista and the rest of the staff at the Caltech Health Center. Many thanks also go out to our high school volunteers who poured countless SDS-PAGE gels and assay quench tubes – Kevin Kim, Catherine Chan, Irene Chen, Albert Gianatan, Chris Chi and Mark Liu.

Lastly, I would like to acknowledge the love and support of my family and friends. To all the Ariosas, Renias and Shafers, thank you for being the most enthusiastic, loyal cheerleaders! To my grandparents, Vic and Dely, and, Cosme and Abundia, thank you for instilling the importance of education to your children and grand children and for your unconditional love. To my parents, Becca and Ting, thank you for working hard and doing your best. To my siblings and cousins, Adrian, Annette, Luke, Nathan and Zacc, thank you for the innumerable laugh-out-loud moments and for always being there no matter what. To my Uncle Restie and Tita Nikki, thank you for being the best second set of parents one could ever hope for. Finally, I would like to thank my best friend and the love of my life, Otto Shafer. Thank you for being my rock and my own personal ninja bear.

ABSTRACT

The signal recognition particle (SRP) targets membrane and secretory proteins to their correct cellular destination with remarkably high fidelity. Previous studies have shown that multiple checkpoints exist within this targeting pathway that allows 'correct cargo' to be quickly and efficiently targeted and for 'incorrect cargo' to be promptly rejected. In this work, we delved further into understanding the mechanisms of how substrates are selected or discarded by the SRP. First, we discovered the role of the SRP fingerloop and how it activates the SRP and SRP receptor (SR) GTPases to target and unload cargo in response to signal sequence binding. Second, we learned how an 'avoidance signal' found in the bacterial autotransporter, EspP, allows this protein to escape the SRP pathway by causing the SRP and SR to form a 'distorted' complex that is inefficient in delivering the cargo to the membrane. Lastly, we determined how Trigger Factor, a co-translational chaperone, helps SRP discriminate against 'incorrect cargo' at three distinct stages: SRP binding to RNC; targeting of RNC to the membrane via SRP-FtsY assembly; and stronger antagonism of SRP targeting of ribosomes bearing nascent polypeptides that exceed a critical length. Overall, results delineate the rich underlying mechanisms by which SRP recognizes its substrates, which in turn activates the targeting pathway and provides a conceptual foundation to understand how timely and accurate selection of substrates is achieved by this protein targeting machinery.

TABLE OF CONTENTS

Dedication……..……..iii

Acknowledgement……..iv

Abstract……...……....vi

Table of Contents……..…….vii

Chapter I:……1

Fingerloop activates cargo delivery and unloading during co-translational protein targeting

Chapter II:...…….…….46

Mechanism of signal sequence surveillance by the signal recognition particle

Chapter III:……76

Molecular interplay with a co-translational chaperone improves the fidelity of SRP-dependent protein targeting

References……....113

CHAPTER I

Fingerloop activates cargo delivery and unloading during co-translational protein targeting

A version of this chapter has been published as:

Ariosa, A.R., Duncan., S., Saraogi, I., Lu, X., Brown, A., Phillips, G.J., and Shan, S. (2012) *Mol. Biol. Cell.* "Fingerloop activates cargo delivery and unloading during co-translational protein targeting." PMID: 23135999

ABSTRACT

During co-translational protein targeting by the Signal Recognition Particle (SRP), information about signal sequence binding in the SRP's M-domain must be effectively communicated to its GTPase domain to turn on its interaction with the SRP receptor (SR) and thus deliver the cargo proteins to the membrane. A universally conserved 'fingerloop' lines the signal sequence binding groove of SRP; the precise role of this fingerloop in protein targeting has remained elusive. Here, we show that the fingerloop plays an essential role in SRP function by helping to induce the SRP into a more active conformation that facilitates multiple subsequent steps in the SRP pathway, including efficient recruitment of SR, GTPase activation in the SRP•SR complex and most significantly, the unloading of cargo onto the target membrane. Contrary to previous suggestions, the fingerloop is not essential for signal sequence recognition by the SRP. Based on these results and recent structural work, we propose that the fingerloop is the first structural element to detect signal sequence binding; this information is relayed to the linker connecting the SRP's M- and G-domains and thus activates the SRP and SR for carrying out downstream steps in the pathway.

INTRODUCTION

Membrane and secretory proteins, whose syntheses are initiated in the cytosol, must be efficiently localized to their correct cellular destinations to assume their function. The signal recognition particle (SRP) is part of the essential cellular machinery responsible for the co-translational recognition and delivery of proteins destined to the eukaryotic endoplasmic reticulum (ER), or the bacterial plasma membrane (Akopian et al., 2013). As a nascent polypeptide emerges from a translating ribosome, SRP recognizes the ribosome nascent chain complex (termed RNC or the cargo), through interaction with both the ribosome exit site and with N-terminal signal sequences on its substrate protein (Halic et al., 2004; 2006; Pool et al., 2002; Schaffitzel et al., 2006). The cargo is delivered to the membrane via the interaction of SRP with the SRP receptor (called FtsY in bacteria). Subsequently, the RNC is transferred to the protein translocation machinery (Sec61p in eukaryotes or SecYEG in bacteria), where the nascent protein is either translocated across or integrated into the membrane (Gilmore et al., 1982a; 1982b).

The composition of the SRP varies across different species, but its functional core is highly conserved and is comprised of two essential components: the SRP54 protein subunit and the SRP RNA (called Ffh and 4.5S, respectively, in bacteria) (Walter and Blobel, 1981a). SRP54 (Ffh) contains two structurally and functionally distinct domains connected by a ~30 amino acid long linker: (i) a methionine-rich M-domain, which contains a hydrophobic groove that serves as the signal sequence binding site and a helix-turn-helix motif that binds the 4.5S RNA (Batey et al., 2000; Freymann et al., 1997; Janda et al., 2010; Keenan et al., 1998); and, (ii) a special GTPase, NG-domain

responsible for interacting with the SRP receptor (Egea et al., 2004; Focia et al., 2004) and for contacting the ribosome exit site (Pool et al., 2002; Schaffitzel et al., 2006). The SRP receptor, FtsY, also contains an NG-domain highly homologous to that in Ffh (Montoya et al., 1997). During protein targeting, the GTP-dependent assembly of a stable complex between the NG-domains of Ffh and FtsY mediates the delivery of cargo proteins to the target membrane (Egea et al., 2004). Subsequent rearrangements in the Ffh•FtsY complex further induce the reciprocal activation of their GTPase activity; this late rearrangement is essential for driving the unloading of cargo to the translocation machinery (Zhang et al., 2008; 2009). Hydrolysis of GTP then drives the rapid disassembly of the SRP-FtsY complex, allowing the two proteins to be recycled for additional rounds of targeting.

The SRP RNA is a ubiquitous and indispensible component of the SRP. The *E. coli* 4.5S RNA contains the universally conserved domain IV of eukaryotic SRP RNA, which forms a hairpin structure capped by a highly conserved GGAA tetraloop (Batey et al., 2000). The SRP RNA binds with picomolar affinity to the SRP54 (or Ffh) M-domain in the vicinity of the signal sequence binding site (Batey et al., 2001). It also regulates the interaction between the Ffh and FtsY GTPases during protein targeting. The tetraloop of the SRP RNA mediates a key electrostatic interaction with FtsY, which accelerates the stable association between the SRP and FtsY GTPases by a factor of 200-3000. This stimulation occurs only in the presence of RNC bearing correct signal sequences, or stimulatory detergents and signal peptides that partially mimic the effect of RNC, ensuring that the recognition of cargo is tightly coupled to its membrane delivery during protein targeting (Bradshaw et al., 2009; Shen et al., 2011; Siu et al., 2007; Zhang et al.,

2010). In addition, the SRP RNA also activates GTP hydrolysis in the SRP•FtsY complex ~10-fold, whereas the cargo negatively regulates this GTPase activation (Peluso et al., 2001; Zhang et al., 2010). Thus, there is extensive molecular communication between the cargo, the SRP RNA, and the GTPases throughout different stages of protein targeting. However, the precise molecular mechanism that allows information to be propagated from the signal sequence binding site in the M-domain to the SRP RNA and the GTPases remains to be defined.

Flanking the signal sequence binding site is an evolutionarily conserved flexible region, the fingerloop, which forms a 'flap' over the hydrophobic binding groove. In the absence of a signal sequence, the M-domain can adopt a 'closed' conformation in which the fingerloop inserts several of its hydrophobic residues into the signal sequence binding site; this conformation was proposed to stabilize the hydrophobic signal sequence binding pocket in the free SRP (Rosendal et al., 2003). The fingerloop has also been crystallized in an 'open' conformation, in which it folds back from the signal sequence binding pocket (Keenan et al., 1998). In a recent crystal structure of the M-domain in complex with a signal peptide, several residues of the fingerloop directly interact with the hydrophobic signal peptide (Janda et al., 2010). These observations have led to the suggestion that the fingerloop forms a flexible 'lid' that closes down on the signal sequence binding groove upon cargo binding to the SRP, which provides additional hydrophobic contacts with the hydrophobic signal peptide (Keenan et al., 1998; Rosendal et al., 2003). In addition, the fingerloop, along with the abundance of methionine residues in the M-domain, is thought to provide the flexibility required to bind a variety of signal sequences (Halic and Beckmann, 2005). Nevertheless, no direct experimental

support for this model has been available, and the role of this highly conserved fingerloop in SRP function has remained unclear.

Given its proximity to the signal sequence binding site, the fingerloop is in an ideal position to sense information about signal sequences; the conformational plasticity of the fingerloop also makes it a good candidate to transmit this information to the GTPases. In support of this notion, a previous study reported that mutations in the fingerloop disrupt the ability of the SRP RNA to stimulate Ffh-FtsY complex assembly (Bradshaw and Walter, 2007; Hainzl et al., 2011). However, these defects could also be explained by the inability of the fingerloop mutants to bind signal sequences. In this work, we defined the precise role of the SRP's fingerloop on individual molecular steps during the protein targeting reaction. Our results showed that, although essential for SRP function, the fingerloop is not required for signal sequence binding but rather, mediates the flow of information from signal sequence binding to the remainder of Ffh to activate the SRP and FtsY GTPases along with facilitating the unloading of cargo to the translocon.

RESULTS

The fingerloop domain is essential for Ffh function

To characterize the fingerloop (FL) of Ffh, we first constructed strain SLD108 to facilitate complementation tests (Materials and Methods). SLD108 is not viable at 42°C since the sole functional copy of *ffh* is expressed from a temperature-sensitive plasmid, pFfhTSpc (Table 1). Growth can be restored at 42 °C if the strain is also transformed with a plasmid expressing a functional copy of *ffh*, pBAD*ffh*N6x, which expresses *ffh* under control of the *araBAD* operator and promoter. To determine the importance of the fingerloop for Ffh function, we also constructed the *ffh*ΔFL allele by deleting a 60-bp region that encodes the finger loop (Figure 1A) on pBAD*ffh*N6x (Materials and Methods).

In cells carrying pBAD*ffh*N6x, we observed growth at both the permissive temperature of 30°C, as well as at 42°C, the non-permissive temperature for pFfhTSpc replication (Figure 1B). We observed, conveniently, that arabinose was not necessary for this plasmid to complement *ffh::kan*1 when grown at 42 °C, due to leaky expression from the *araBAD* promoter at the elevated temperature (Figure 1B). Colonies that appeared at 42 °C were re-tested and confirmed to be Spc^S (spectinomycin sensitive), indicating loss of the pFfhTSpc plasmid. Moreover, the Spc^S transformants were only able to grow at 30 °C when provided with 0.01% L-arabinose (data not shown). In contrast to the wild-type control, expression of *ffh*ΔFL failed to complement *ffh::kan*1 in SLD108 (Figure 1B). Consistent with this result, none of the cells recovered from the heavy portion of the streak were Spc^S, nor were they able to grow at 30°C.

The finger loop is often unstructured in crystallographic and biochemical studies of the SRP (Cleverley et al., 2001; Doudna and Batey, 2004; Janda et al., 2010; Zheng and Gierasch, 1997). As an alternative approach to identify key features of the FL, we compared the amino acid sequences of this loop from 109 distinct species, representing all three domains of life using multiple sequence alignment (Thompson et al., 1994). These analyses identified two amino acid pairs, Leu350/Met351 and Pro355/Gly356 from *E. coli*, that are highly conserved (Figure 1A). To assess the importance of these residues, we generated mutant alleles where each amino acid pair was converted to alanines. When expressed in SLD108, the *ffh*LM→AA allele complemented only slightly better than *ffh*ΔFL, while expression of *ffh*PG→AA complemented as well as *ffh*$^{+}$ (Figure 1B). Expression levels of all Ffh constructs were consistent across the board (Figure S1).

To further test the function of the *ffh* mutants, we took advantage of the features of SLD108, as described in Materials and Methods, that allow L-arabinose to induce gene expression at levels that directly correlate with its concentration homogeneously throughout the population of cells (Morgan-Kiss et al., 2002). We used this system to determine if elevated gene expression of the mutant *ffh* alleles could restore growth to SLD108 at the non-permissive temperature. As expected, increased expression of *ffh*ΔFL failed to restore viability to SLD108, and only a minor increase in growth was observed when *ffh*LM→AA was expressed at higher levels. As observed previously, expression of the *ffh*PG→AA allele supported growth of SLD108 at levels indistinguishable from wild-type *ffh* (Figure 1C).

Fingerloop is important for SRP-mediated protein targeting and translocation

To directly test the effect of the fingerloop mutations on co-translational protein targeting, we used a well-established *in vitro* assay that examines the ability of purified SRP and FtsY to target a model SRP substrate, preprolactin (pPL), to ER microsomal membranes (Powers and Walter, 1997; Shan et al., 2007).The efficiency of targeting and translocation can be quantified based on cleavage of pPL signal sequence upon its successful incorporation into the membrane (Figure 2A). Wild-type SRP efficiently targeted pPL, reaching a translocation efficiency over 60% at saturating FtsY concentrations (Figures 2A and B). Deletion of the fingerloop significantly reduced the targeting efficiency, with only ~30% successful targeting and translocation at saturating FtsY concentrations (Figures 2A and B). Further, a much higher FtsY concentration was required to reach saturation for the targeting reaction mediated by SRP(ΔFL). The LM→AA mutant also displayed impaired targeting of pPL, but the defect is milder than that of mutant SRP(ΔFL) (Figures 2A and B). Qualitatively and in a relative sense, the results from Figure 2 agreed with the *in vivo* observations and together provided direct evidence that the conserved fingerloop plays an important role in co-translational protein targeting. We note that several factors could contribute to the stronger phenotype of fingerloop mutants *in vivo* than *in vitro*. The *in vitro* assay represents a single round of targeting and translocation, whereas *in vivo*, SRP needs to mediate multiple rounds of targeting and defects in translocation can accumulate. In addition, the slower translation rate *in vitro* compared to *in vivo* gives the SRP and FtsY a longer time window to complete the targeting reaction, so that defects in their assembly (see below) could be

masked. Finally, SRP is limiting *in vivo* and is competed among a much larger number of translating ribosomes than in translation extracts, thus mild mutational effects on SRP-RNC interaction (see below) are easily masked in the *in vitro* targeting assay but could contribute more significantly *in vivo.*

The fingerloop is not essential for SRP to bind cargo

It was often thought that the highly conserved fingerloop plays an important role in signal sequence binding by the SRP. To test this hypothesis and to determine whether compromised signal sequence binding accounts for the defects of fingerloop mutants in protein targeting, we compared the binding affinities of the wild-type and mutant SRPs for RNCs bearing the nascent chain of FtsQ, a bona-fide SRP substrate (RNC_{FtsQ}) (Zhang et al., 2010). RNCs bearing the nascent chain of firefly luciferase (RNC_{Luc}), which contains no signal sequences, served as a control for the ability of SRP to bind ribosomes translating incorrect cargos. SRP was labeled with fluorescein at Cys421 near the signal sequence binding groove, and SRP-RNC binding was monitored as a change in the fluorescence anisotropy of Ffh(C421)-fluorescein (Zhang et al., 2010). Equilibrium titrations based on this anisotropy signal showed that wild-type SRP binds to RNC_{FtsQ} and RNC_{Luc} with equilibrium dissociation constants (K_d) of 1.7 nM and 128 nM, respectively (Figures 3A and B, closed circles), reflecting a 10^2-fold contribution of the signal sequence to cargo binding. Unexpectedly, both the ΔFL and LM→AA mutants of SRP were able to bind tightly to RNC_{FtsQ}, with less than three-fold change in the value of K_d (Figure 3A, open symbols and Figure 3C). The binding affinity of SRP for RNC_{Luc} was also not substantially affected by the fingerloop mutations (Figure 3B, open symbols and Figure 3C).

To directly monitor signal sequence interactions with the Ffh M-domain, the binding of wild-type and mutant SRPs to the RNC were measured using a fluorescent non-natural amino acid, 7-hydroxycoumaryl ethylglycine (Cm), incorporated near an engineered signal sequence, 1A9L, on the nascent chain (Saraogi et al., 2011). FRET between Cm-labeled RNC_{1A9L} and BODIPY-FL labeled at residue 421 of Ffh M-domain reports directly on the docking of the signal sequence into its binding groove (Saraogi et al., 2011). This assay allowed us to measure, in real time, the association and dissociation rate constants of cargo-SRP binding (Figures 3D and 3E, respectively). The results showed that mutants SRP(ΔFL) and SRP(LM→AA) bind and dissociate from RNC_{1A9L} with rate constants that differ by no more than three-fold from wild-type SRP (Figure 3F). The values of K_d, calculated from these rate constants, is only two-fold weaker with mutant SRP(ΔFL) and six-fold weaker with mutant SRP(LM→AA) (Figure 3F). These results support conclusions from the anisotropy assay and together they indicate that, contrary to previous speculations, the fingerloop is not essential for cargo recognition by the SRP. Although this mild defect could contribute, in part, to the phenotype of fingerloop mutants *in vivo*, it would be easily masked in the *in vitro* targeting reaction where the concentration of SRP is >50-fold above the K_d values even with SRP(LM→AA) . Thus, the observed defects of fingerloop mutants in the *in vitro* targeting assay could not solely arise from their defects in binding the RNC and instead, may arise from subsequent steps in the SRP pathway.

The fingerloop is necessary for signal sequence induced stimulation of SRP-FtsY complex assembly

To efficiently deliver its substrate proteins to the membrane, SRP must rapidly assemble a stable complex with its receptor FtsY. However, to ensure fidelity of protein targeting, complex assembly between free SRP and FtsY is extremely slow but is substantially accelerated by correct cargos (Zhang et al., 2010) and, to a lesser extent, by signal peptides or the detergent Nikkol that mimics the effect of signal peptides (Bradshaw et al., 2009). We therefore asked whether efficient SRP-FtsY complex assembly in response to cargo is affected by deletion or mutation of the fingerloop. To this end, we measured the rate constants for formation of the GppNHp-stabilized complex between SRP and FtsY, using either FRET between DACM-labeled SRP(C235) and BODIPY-FL-labeled FtsY(C487), or acrylodan-labeled SRP(C235) which specifically changes fluorescence upon GTP-dependent formation of the stable complex (Zhang et al., 2008; 2009). We determined complex assembly rate constants under three conditions: (1) without any stimulant; (2) in the presence of the signal peptide mimic Nikkol; and (3) in the presence of RNC_{FtsQ}. In the latter cases, SRP was preincubated with saturating concentrations of Nikkol or RNC based on the information from previous studies (Bradshaw et al., 2009; Zhang et al., 2010) to ensure that >98% of SRP is loaded with cargo or the signal peptide mimic, so that effects of the fingerloop mutations on cargo/signal sequence binding are bypassed.

In the absence of any stimulant, complex assembly for wild-type SRP and the fingerloop mutants were slow and differed by no more than three-fold, ranging from 250 – 610 $M^{-1}s^{-1}$ (Figures 4A and C). Consistent with previous results (Bradshaw and Walter,

2007; Bradshaw et al., 2009), stable SRP-FtsY complex assembly was accelerated 50-fold with wild-type SRP in the presence of Nikkol, but this stimulation was abolished with the ΔFL and LM→AA mutations (Figures 4B and C). These data support the notion that the fingerloop plays an important role in mediating the signal peptide-induced stimulation of complex assembly (Bradshaw and Walter, 2007).

As previously demonstrated, RNC_{FtsQ} exerts a larger stimulatory effect on SRP-FtsY complex assembly than signal peptides or Nikkol, accelerating their complex assembly over 10^3-fold (Figures S2 and 4C) (Bradshaw et al., 2009; Shen et al., 2011; Zhang et al., 2010). Intriguingly, RNC_{FtsQ} also provided significant stimulation for mutants SRP(ΔFL) and SRP(LM→AA), increasing their complex assembly rate constants by 360- and 620-fold, respectively (Figure S2 and 4C). In contrast to the observations in the presence of Nikkol, mutants SRP(ΔFL) and SRP(LM→AA) exhibited only 10- and 2.5-fold slower complex assembly kinetics in the presence of RNC_{FtsQ}. Thus, the additional presence of the ribosome in a complete cargo partially rescued the defects of the fingerloop mutants in mediating efficient SRP-FtsY complex assembly in response to a signal peptide mimic.

GTP-dependent assembly of the stable SRP-FtsY complex comprises two steps, the formation of a transient *early* intermediate, followed by a GTP-dependent rearrangement of this intermediate into a stable *closed* complex (Zhang et al., 2008; 2009). Using established fluorescence assays and conditions (see Methods), we further dissected which of these steps were affected by the fingerloop mutations. In the presence of cargo, the *early* intermediate formed by the SRP(ΔFL) and SRP(LM→AA) mutants were two to three fold weaker compared to that formed by wild-type SRP (Figure S3 and

Table 2). In addition, this intermediate rearranges to the *closed* complex two to four fold slower with mutant SRP(ΔFL) and SRP(LM→AA) than with wild-type SRP (Figure S4 and Table 2). Thus, the combination of defects in stabilizing the *early* intermediate and in mediating the *early* → *closed* rearrangement accounted for the overall defect of fingerloop mutants in assembling the stable SRP-FtsY complex.

The fingerloop is essential for GTPase activation and cargo unloading.

Although the fingerloop mutants exhibited defects in signal peptide-induced stimulation of complex assembly, in the presence of RNC these defects were mild and not sufficient to account for their defects in co-translational protein targeting, especially for the ΔFL mutant. We therefore asked whether additional downstream steps in the SRP pathway were also impaired by these mutations. Previous work has shown that after a stable SRP•FtsY complex is assembled, GTPase activation in this complex is crucial for the successful unloading of cargo from the SRP to the translocation machinery on the target membrane (Shan et al., 2007). We therefore asked whether the fingerloop mutations impaired the ability of the SRP•FtsY complex to activate its GTPase sites.

To this end, we monitored the reciprocally stimulated GTPase reaction between SRP and FtsY (Peluso et al., 2001). In this assay, the observed reaction rates at subsaturating FtsY concentrations are rate-limited by and reflect the assembly of the SRP-FtsY complex, whereas the rate constant at saturating FtsY concentrations (k_{cat}) reports on the GTP hydrolysis rate once a stable complex is formed (Figure S5 and 5). The complex formed by the wild-type SRP hydrolyzed GTP efficiently, with a k_{cat} of 100 min^{-1} (Figure 5 and S5). For both fingerloop mutants, the observed GTPase rates at

subsaturating FtsY concentrations were much slower (Figures S5A and B, k_{cat}/K_m), reflecting their kinetic defects in complex assembly in the presence of the signal peptide mimic Nikkol (Figure S2 and 4C). However, once a stable GTPase complex is formed at saturating FtsY concentrations, mutant SRP(LM→AA) exhibited minimal defects in activated GTP hydrolysis, whereas mutant SRP(ΔFL) had a significantly reduced GTPase rate (Figures 5 and S5, k_{cat}), indicating an additional defect of this mutant in undergoing GTPase activation.

GTPase activation was proposed to be essential for the unloading and transfer of the cargo (Shan et al., 2007). We therefore asked whether the fingerloop also plays an important role in the timely and efficient transfer of cargo to translocation sites on the target membrane. To address this question, we modified our targeting assay to more specifically isolate this cargo unloading step (Figure 6A). We generated ^{35}S-methionine labeled, stalled RNCs bearing the pPL_{86} nascent chain (RNC_{pPL86}) via *in vitro* translation. RNC_{pPL86} was incubated with saturating SRP (wild-type or ΔFL), FtsY and GTP for sufficient time to allow the formation of a stable RNC_{pPL86}•SRP•FtsY complex, such that the kinetic defect of mutant SRP(ΔFL) in complex assembly was bypassed. Microsomes were then added to trigger the transfer of RNC_{pPL86} from the targeting complex to translocation sites on the ER membrane, which was monitored at different time points by sedimentation (Figure 6A). This experiment showed that the targeting complex formed by wild-type SRP was able to unload ~35% of RNC_{pPL86} to the membrane, and the unloading reaction was complete as early as 15 seconds (Figure 6B, white bars). In contrast, cargo transfer proceeded much more slowly with mutant SRP(ΔFL), and even after two minutes, less than 20% of RNC_{pPL86} stably engaged with the microsomal

membrane (Figure 6B, black bars). These results directly demonstrated that the fingerloop plays an important role in the cargo handover event at the last stage of the protein targeting reaction.

The fingerloop is crucial for SRP RNA-mediated stimulatory effects

The effects of the fingerloop mutants, especially Ffh(ΔFL), in the GTPase assay above were reminiscent of the effects of removing the SRP RNA (Peluso et al., 2001; 2000; Shen et al., 2011), which accelerates complex assembly between SRP and FtsY and promotes their subsequent GTPase activation. This raises the possibility that the defects of the fingerloop mutants were caused by defective function of the SRP RNA. To test whether this is the case, we measured the GTPase activity for wild-type and mutant Ffh in the absence of the SRP RNA. Under these conditions, both Ffh(ΔFL) and Ffh(LM→AA) exhibited k_{cat} and k_{cat}/K_m values similar to those of wild-type Ffh (Figures 7A and D), indicating that the intrinsic ability of Ffh to form a complex with FtsY and to hydrolyze GTP are unaffected by the fingerloop mutations. Thus, the defects of the fingerloop mutants in complex assembly and GTPase activation described above likely arise from the inability of the SRP RNA to exert its stimulatory effect on the GTPase interactions.

To provide additional evidence for this notion, we tested another unique signature of the action of SRP RNA: its ability to accelerate the disassembly as well as the assembly of the Ffh•FtsY complex, without perturbing the equilibrium stability of this complex (Peluso et al., 2000; Shen et al., 2011). If the defects exhibited by the fingerloop mutants are associated with defective function of the SRP RNA, then these mutants will

phenocopy the effect of SRP RNA deletion and exhibit much slower complex dissociation rates (k_{off}). Using acrylodan-labeled SRP(C235), we measured the dissociation rate constants of the stable SRP•FtsY complex with the fingerloop mutants. The GTPase complex assembled by SRP(ΔFL) exhibited a dissociation rate constant 80-fold slower than that of wild-type SRP (Figures 7B and E), approaching the value observed in the absence of the SRP RNA (Peluso et al., 2000; Shen et al., 2011). Mutant SRP(LM→AA) exhibited a similar, albeit milder reduction in complex disassembly kinetics (Figures 7C and E). The equilibrium stability of the SRP•FtsY complex, derived from the complex assembly and disassembly rates, were unaffected by the fingerloop mutants (Figure 7E), analogous to the effects of the effects of mutating or removing the SRP RNA. Together, these results strongly suggested that the fingerloop is essential for the SRP RNA to exert its stimulatory effects on the SRP and FtsY GTPases during co-translational protein targeting.

DISCUSSION

Co-translational protein targeting by SRP is essential for maintaining the proper localization of proteins in all cells. During this process, recognition of signal sequences on the cargo protein must be tightly coupled to rapid delivery of the translating ribosomes to the target membrane and its efficient unloading onto the translocation machinery. This coupling requires that the GTPase domains in the SRP and the SRP receptor FtsY actively communicate with spatial and temporal cues from the cargo and the target membrane. In this work, we showed that the universally conserved SRP fingerloop is essential for conveying the information about signal sequence binding in the M-domain to the NG-domain and regulates multiple stages of the targeting reaction, including recruitment of the SRP receptor, subsequent activation of the GTPases and the handover of cargo to the translocation machinery in the membrane.

The fingerloop flanks the signal sequence binding site, forming a flexible 'flap' that has been proposed to close down on the signal sequence binding groove upon cargo binding to the SRP (Keenan et al., 1998; Rosendal et al., 2003). Further, the structural plasticity of the fingerloop together with the richness of methionine residues in the M-domain was proposed to provide the conformational flexibility necessary for the SRP to bind diverse signal sequences (Bernstein, 1998). Given this, it was surprising to find that mutation or even deletion of the entire fingerloop did not give rise to significant defects in the ability of SRP to bind cargo. One possible explanation is that the fingerloop exerts a similar effect on both sides of the binding equilibrium: the free Ffh and Ffh bound to the signal sequence. Crystallographic studies showed that in the absence of signal sequences, the fingerloop could insert into the hydrophobic signal sequence binding

groove to stabilize the free Ffh (Figure 8A, SRP) (Rosendal et al., 2003). Upon cargo recognition, the interaction of the fingerloop with the binding groove is replaced by interaction with the signal peptide (Figure 8A, RNC•SRP), thereby giving rise to an apparent 'isoenergetic' effect on cargo binding. Alternatively, the fingerloop might stably 'close down' on the signal sequence binding site to provide additional binding interactions (Hainzl et al., 2011; Janda et al., 2010). Despite the absence of a significant contribution of this loop to SRP's cargo binding affinity, the results here strongly suggest that signal sequence binding induces important conformational changes in the fingerloop as well as the remainder of the M-domain, as manifested by the defects of these mutants in subsequent steps of protein targeting.

A major effect of fingerloop mutations is that the SRP and FtsY GTPases lose their ability to respond to the binding of the signal peptide mimic, Nikkol, and efficiently assemble a complex with one another. How does the fingerloop exert this effect? Several observations here and from previous work offered a few clues. The fingerloop mutations phenocopied the effects of deleting the SRP RNA on the GTPases' interactions, suggesting that they abolished the ability of this RNA to accelerate complex formation between the SRP and FtsY. It has been shown that the conserved tetraloop of the SRP RNA provides a tethering interaction that holds FtsY near the SRP GTPase to facilitate their initial encounter (Shen and Shan, 2010; Siu et al., 2007). In this mechanism, the SRP's NG-domain must be properly positioned close to the RNA tetraloop; this likely requires a re-orientation of the relative position of the M- and NG-domains from that in the free SRP, which appears to be triggered by the cargo, the signal peptide or the signal peptide mimic Nikkol (Figure 8A, step 1) (Ataide et al., 2011; Batey

et al., 2001; Bradshaw et al., 2009; Hainzl et al., 2011; Halic et al., 2006; Shen et al., 2011; Zhang et al., 2009; 2010). We therefore deem it most likely that the SRP fingerloop plays an important role in enabling the SRP to undergo this structural rearrangement in response to signal sequence binding, inducing it into a more active conformation for FtsY recruitment.

This hypothesis is further supported by the observation that mutation of the SRP fingerloop has a much less deleterious effect when the SRP is bound to a complete cargo, RNC_{FtsQ}, than to the less effective signal peptide mimic Nikkol. This intriguing relationship between the SRP fingerloop and the RNC is akin to 'synthetic lethality' effects, which suggests that the fingerloop and the RNC play overlapping and redundant roles in inducing a more active conformation of SRP for complex assembly (Figure 8B). The RNC, by interacting with both the M- and N-domains of the SRP, is highly effective in bringing the SRP's NG-domain into close proximity to the RNA tetraloop. Thus in the presence of RNC, the SRP is predominantly in the active conformation (Figure 8B, $K>1$). This redundancy would compensate for a fraction of the destabilizing effect of the fingerloop mutations, thus partially masking their deleterious effect (Figure 8B, $\Delta\Delta G^{\ddagger}_{RNC} < \Delta\Delta G_{FL}$). In contrast, in the presence of Nikkol only a small fraction of SRP molecules reach the 'active' structure (Figure 8B, $K<1$). Although mutation of the fingerloop exerts the same destabilizing effect on the active conformation, the full extent of this effect is manifested (Figure 8B, $\Delta\Delta G^{\ddagger}_{Nikkol} = \Delta\Delta G_{FL}$) as there is no redundancy to buffer the deleterious effect of these mutations.

Once the *early* RNC•SRP•FtsY complex is formed (Figure 8A, step 2) (Estrozi et al., 2011; Zhang et al., 2008; 2009), it undergoes additional conformational changes that

are essential for subsequent steps of the pathway that ultimately leads to unloading the cargo (Figure 8A, steps 3) (Ataide et al., 2011; Hainzl et al., 2011; Shan et al., 2007) and activating GTP hydrolysis (Shan et al., 2007; Siu et al., 2007; Zhang et al., 2009). The SRP RNA also facilitates GTPase activation (Peluso et al., 2001; Shen et al., 2011; Siu et al., 2007) and recent work further suggested a potential model for this stimulatory effect: at late stages of the GTPase rearrangements, the Ffh•FtsY NG-domain complex could detach from SRP RNA's tetraloop and instead, interact with the 5', 3'-distal end of the SRP RNA where GTP hydrolysis can be stimulated (Figure 8A, step 3) (Ataide et al., 2011). In this structure, the NG-domain complex would be removed from the signal sequence binding site and the ribosome exit site, which could represent a conformation more conducive to the release of cargo. Regardless of whether this speculative model is true, our observations here that deletion of the fingerloop abolishes SRP RNA-dependent GTPase activation and also impairs the unloading of cargo strongly suggest that the fingerloop is also intimately involved in late conformational rearrangements of SRP that mediate the last stages of the protein targeting reaction (Figure 8A, step 3).

Together, the results presented here demonstrate that the SRP fingerloop is not essential for the initial recognition of cargo. Instead, it mediates conformational rearrangements in the SRP essential for subsequent steps throughout the targeting reaction, including the recruitment of the SRP receptor and subsequent GTPase activation that leads to cargo unloading. In light of the recent structural work, it is intriguing to observe that all of these molecular steps require global re-organization of the relative position of the M- and NG-domains of the SRP, during which the linker connecting its G- and M-domains undergoes major restructuring (Figure 8A). Because of its proximity to

the signal sequence binding site, we speculate that the fingerloop is the first structural element that senses signal sequences and changes conformation. Through the remainder of the M-domain, this information is amplified and leads to the restructuring of the M-G domain linker, thus inducing more global rearrangements of the SRP in both the early and late stages of the protein targeting reaction.

MATERIALS AND METHODS

Materials

The strains and plasmids used in this study are shown in Table 1. All antibiotics and other chemicals were obtained from Sigma Chemical Co. (St. Louis, MO). Restriction enzymes used for cloning were obtained from New England Biolabs (Ipswich, MA) and Fermentas Life Sciences (Glen Burnie, MD). Oligonucleotide primers were synthesized by Integrated DNA Technologies (Coralville, IA). Antibiotics were used at the following concentrations: ampicillin (Amp), 100 μg/ml; kanamycin (Kan), 30 μg/ml; spectinomycin (Spc), 100 μg/ml.

Ffh, FtsY, and 4.5S RNA were expressed and purified using established protocols (Peluso *et al*. 2001). Single cysteine mutations were constructed using the QuickChange mutagenesis protocol (Stratagene) and were purified using the same procedures as wild-type protein. Fluorescent dyes fluorescein, BODIPY-FL, DACM, and acrylodan were purchased from Invitrogen. RNCs were prepared and purified as described (Saraogi et al., 2011; Schaffitzel and Ban, 2007). Single cysteine mutants of Ffh and FtsY were labeled using maleimide chemistry and purified as described (Zhang *et al*. 2008). Labeling efficiency was usually >95%.

Plasmid constructions

All plasmids are derivatives of pBAD*ffh*6x, a plasmid that expresses an allele of *ffh* that expresses a hexahistidine epitope tag at the carboxy terminus of Ffh (Table 1). This plasmid was made by PCR amplification of *ffh* from *E. coli* genomic DNA using primers *ffh*N.S (A**CCATGG**TTGATAATTTAACCGATCGTTTGTCGC) and *ffh*C-AS (TCAATGGTGATGGTGATGATGACCGGTACG). The primers were designed so as

to introduce an *Nco*I restriction site (shown in bold in primer ffhN-F) to the PCR product. The amplification product was introduced to pBAD-topo (Invitrogen, Carlsbad, CA) such that the 3' end of *ffh* was fused in-frame with a hexahistidine coding sequence. The resulting plasmid was subsequently digested with *Nco*I and religated yielding pBAD*ffh*6x.

This plasmid was further modified using site directed mutagenesis to introduce an *Nhe*I restriction site at the start of the finger loop-coding region, yielding pBAD*ffh*N6x. No amino acid substitutions resulted from this change. The finger loop region of Ffh, corresponding to amino acids 350-369 (Figure 1A), was deleted in plasmid pBAD*ffh*N6xΔFL. This plasmid was made by PCR amplification of *ffh* using primers *ffh*NheI-FL.S (ATG**GCTAGC**AAAGTGCTGGTGCGTATGGAAGCC) and *ffh*Nhe-FL.AS (CCCCCAGGCTTCCCTGGTCC). The PCR product was digested with *Nhe*I (site shown in bold) and *Blp*I (site contained within the PCR product) and the gel-purified DNA was ligated into pBAD*ffh*N6x digested with the same enzymes.

Two additional *ffh* alleles were also constructed by site-directed mutagenesis of pBAD*ffh*N6x (*ffh*LM→AA and *ffh*PG→AA) (Figure 1A). The relevant region of each plasmid construct was confirmed by DNA sequencing (DNA Facility of Iowa State University). Expression of *ffh* from all plasmids was confirmed by using the InVision His-Tag In Gel Stain (Invitrogen, Carlsbad, CA), which was used to detect the hexahistidine epitope tag at the carboxy terminus of Ffh (Figure S1).

Strain constructions

To characterize function of the finger loop mutants *in vivo*, we constructed SLD108. This strain is deleted for genes whose products are necessary for arabinose

transport (*araFGH*, *araE*) and utilization (*araBAD*). In addition, SLD108 expresses a mutant LacY permease that allows homogenous uptake of arabinose throughout the population so that the heterogeneity of gene expression of genes under *araC* control is eliminated (Morgan-Kiss et al., 2002). To construct SLD108, ECF529 {Bowers, 2004 #586} was first modified by lambda Red homologous recombination to inactivate *bla* (Amp^R) encoded on the chromosome of this strain and replacing it with a Kan^R gene cassette. For this, primers bla-KD4.S (ATGAGTATTCAACATTTCCGTGTCGCCCTTATTCCCTTTTTTGCGGCATTtgtgtaggctggagctgcttc) and bla-KD4.AS (TTACCAATGCTTAATCAGTGAGGCACCTATCTCAGCGATCTGTCTAcatatgaatatcctccttag), were used to amplify a PCR product using pKD4 as a template (Datsenko and Wanner, 2000). Sequences in upper case designate the portions of the primers with homology to *bla* and sequences in lower case are homologous to pKD4 (Datsenko and Wanner, 2000). The gel-purified PCR product was electroporated into ECF529 transformed with pSIM5, as described (Datta et al., 2006) and Kan^R, Amp^S recombinants were identified.

The Kan^R cassette was subsequently deleted using Flp-mediated site-specific recombination, as described (Datsenko and Wanner, 2000). To complete construction of SLD108, the resulting Kan^S (sensitive) strain was subsequently transformed with pFfhTSpc, expressing ffh^+ from a temperature sensitive replicon (Phillips, 1999) and imparting Spc^R (spectinomycin resistant) and the *ffh*::*kan*1 allele (Phillips and Silhavy, 1992) was introduced by P1 transduction, as described (Peterson and Phillips, 2008).

For complementation tests, plasmids expressing the different *ffh* alleles were

transformed into SLD108 and Amp^R colonies restreaked on LB+Amp agar plates and incubated at 30°C and 42°C. Where indicated, dilutions of saturated cultures were spotted onto LB+Amp plates containing 0%, 0.01%, and 0.02% of L-arabinose and incubated overnight at 42°C.

Fluorescence measurements

Fluorescence measurements were carried out on a FluoroLog-3-22 spectrofluorometer (Jobin-Yvon) in assay buffer (50 mM KHEPES pH 7.5, 150 mM KOAc, 10 mM $Mg(OAc)_2$, 2 mM DTT, 10% glycerol, with or without 0.01% Nikkol). The buffer also contained 100-200 μM GppNHp, a non-hydrolyzable GTP analogue. All reactions were carried out at 25 ºC unless otherwise stated.

The binding affinities of SRP for RNCs or ribosomes were determined using two methods. In the first approach, fluorescence anisotropy measurements were carried out with 5-10 nM of fluorescein labeled Ffh(C421) and varying concentrations of RNC_{FtsQ} or RNC_{Luc}. Observed anisotropy values (A) are fit to equation 1,

$$A = A_0 + (A_1 - A_0)\left\{\frac{[SRP] + [RNC] + K_d - \sqrt{([SRP] + [RNC] + K_d)^2 - 4[SRP][RNC]}}{2[SRP]}\right\}$$

(1)

in which A_0 is the anisotropy value of free SRP, A_1 is the anisotropy value when SRP is bound to cargo, and K_d is the equilibrium dissociation constant of SRP for the RNC (Zhang *et al*. 2010). In a second approach, the binding of SRP to the RNC was determined using Förster Resonance Energy Transfer (FRET) between 7-hydroxycoumarin labeled RNC_{1A9L} and BODIPY-labeled SRP (Saraogi and Shan, 2011). Time courses for SRP-RNC assembly (k_{on}) and disassembly (k_{off}) were determined using

either a FluoroLog-3-22 spectrofluorometer (Jobin-Yvon) or an SF-2004 stopped-flow apparatus (KinTek). To determine SRP-RNC assembly rates, 20 nM RNC_{1A9L} was mixed with varying concentrations of SRP. Linear fits (eq 2) of the observed rate constants for SRP-RNC binding (k_{obsd}) was plotted as a function of SRP concentration to give the second-order association rate constant, k_{on}.

$$k_{obsd} = k_{on}[\text{SRP}] + k_{off} \quad (2)$$

To determine SRP-RNC disassociation rate constants, 20 nM RNC_{1A9L} was pre-incubated with saturating amounts of labeled SRP. The pre-formed RNC-SRP complex is then chased with >10-fold excess unlabeled SRP. Exponential fits to the time course gives the dissociation rate constant.

Association rate constants for SRP–FtsY complex formation were determined using two different assays (Zhang et al, 2009): (1) FRET between donor (DACM) and acceptor (BODIPY-FL)-labeled SRP(C235) and FtsY(C487), respectively; or (2) change in the fluorescence of SRP(C235) labeled with acrylodan, an environmentally sensitive dye. In all cases, saturating concentrations of RNCs (50- or 100-fold above the respective K_d value) were used to ensure that SRP was bound with cargo. Complex assembly was initiated by mixing SRP with varying amounts of FtsY in the presence of 100 μM GppNHp, and the time course of fluorescence change was monitored using a FluoroLog-3-22 spectrofluorometer (Jobin-Yvon) or an SF-2004 stopped-flow apparatus (KinTek). The data were fit to Eq 2, except that the term [SRP] was replaced by [FtsY].

Equilibrium titrations of the early intermediate were carried out using FRET as described previously (Zhang et al. 2008). Rate constants for rearrangement of the early intermediate to the stable complex were measured using Ffh-C235 labeled with

acrylodan. An RNC-SRP-FtsY early intermediate was preformed in the presence of saturating SRP/Ffh and FtsY with respect to the K_d value of the early intermediate. The reaction was initiated by mixing 500 mM GppNHp with the early intermediate. The time course of fluorescence change was fit to single-exponential functions to give the rearrangement rate constants. For experiments concerning SRP or Ffh loaded with different RNCs, concentrations 50- to 100-fold above their respective K_d for Ffh were used to ensure >90% occupancy of SRP by the cargo.

GTPase Assay

All GTPase assays were performed at 25°C in assay buffer [50 mM KHEPES, pH 7.5, 150 mM KOAc, 10 mM $Mg(OAc)_2$, 2 mM dithiothreitol (DTT), 0.01% Nikkol, and 10% glycerol]. GTP hydrolysis reactions were followed and analyzed as described previously (Peluso et al., 2001). In general, reciprocally stimulated GTPase reactions between SRP and FtsY were determined in reactions containing 100-500 nM wild-type or mutant Ffh, 200-1000 nM 4.5S RNA (where applicable), 100 μM GTP, doped with γ-^{32}P-GTP (MP Biomedicals, Solon, OH), and varying concentrations of FtsY. The concentration dependence of the observed rate constant (k_{obsd}) is fit to equation 3, in which k_{cat} is the rate constant at saturating FtsY concentrations, and K_m is the concentration of FtsY that gives half the maximal rate.

$$k_{obsd} = k_{cat} \times \frac{[FtsY]}{[FtsY] + K_m} \quad (3)$$

Translocation Assay

The protein targeting efficiency of wild-type Ffh and mutants ΔFL and LM→AA were determined by a co-translational translocation assay using preprolactin (pPL) as a substrate, as described previously (Shan et al., 2007). Reactions were carried out using

333 nM SRP, varying concentrations of FtsY, and 2 eq of trypsin-digested, salt-washed ER microsomal membranes (TKRM).

Cargo-Unloading Assay

The targeting of RNC_{pPL86} was performed with slight modifications of the procedures used by Wilson *et al*. (1988). Stalled RNCs bearing pPL_{86} were generated by *in vitro* translation using wheat germ translation extract (Promega Corporation, Madison, WI) in the presence of ^{35}[S]-methionine (MP Biomedicals, Solon, OH). The stalled RNC_{pPL86} were incubated with saturating SRP or SRP(ΔFL), FtsY and GTP (to final concentrations of 250 nM, 1 μM and 3 mM, respectively) for 30 minutes at room temperature to ensure that the ternary complex, RNC_{pPL86}•SRP/SRP(ΔFL)•FtsY, was formed. Cargo unloading was initiated by addition of 2 eq of TKRM at 25°C. The reaction was stopped at different time points (15, 30, 60, 90 and 120 seconds) by flash freezing with liquid nitrogen. The samples were thawed on ice and immediately layered onto a sucrose cushion [0.5 M sucrose, 50 mM KHEPES pH 7.5, 150 mM KOAc, 10 mM $Mg(OAc)_2$, and 2 mM dithiothreitol (DTT)]. Membrane-bound RNCs were sedimented by centrifugation at 55,000 rpm at 4°C for 3 minutes (TLA100, Beckman) (Beckman Coulter Optima TLX Ultracentrifuge). The reaction was analyzed by 15% SDS-PAGE and autoradiography.

TABLES

Table 1. Bacterial strains and plasmids.

Strain or plasmid	Relevant genotype or description	Source or reference
E. coli strains		
NEB5a	*fhuA2*Δ(*argF-lacZ*)*U169 phoA glnV44 80* Δ(*lacZ*)*M15 gyrA96 recA1 relA1 endA1 thi-1 hsdR17* (general cloning host)	New England Biolabs
ECF529	Δ*araBAD*, Δ*rhaBAD*, Δ*araFGH*, Δ*araE*, *rrnB*PI(CTC-AGA)-*lacYA177C*	Bowers *et al*., 2004
XLU102	ECF529, Δ*bla*::*frt*	This study
SLD108	XLU102, *ffh*::*kan*1, pFfhTSpc	This study
Plasmids		
pFfhTSpc	$pSC101_{ts}$, *ffh*$^{+}$, *spc* (Spc^{R})	Lab collection
pBAD*ffh*6x	*araC*, *ffh*$^{+}$, *bla* (Amp^{R}), ColE1 (vector for expressing *ffh* under P_{araBAD} control)	This study
pBAD*ffh*N6x	pBAD*ffh*6x (*Nhe*I)	This study
pBAD*ffh*N6xDFL	pBAD*ffh*N6x with fingerloop deleted	This study
pBAD*ffh*N6xLM-AA	pBAD*ffh*N6x with LM→AA mutation	
pBAD*ffh*N6xPG-AA	pBAD*ffh*N6x with PG→AA mutation	

Table 2. Effects of fingerloop mutations on the equilibrium stability of the *early* complex in the presence of RNC_{FtsQ} ($K_{d,early}$), and on the rate constants for rearrangement of the cargo-SRP-FtsY *early* complex to the stable *closed* complex ($k_{rearrange}$). The rate and equilibrium constants are derived from the data in Figures S2 and S3.

	SRP	**ΔFL**	**LM→AA**
$K_{d,early}$ (nM)	86 (1)	175 (2)	236 (4)
$k_{rearrange}$ (s^{-1})	0.6 (1)	0.18 (0.3)	0.3 (0.5)

FIGURES

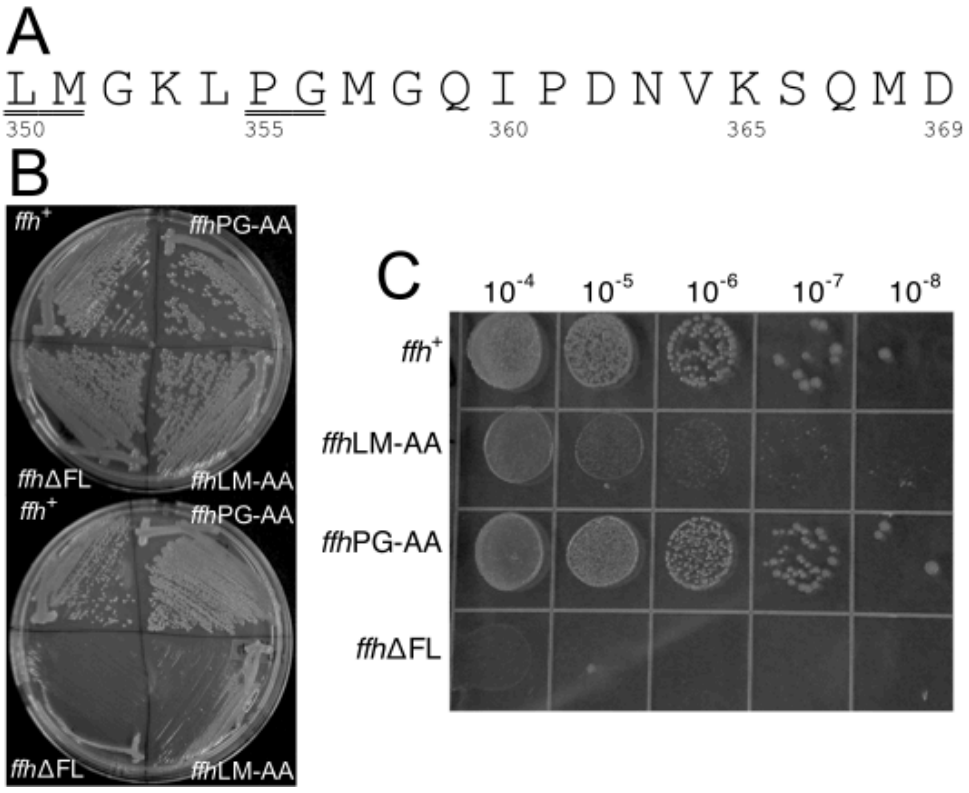

Figure 1. Phenotypes of *ffh* fingerloop mutants. (A) The amino acid sequence of finger loop domain of Ffh deleted in the *ffh*ΔFL allele. Positions of amino acids of the *E. coli* Ffh protein are shown. The underlined amino acids were converted to alanine in the *ffh*LM→AA and *ffh*PG→AA alleles. (B) Plasmids expressing *ffh*ΔFL, *ffh*PG→AA, *ffh*LM→AA and *ffh*$^+$ alleles were transformed into the temperature-sensitive strain SLD108 and cultured at 30^{o}C (top) or 42^{o}C (bottom) as shown. (C) SLD108 transformants expressing each of the four *ffh* alleles were spotted onto LB+Amp+L-arabinose plates at the dilutions shown at the top, and incubated at 42^{o}C overnight.

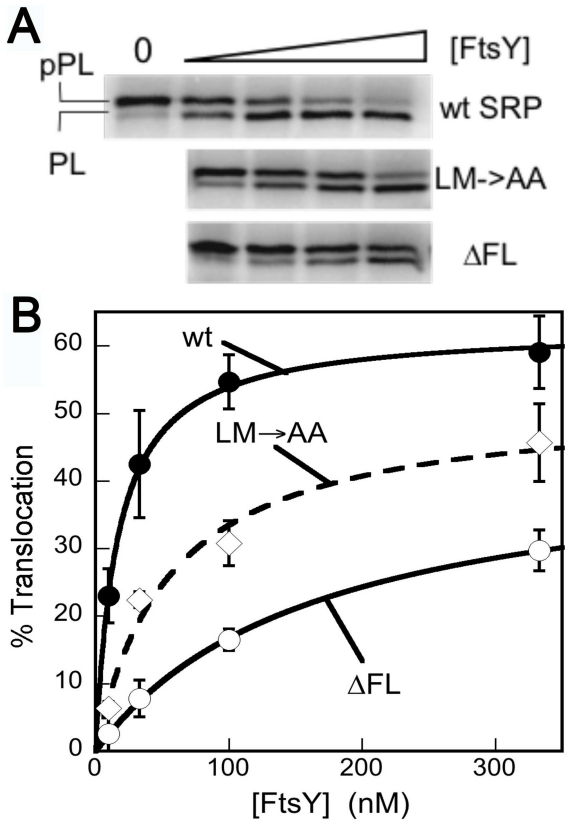

Figure 2. SRP fingerloop mutants are defective in protein targeting and translocation. (A) Co-translational targeting and translocation of ^{35}S-labeled pPL into ER microsomal membranes by wild-type and mutant SRP. (B) Quantification of the data in part A for wild-type SRP (●), SRP(LM→AA) (◇), and SRP(ΔFL) (○).

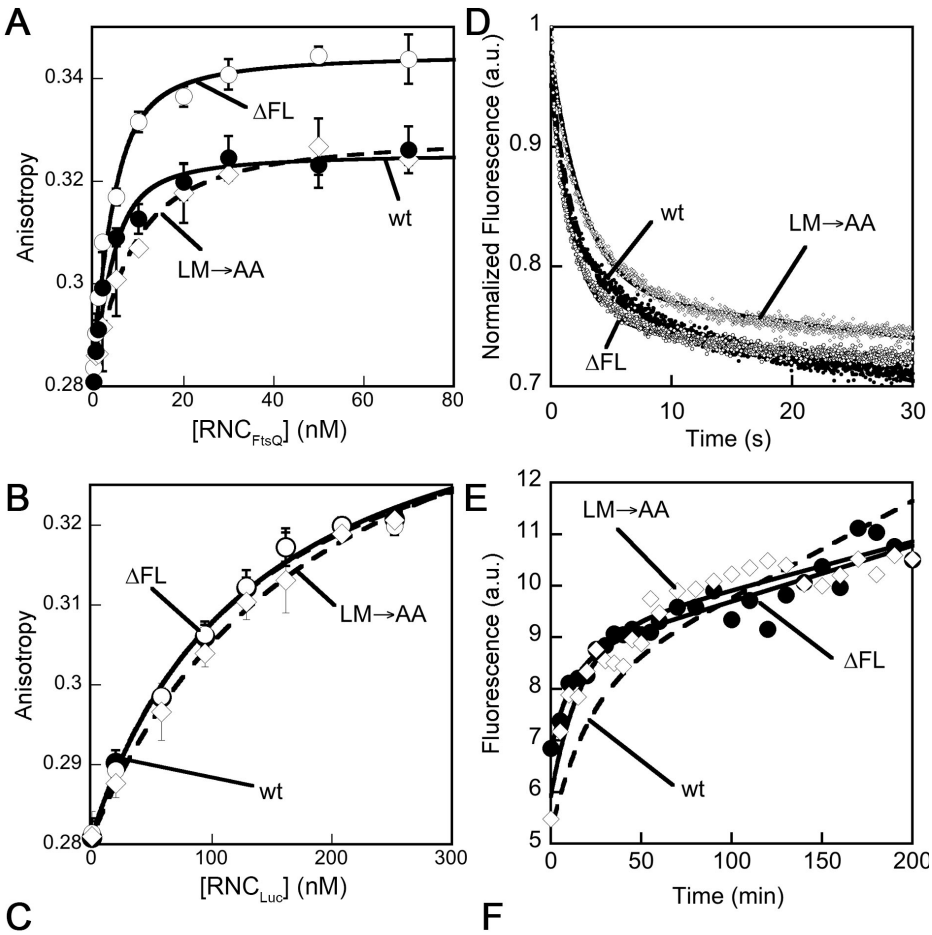

C

K_d (nM)	SRP	ΔFL	LM→AA
RNC_{FtsQ}	≤ 1.8	≤ 1.7	≤ 5.4
RNC_{Luc}	133	128	190

F

RNC_{1A9L}	SRP	ΔFL	LM→AA
k_{on} ($\mu M^{-1}s^{-1}$)	2.3	1.4	0.90
k_{off} (s^{-1})	1.8×10^{-4}	2.4×10^{-4}	4.8×10^{-4}
K_d (nM)	0.08	0.17	0.53

Figure 3. Fingerloop mutants did not exhibit significant defects in cargo binding. (A, B) Equilibrium titrations to measure the binding of wild-type Ffh (●), mutant Ffh(ΔFL) (○), and mutant Ffh(LM→AA) (◇) to RNCs bearing the nascent chain from FtsQ (A) or luciferase (B). The lines are quadratic fits of data to Eq. 1 in *Methods*. (C) Summary of the binding affinities from parts A-B. FRET was used to monitor the association (D) and dissociation (E) of wild-type SRP, SRP(ΔFL) (●) and SRP(LM→AA) (◇)for binding

RNC_{1A9L}, as described in the *Methods*. The results with wt SRP (dotted line) are from Saraogi et al., manuscript in preparation. (F) The association and dissociation rate constants (k_{on} and k_{off}, respectively) of wild-type SRP, SRP(ΔFL) and SRP(LM→AA). The K_d values were calculated according to $K_d = k_{off}/k_{on}$.

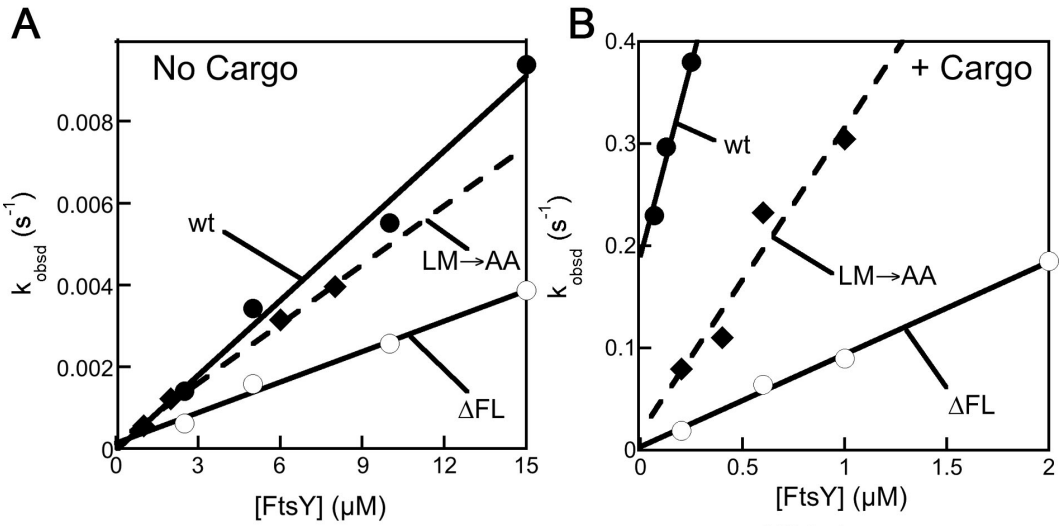

C

k_{on} ($M^{-1}s^{-1}$)	- Cargo	+ Nikkol	+ Cargo	+ Nikkol / - Cargo	+ Cargo / - Cargo
SRP	6.1×10^{2} (1)	3.2×10^{4} (1)	7.5×10^{5} (1)	52	1230
ΔFL	2.5×10^{2} (0.41)	3.7×10^{2} (0.012)	9.0×10^{4} (0.12)	1.5	360
LM→AA	4.8×10^{2} (0.78)	5.4×10^{2} (0.017)	3.0×10^{5} (0.4)	1.1	620

Figure 4. The effects of fingerloop mutants on SRP-FtsY complex assembly. (A-C) Measurements of SRP-FtsY complex assembly kinetics of wild-type SRP (●), mutant SRP(ΔFL) (○) and mutant SRP(LM→AA) (◇) without any stimulants (A) and in the presence of RNC_{FtsQ} (B). The lines are linear fits of the data to Eq 2. (C) Summary of the complex formation rates from 4A-B and S2.

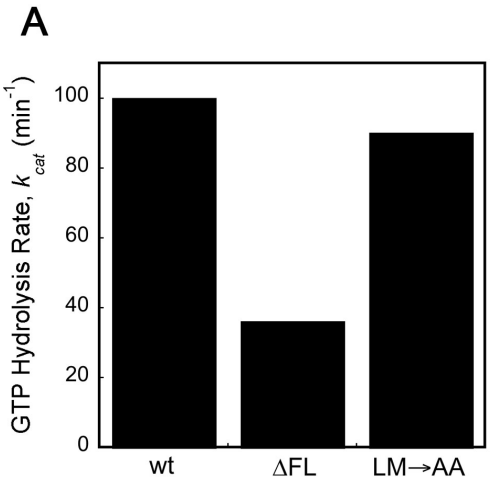

Figure 5. Deletion of the fingerloop results in inefficient GTPase activation. The reciprocally stimulated GTPase reaction between SRP and FtsY were determined for wild-type SRP and mutants SRP(LM→AA) and SRP(ΔFL).

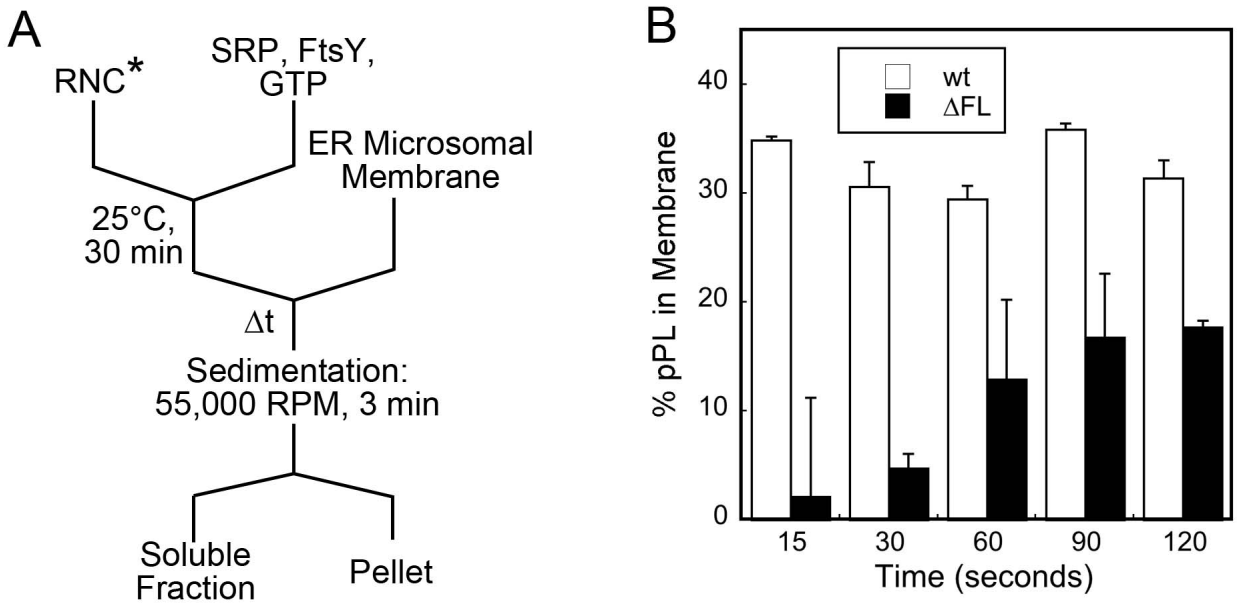

Figure 6. Deletion of the fingerloop impaired unloading of cargo to the ER membrane. (A) Schematic of the experiment to isolate the cargo unloading process. (B) Percentage of RNC_{pPL86} stably engaged with the membrane mediated by wild-type SRP and mutant SRP(ΔFL).

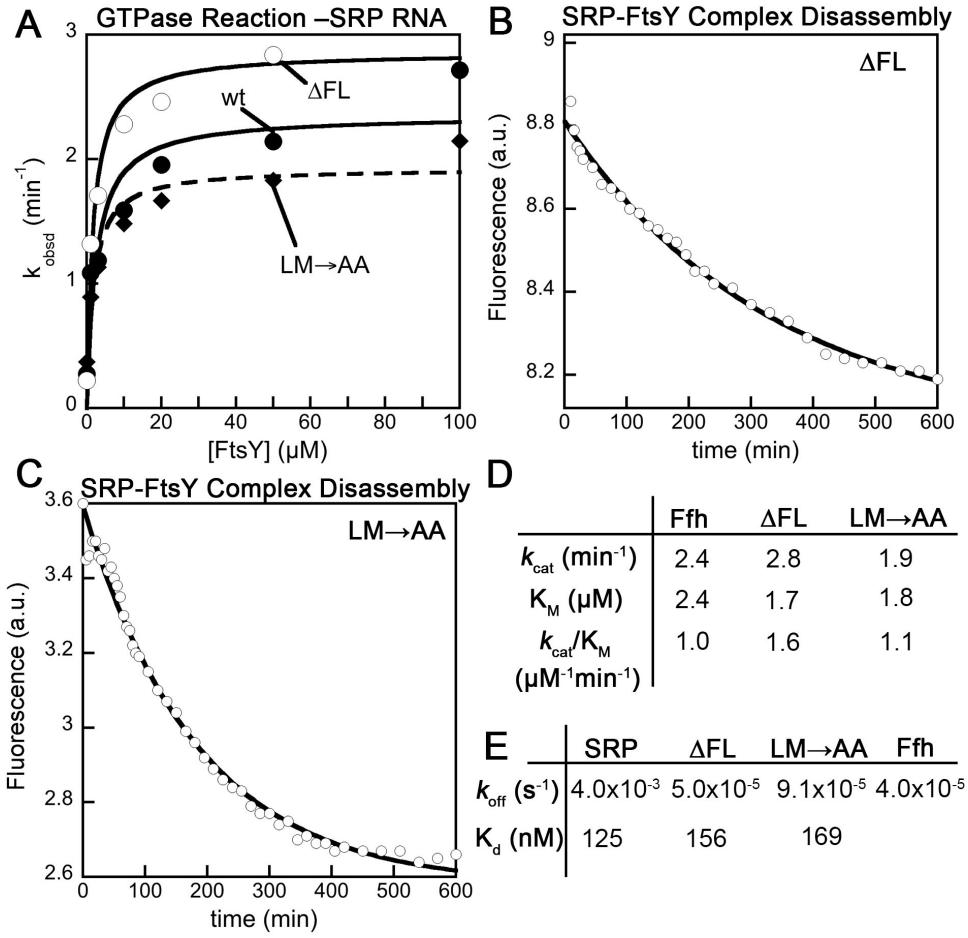

	Ffh	ΔFL	LM→AA
k_{cat} (min^{-1})	2.4	2.8	1.9
K_M (μM)	2.4	1.7	1.8
k_{cat}/K_M (μM^{-1}min^{-1})	1.0	1.6	1.1

	SRP	ΔFL	LM→AA	Ffh
k_{off} (s^{-1})	4.0x10^{-3}	5.0x10^{-5}	9.1x10^{-5}	4.0x10^{-5}
K_d (nM)	125	156	169	

Figure 7. Effects of fingerloop mutants on complex assembly and GTPase activation are linked to the SRP RNA. (A) Reciprocally stimulated GTPase reaction in the absence of SRP RNA for wild-type Ffh (●) and mutants Ffh(LM→AA) (◇) and Ffh(ΔFL) (○). The lines are fits of data to Eq. 3 in the *Methods.* Measurement of the disassembly of the SRP•FtsY complex formed by Ffh(ΔFL) (B) and Ffh(LM→AA) (C). The lines are single exponential fits of the data, which gave the dissociation rate constants. (D) Summary of the k_{cat} and K_m values from the data in part A. (E) Summary of the rate constants obtained from parts B and C. The equilibrium stability (K_d) of the SRP•FtsY closed complex (wild-type and mutants) were calculated according to $K_d = k_{off}/k_{on}$ based on rates obtained in parts 7B, 7C and Figure 4B.

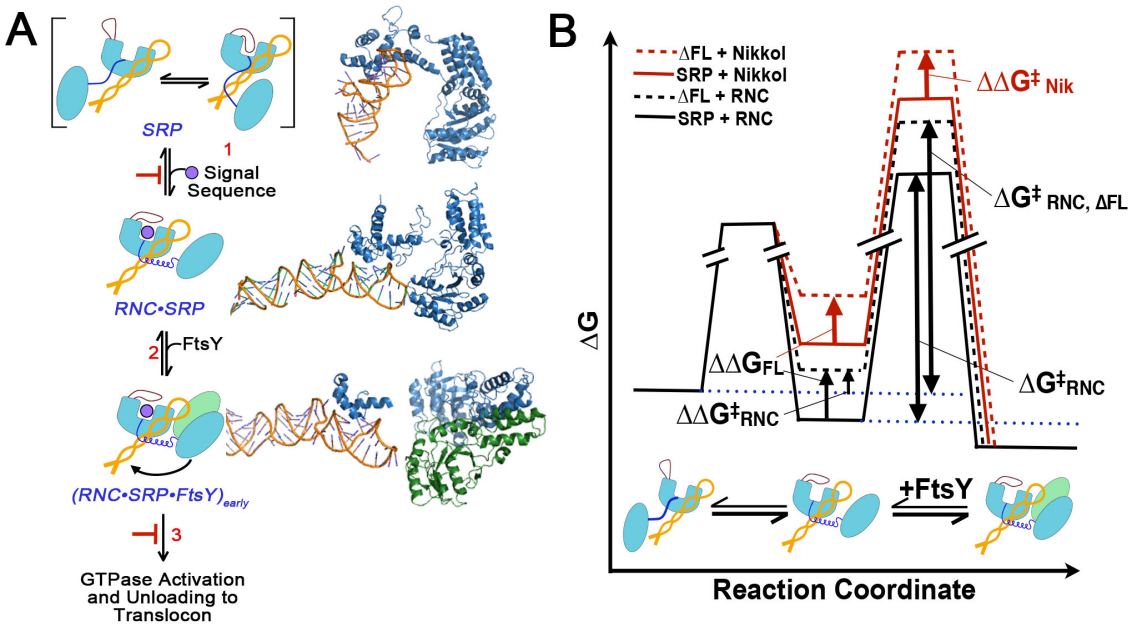

Figure 8. A model for the role of SRP fingerloop (brown) in relaying the information of signal sequence binding to the GTPases and enabling multiple stages of SRP-FtsY interactions during protein targeting is shown in (A). Step 1, the presence of a signal sequence in the M-domain is propagated to the NG-domain (both in light blue, connected by the flexible linker in dark blue) by the fingerloop, priming the SRP for binding its receptor, FtsY (green), near the SRP RNA's tetraloop end (orange). In step 2, FtsY associates with SRP to form the $[RNC•SRP•FtsY]_{early}$ intermediate. During step 3, $[RNC•SRP•FtsY]_{early}$ rearranges to activate GTP hydrolysis and facilitate the transfer of the RNC to the translocation machinery. Structures or structural models for each complex (from top to bottom, PDB IDs: 1QZW, 2J28 and 2XKV; {Estrozi, 2011 #610;Halic, 2006 #605;Rosendal, 2003 #496}) are shown adjacent to the respective SRP/FtsY diagrams. (B) Free-energy profile explaining the different manifestations of the effects of fingerloop in the presence of the signal sequence mimic Nikkol (red) or the RNC (black). In both cases, removal of the fingerloop (dash line) disfavored the conformational change of SRP to an active conformation (ΔΔG) more conducive to complex assembly with

FtsY. In the presence of Nikkol, this conformational change is unfavorable even with wild-type SRP, thus the effect of the fingerloop is fully manifested ($\Delta\Delta G = \Delta\Delta G^{\ddagger}_{Nik}$). In contrast, when bound to the RNC the SRP is pre-organized into the active conformation; thus, although removal of the fingerloop exerts the same destabilizing effect, the full extent of its defect is masked in the observed complex assembly rates ($\Delta\Delta G^{\ddagger}_{RNC} < \Delta\Delta G$).

ACKNOWLEDGEMENTS

We thank members of the Shan group for helpful comments on the manuscript. This work was supported by National Institutes of Health (NIH) grant GM078024, the Beckman Young Investigator Award, the David and Lucile Packard Fellowship in Science and Engineering, and the Henry Dreyfus Teacher-Scholar Award to S.-O.S. G.J.P. was supported by NIH grant R01 GM069628. A.R.A. was supported by NIH/NRSA training grant 5T32GM07616 and by the Betty and Gordon Moore Foundation.

SUPPLEMENTARY FIGURES

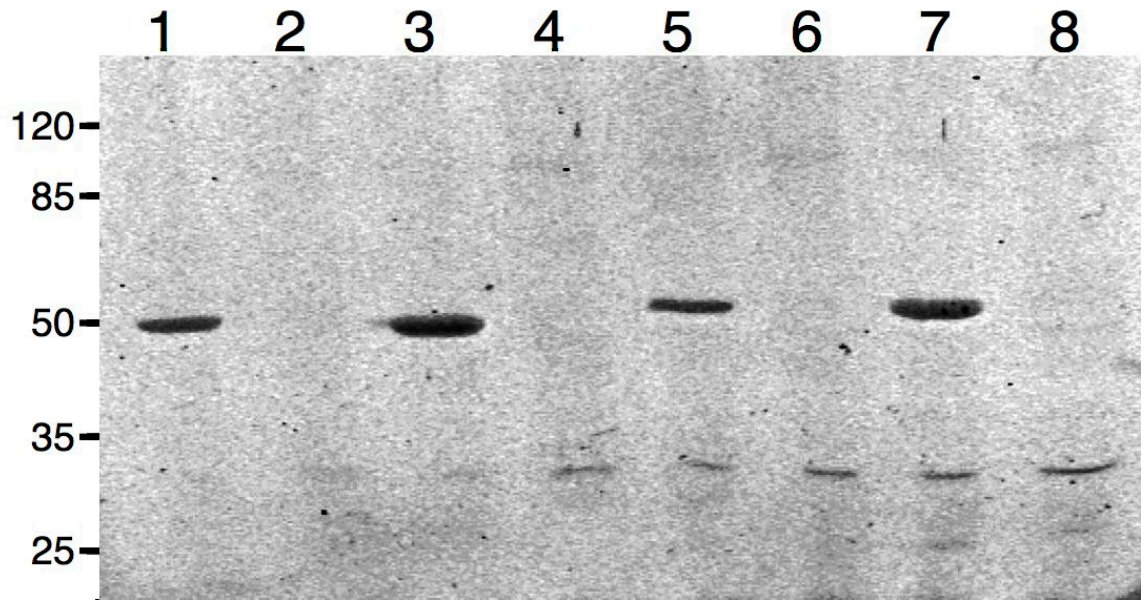

Figure S1. Expression of *ffh* alleles analyzed by SDS-PAGE. Proteins were resolved and detected as described in Materials and Methods. Lanes 1-2: *ffh*PG→AA; 3-4: *ffh*ΔFL; 5-6: *ffh*$^{+}$, 7-8: *ffh*LM→AA. Lanes 1, 3 5, 7: + L-arabinose; 2, 4, 6, 8: – L-arabinose. Molecular weight standards are shown on the left, the relative positions of which were identified using a corresponding SDS-PAGE gel stained with Coomassie Brilliant Blue.

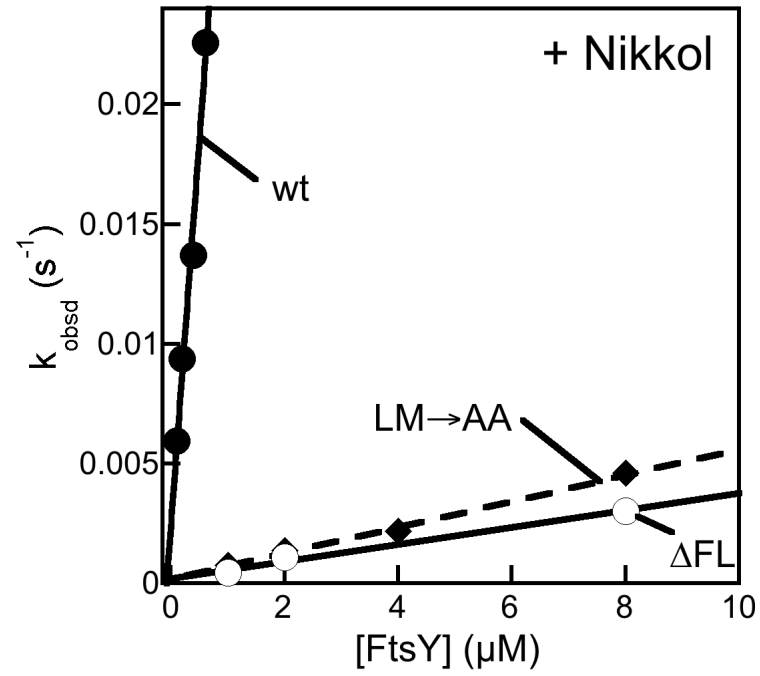

Figure S2. The effects of fingerloop mutants on SRP-FtsY complex assembly. Measurements of SRP-FtsY complex assembly kinetics of wild-type SRP (●), mutant SRP(ΔFL) (○) and mutant SRP(LM→AA) (◇) in the presence of Nikkol.

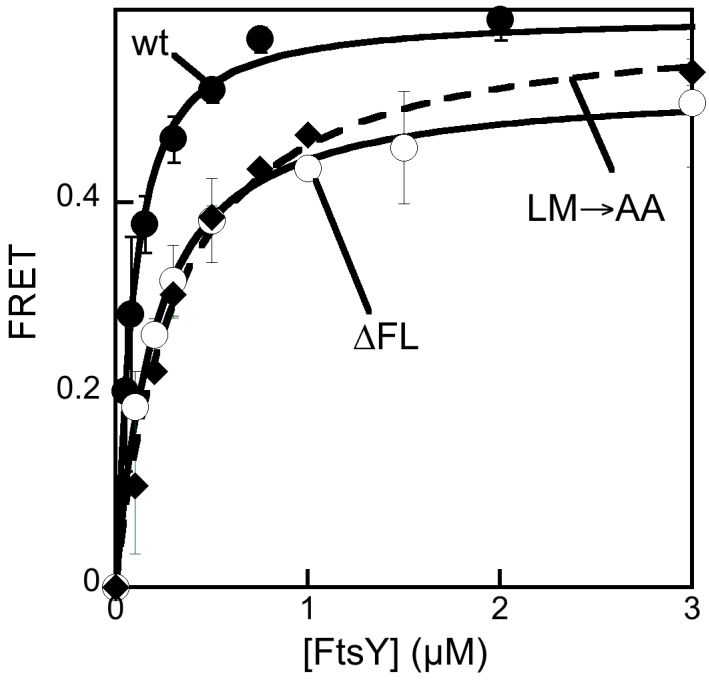

Figure S3. Effects of the fingerloop on the equilibrium stability of the early complex in the presence of RNC_{FtsQ}.

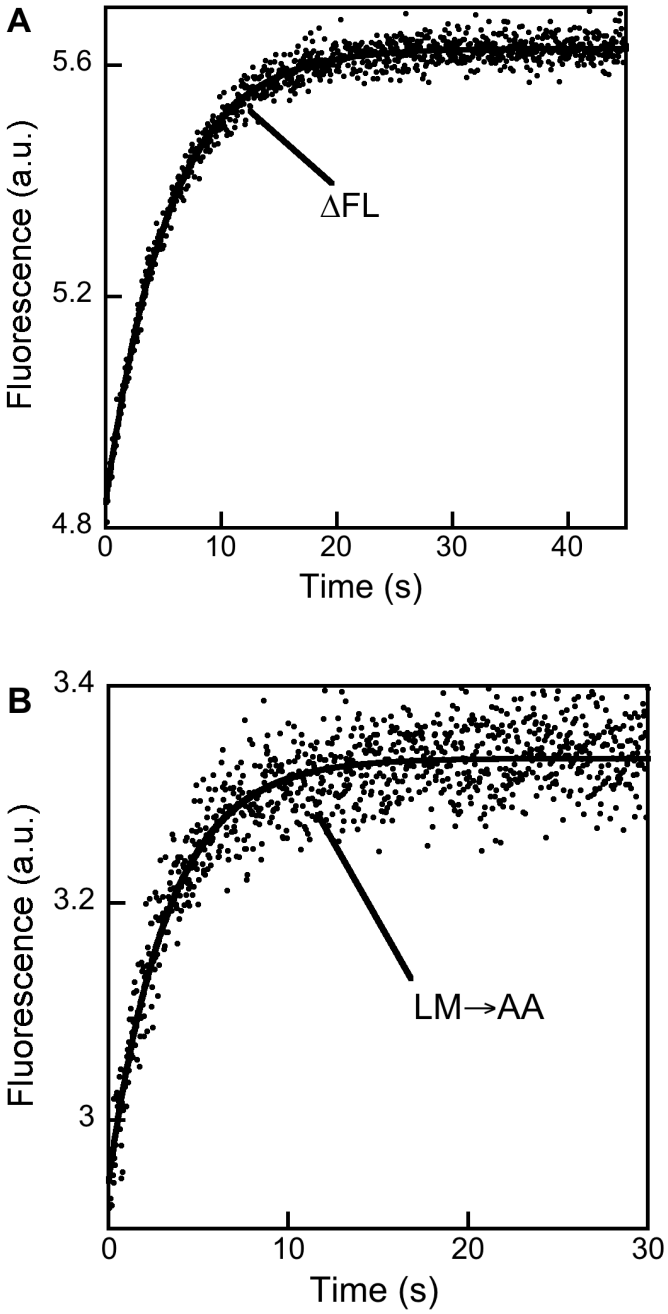

Figure S4. Rate constants for formation of the stable complex starting from a preformed RNC•SRP•FtsY early complex using either (A) SRP(ΔFL) or (B) SRP(LM→AA).

A

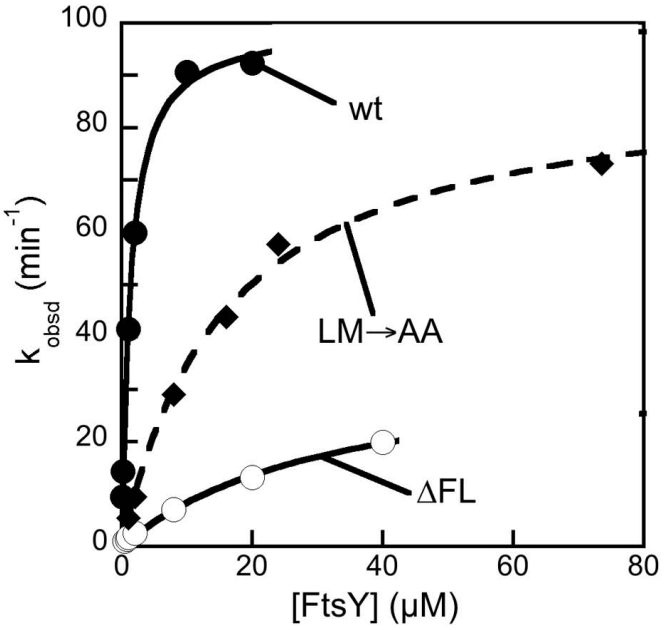

B

	SRP	ΔFL	LM→AA
k_{cat} (min^{-1})	100 (1)	36 (0.36)	90 (0.90)
K_M (μM)	1.3 (1)	32 (25)	6 (4.6)
k_{cat}/K_M ($\mu M^{-1}min^{-1}$)	77 (1)	1.1 (0.01)	15 (0.19)

Figure S5. Deletion of the fingerloop results in inefficient GTPase activation. (A) The reciprocally stimulated GTPase reaction between SRP and FtsY were determined for wild-type SRP (●) and mutants SRP(LM→AA) (◇) and SRP(ΔFL) (○). The data were fit to Eq. 3 in the *Methods*. (B) Summary of the k_{cat} and K_m values from the data in part A.

CHAPTER II

Mechanism of signal sequence surveillance by the signal recognition particle

A version of this chapter has been published as:

Von Loeffelholz, O., Knoops, K., Ariosa, A.R., Zhang, X., Karuppasamy, M., Huard, K., Schoehn, G., Berger, I., Shan, S. and Schaffitzel, C. (2013) *Nat. Struct. Mol. Biol.* Epub ahead of print. "Structural Basis of Signal Sequence Surveillance and Selection by the SRP-FtsY Complex." PMID: 23563142.

ABSTRACT

The signal recognition particle (SRP) utilizes a multistep quality control process to deliver its substrates, ribosome-nascent chain complexes (RNCs), to the membrane. Checkpoints exist in this targeting pathway such that ribosomes translating weakly hydrophobic signal sequences can be rejected *after* SRP binding from the targeting reaction. Here, we show that the *early* targeting complex, formed by SRP and its receptor FtsY with ribosomes translating the incorrect cargo EspP, is unstable and rearranges inefficiently into subsequent conformational states, such that FtsY dissociation is favoured over successful completion of the targeting reaction. The N-terminal extension of EspP acts as an SRP-avoidance sequence and is responsible for these defects in the early targeting complex. These biochemical observations are further supported by the cryo-electron microscopy structure of this 'false' *early* complex with EspP reveals that the NG-domains of Ffh (SRP protein) and FtsY form a distorted, flexible heterodimer. Our results provide a strong evidence for SRP-mediated signal sequence selection during the recruitment of the SRP receptor.

INTRODUCTION

The universally conserved signal recognition particle (SRP) targets nascent proteins with hydrophobic signal sequences to translocation machineries at the target membrane (Akopian et al., 2013). *Escherichia coli* contains a minimal SRP consisting of the protein, Ffh (SRP54 homologue), and the 4.5S RNA, which forms a stable hairpin structure with an evolutionary conserved tetraloop. Ffh is composed of three domains: the N-terminal four-helix bundle and the GTPase domain that together form the functional NG-domain as well as the M-domain which binds the 4.5S RNA and the hydrophobic signal sequence (Batey et al., 2000; Hainzl et al., 2011; Janda et al., 2010; Montoya et al., 1997). FtsY, the bacterial SRP receptor, also contains an NG-domain (Montoya et al., 1997) preceded by an A-domain implicated in membrane and translocon (SecYEG in bacteria) binding (Angelini et al., 2005; Weiche et al., 2008). The Ffh and FtsY NG-domains form a heterodimeric complex with a composite active site (Egea et al., 2004; Focia et al., 2004), in which GTP hydrolysis is activated without requiring an external GTPase activating protein.

During co-translational targeting, both the SRP and FtsY undergo sequential and discrete conformational states in the SRP/FtsY heterodimer, which have been characterized by fluorescence spectroscopy, mutational and structural analyses (Akopian et al., 2013). First, SRP binds with high affinity and is retained longer on ribosomes with a nascent chain in the exit tunnel or exposing a hydrophobic signal sequence (RNC, cargo) (Holtkamp et al., 2012; Zhang et al., 2010). In these cargo-SRP complexes, the Ffh NG-domain is positioned close to the SRP RNA tetraloop (Halic et al., 2006) which accelerates FtsY docking (Peluso et al., 2001) and stabilizes the *early* SRP-FtsY targeting

complex (Shen et al., 2012; Zhang et al., 2010). Subsequently, phospholipids and SecYEG drive GTP-dependent rearrangement from the transient *early* state, which lacks tight interaction between the Ffh/FtsY NG-domains, into the *closed* state (Lam et al., 2010; Shen et al., 2012; Zhang et al., 2010). Rearrangement into the *closed* state involves formation of a stable NG-domain complex with a continuous interface around the GTP molecules (Egea et al., 2004; Focia et al., 2004). Subsequent GTPase activation, involving optimization of the GTPase active site and relocation of the entire NG-domain complex to the opposite end of the SRP RNA (Ataide et al., 2011; Shen et al., 2012), drives the delivery of the cargo onto the SecYEG protein-conducting channel and the disassembly of the SRP-FtsY complex after GTP hydrolysis (Connolly et al., 1991). Throughout the targeting cycle, these GTPase rearrangements allow the SRP and FtsY to actively sense and respond to the presence of the cargo to achieve accurate temporal and spatial control (Zhang et al., 2008; 2009).

In *E. coli*, the co-translational SRP pathway is mostly used for the integration of inner membrane proteins (Tian et al., 2000; Valent et al., 1995). The hydrophobicity of the nascent chain is the main criterion for whether a nascent polypeptide is targeted co-translationally by the SRP pathway or post-translationally via SecA/SecB (Lee and Bernstein, 2001; Valent et al., 1995). A threshold level of hydrophobicity appears to exist for SRP targeting because overexpression of the SRP cannot reroute a model substrate (maltose binding protein) from the post- to the co-translational targeting pathway(Lee and Bernstein, 2001), indicating a high degree of specificity of the SRP pathway. More recent work suggests that the selection of cargos by the SRP is a multistep quality control process (Zhang et al., 2010). If “incorrect cargos” containing weak or no signal sequences

are bound to the SRP, they can be rejected after FtsY docking as the SRP-FtsY complex undergoes sequential conformational changes during the delivery and unloading of cargo. Amongst them, a critical checkpoint is the *early* RNC-SRP-FtsY targeting complex (Zhang et al., 2009), which is stabilized at least 50-fold by a correct cargo compared to incorrect cargos or non-translating ribosomes (Zhang et al., 2009; 2010).

A striking example of an "incorrect cargo" is the bacterial autotransporter EspP. The N-terminus of EspP comprises an unusual 55 amino acid signal sequence composed of a classical signal sequence and an N-terminal extension conserved among autotransporters (Peterson et al., 2006; Szabady et al., 2005) (Figure 1A). *In vivo*, EspP is recognized by SRP, but translocated post-translationally using the SecA/B pathway(Peterson et al., 2006). *In vitro*, the RNC_{EspP} (RNC displaying the EspP signal sequence) is bound by the SRP with high affinity (13.6 nM) (Zhang et al., 2010). However, the *early* SRP-FtsY targeting complex formed in the presence of RNC_{EspP} yields a lower fluorescence resonance energy transfer (FRET) signal between donor-labeled Ffh and acceptor-labeled FtsY as compared to RNCs carrying strong signal sequences from bona-fide SRP substrates (Zhang et al., 2010). This indicates that the *early* targeting complex formed with RNC_{EspP} adopts a different structure than that formed with a strong SRP cargo, such as FtsQ (RNC_{FtsQ}) (Estrozi et al., 2011).

To provide insights into the molecular mechanism of signal sequence selection by the SRP, we further investigated how this unique N-terminal amino acid extension allows EspP to avoid the SRP pathway by creating different variants of RNC_{EspP}. We either deleted the N-terminal extension ($RNC_{EspP\Delta N}$), increased the hydrophobicity of the signal sequence ($RNC_{EspP\text{-}Hydro}$) or both ($RNC_{EspP\Delta N\text{-}Hydro}$). Biochemical analyses show that

despite the presence of a more hydrophobic signal sequence, SRP bound to $RNC_{EspP\text{-}Hydro}$ remains incapable of forming a stable *early* complex with FtsY. Furthermore, both RNC_{EspP} and $RNC_{EspP\text{-}Hydro}$ kinetically disfavor the rearrangement of the SRP-FtsY *early* intermediate to the *closed* state and the overall rate of SRP-FtsY *closed* complex assembly. In addition to these analyses, our collaborator, the Schaffitzel Group, determined the structure of the RNC_{EspP}-SRP-FtsY *early* targeting complex by single particle cryo-EM. This quasi-atomic model of the RNC_{EspP}-SRP-FtsY complex represents an unstable, 'false' *early* targeting complex, which is destined to be rejected from the SRP pathway. Functionally important differences in the conformation of the Ffh M- and NG-domains in the EM structure of this 'false' *early* targeting complex with RNC_{EspP} as compared to the RNC-SRP complex (Halic et al., 2004; Schaffitzel et al., 2006) and the *early* state complex formed with RNC_{FtsQ} (Estrozi et al., 2011) were identified. Our biochemical work, strengthened by structural information, provides a rationale for the rejection of this substrate from the SRP targeting pathway.

RESULTS

RNC-SRP binding alone cannot account for the rejection of EspP

We first asked whether deleting the N-terminal extension and increasing the hydrophobicity of the signal sequence may lead to a higher efficiency in the SRP-dependent targeting of EspP. To this end, the wildtype and three variants of the EspP signal sequence were fused to Prolactin as a model substrate, which is efficiently translocated across the membrane. One EspP signal sequence variant had the N-terminal extension of EspP deleted (EspPΔN), the second variant contained two leucine mutations (C42L/G45L; EspP-Hydro), and the third variant comprised both of these alterations (EspPΔN-Hydro) (Figure 1A). The efficiency of SRP and FtsY at targeting these cargos was measured in a heterologous *in vitro* protein targeting and translocation assay using microsomal membranes (Powers and Walter, 1997; Shan et al., 2007). EspP is poorly translocated *in vitro* (Figures 1B, Table 1 and Supplementary Figure 1A), thus reproducing *in vivo* experiments (Peterson et al., 2006). Interestingly, increasing the hydrophobicity of the EspP signal sequence (EspP-Hydro) improved the translocation efficiency by less than two-fold, whereas deletion of the N-terminal extension (EspPΔN and EspPΔN-Hydro) led to highly efficient targeting and translocation (Figure 1B and Table 1), in agreement with previous observations *in vivo* (Peterson et al., 2006). These results strongly suggest that the N-terminal extension is the primary cause of the inefficient targeting of EspP.

We then asked whether deletion of the N-terminal extension improves the binding affinity of SRP for EspP cargos. As described earlier, RNC_{EspP} bound to SRP with moderate affinity (K_d ~13.6 nM; Figure 1C), comparable to that of another SRP-

dependent substrate, 3A7L (LALLLLLALA), which is efficiently targeted (Zhang et al., 2010). Deletion of the N-terminal extension ($RNC_{EspP\Delta N}$) did not alter this binding affinity (Figure 1C and Table 1). As expected, $RNC_{EspP\text{-}Hydro}$, which contains a highly hydrophobic signal sequence, bound to SRP strongly (K_d ~1.0 nM; Figure 1C and Table 1). Deletion of the N-terminal extension ($RNC_{EspP\Delta N\text{-}Hydro}$) did not affect the SRP binding affinity either (Figure 1C and Table 1). These results show that the N-terminal extension did not exert its inhibitory role on the SRP pathway by reducing the affinity between the SRP and the RNCs (Table 1). In light of these results and recent work (Zhang et al., 2010), we hypothesize that the N-terminal extension of the EspP signal sequence interferes with subsequent steps of the SRP pathway, such as SRP-FtsY assembly.

The EspP N-terminal extension leads to a weak, distorted *early* targeting complex

The SRP loaded with a correct cargo forms a stabilized RNC-SRP-FtsY *early* targeting complex, whereas incorrect cargos fail to provide this stabilization (Zhang et al., 2010). To test whether this were the case with EspP and its variants, we measured the stability of the *early* complex using FRET between DACM (donor)-labeled Ffh(C235) and BODIPY-FL (acceptor)-labeled FtsY(C487) (Zhang et al., 2011). The *early* targeting complexes formed with $RNC_{EspP\Delta N}$ and $RNC_{EspP\Delta N\text{-}Hydro}$ are highly stable (Figure 2A and Table 1), whereas inclusion of the N-terminal extension in the EspP signal sequence caused a 6–7 fold reduction in the stability of the *early* targeting complexes formed with RNC_{EspP} and $RNC_{EspP\text{-}Hydro}$ (Figure 2A). In addition, the maximal FRET efficiencies of the *early* targeting complexes are 0.10–0.16 units lower with RNCs containing nascent chains with the N-terminal extension (Figure 2A and Table 1), suggesting that the *early*

targeting complex formed with R RNC_{EspP} positions the SRP and FtsY's GTPase domains differently from that with RNC_{EspPAN} or a correct SRP cargo.

Cryo-EM structure and quasi-atomic model of the RNC_{EspP}-SRP-FtsY *early* complex

To gain insight into the nature of these differences, our collaborator, the Schaffitzel group, determined the structure of the RNC_{EspP}-SRP-FtsY *early* targeting complex by single particle cryo-EM. To efficiently assemble the EspP *early* complex, the C-terminus of FtsY was fused to the N-terminus of Ffh via a 31-amino acid, glycine- and serine-rich linker (~117 Å). The resulting single-chain construct behaved similarly to the unlinked SRP and FtsY in ribosome binding and GTP hydrolysis experiments (Estrozi et al., 2011). Importantly, a similar FtsY-SRP fusion was completely functional *in vivo* (Braig et al., 2011). For cryo-EM, RNC_{EspP} complexes were incubated with a ten-fold excess of single-chain SRP construct in the absence of GTP to prevent subsequent rearrangements of the targeting complex, which may lead to additional conformational heterogeneity. After computational sorting and refinement, the RNC_{EspP}-SRP-FtsY structure was reconstructed at 12 Å resolution (FSC 0.5 criterion).

At the exit of the ribosomal tunnel, distinct elongated density was observed accounting for the SRP-FtsY complex (red in Figure 2C), which had two connections to the large ribosomal subunit (50S; blue in Figure 2C). A two-lobed density is positioned directly above the tunnel exit where the EspP nascent chain emerged. To generate a quasi-atomic model of the EspP *early* state, the crystal structures of the *E. coli* 70S ribosome (Schuwirth et al., 2005), the *E. coli* SRP (Ataide et al., 2011; Freymann et al.,

1997; Janda et al., 2010) and FtsY (Montoya et al., 1997) were placed into the experimental density (Figures 2D and 2E). The NG-domains of Ffh and FtsY were placed into the two-lobed density above the tunnel exit (Figures 2D and 2E). The quasi-atomic model indicates that FtsY forms a contact with the 4.5S RNA tetraloop, which has been shown to stabilize FtsY binding to the SRP in the *early* complex (Figures 2D and 2E) (Estrozi et al., 2011; Shen and Shan, 2010).

The FtsY NG-domain interacts weakly with the RNC_{EspP}-SRP complex

In the *early* targeting complex formed with RNC_{EspP}, the NG-domains of Ffh and FtsY are weakly associated (Figure 3A) compared to the NG-domain arrangement observed in the crystal structures in which extensive contacts are formed between the N- and G-domains (Egea et al., 2004; Focia et al., 2004). Compared to the FtsQ *early* state (Figure 3B), the Ffh NG-domain is closer to the M-domain (~16 Å) in the 'false' *early* complex. The N-domain of Ffh contacts the N-domain and the NG-domain interface of FtsY. Overall, the NG-domain interaction is not very well defined (see below). In contrast, in the *early* complex formed with RNC_{FtsQ}, the Ffh/FtsY N-domains interact to form a pseudo-symmetric V-shaped complex (Figure 3B) (Estrozi et al., 2011; Zhang et al., 2011). In both complexes, the G-domains are not involved in the interaction, and both GTPase active sites are accessible, consistent with the fact that the *early* complexes can form with or without nucleotides (Zhang, 2009). In agreement with the FRET measurements (Figures 2A and 2B), we observe a larger distance of the Ffh/FtsY G-domains (~68 Å) as compared to the FtsQ *early* complex (~60 Å) and to the *closed*

complex in which the G-domains interact tightly (31 Å) (Egea et al., 2004; Focia et al., 2004).

The FtsY NG-domain is tilted in the 'false' *early* complex, and the tip of the N-domain is displaced ~15 Å towards the Ffh NG-domain (Figure 3D). The interaction between the FtsY G-domain and the RNA tetraloop is a major stabilizing interaction of the *early* targeting complex (Figure 3B) (Estrozi et al., 2011; Shen and Shan, 2010). The tilted conformation of the FtsY NG-domain in the EspP 'false' *early* complex likely weakens its interaction with the RNA tetraloop. Together with the weak interaction of the Ffh/FtsY NG-domains, this likely explains the low affinity of the *early* targeting complex formed with RNC_{EspP} (Figures 2A and 2B). In our collaborator's EM structure, FtsY is covalently linked to Ffh by a flexible linker and therefore, this weak interaction is stabilized to prevent the disassembly of the complex.

Slow rearrangement of RNC_{EspP} to the *closed/activated* state

The less favorable Ffh/FtsY NG-domain arrangement observed in the RNC_{EspP} *early* complex likely impedes the formation of the stable *closed* complex, which is the subsequent step in the SRP pathway and required to deliver the RNC to the membrane (Lam et al., 2010). Consistent with this hypothesis, RNC_{EspP} and $RNC_{EspP\text{-}Hydro}$ mediated the rearrangement from the *early* to *closed* complex at rate constants of 0.04 s^{-1} and 0.10 s^{-1}, respectively, which are at least 3-6-fold slower than that previously observed with bona-fide SRP cargos (Figures 4Aa and 4B, Table 1) (Zhang et al., 2010). When the N-terminal extension of EspP is deleted, this rearrangement occurred at 2–3 fold faster rates. Collectively, the lower stability of the *early* targeting complex (Figures 2A and 2B)

and the slower *early*-to-*close* rearrangement (Figure 4A) would lead to less efficient assembly of the *closed* complex, which is evidenced by direct measurements using a FRET assay: RNC_{EspP} and $RNC_{EspP\text{-}Hydro}$ mediated ~10-fold slower assembly of the *closed* complex than $RNC_{EspP\Delta N}$ and $RNC_{EspP\Delta N\text{-}Hydro}$ (Figure 4B and Table 1).

DISCUSSION

Genetic, biochemical and structural analyses of the SRP and its receptor have led to considerable insight into the co-translational targeting cycle (Akopian et al., 2013). However, the molecular mechanism and structural details by which substrate proteins are surveyed and directed into the co- or post-translational targeting pathways have remained elusive to date. Here, we address this question using EspP, a secreted serine protease autotransporter with an unusually long, less hydrophobic signal sequence containing a basic N-terminal extension (Figure 1A) (Bradshaw et al., 2009; Peterson et al., 2006; Szabady et al., 2005), as a model substrate. EspP was chosen because RNCs translating EspP have been shown to interact well with the SRP *in vitro* (Zhang et al., 2010), but EspP is targeted post-translationally *in vivo* (Peterson et al., 2006). We show that the N-terminal extension preceding the signal sequence causes EspP to be rejected from the SRP pathway *after* SRP binding. Furthermore, cryo-EM analysis of the RNC_{EspP}-SRP-FtsY 'false' *early* complex provides a structural basis for rejection of RNC_{EspP} from the SRP pathway.

Our results show that the basic N-terminal extension of the EspP signal sequence provides a strong 'SRP-avoidance' sequence that rejects substrate proteins from the SRP pathway. Even the EspP variant bearing a highly hydrophobic signal sequence is targeted poorly by the SRP in the presence of this extension. Interestingly, the N-terminal extension does not exert its inhibitory effect by disrupting high affinity binding of SRP to the RNC, as both $RNC_{EspP\text{-}Hydro}$ and $RNC_{EspP\Delta N\text{-}Hydro}$ bound the SRP with 1 nM affinity but were targeted with significantly different efficiencies. Rather, this extension compromises the ability of RNCs to stimulate subsequent SRP-FtsY interactions, which

are critical for completing the targeting cycle. In particular, SRP loaded with RNC_{EspP} and $RNC_{EspP\text{-}Hydro}$ forms a less stable and less productive *early* targeting complex with FtsY, leading to two consequences that disfavour the targeting reaction. First, FtsY dissociates more easily from a labile *early* targeting complex, requiring additional rounds of assembly and disassembly for the targeting reaction to proceed. Second, a distorted *early* targeting complex renders the subsequent formation of a *closed/activated* RNC_{EspP}-SRP-FtsY complex slower. For these reasons, we term the *early* complex formed with RNC_{EspP} a 'false' *early* complex that is less conducive to complete a successful protein targeting reaction.

The cryo-EM structure of the RNC_{EspP}–SRP-FtsY complex reveals the structural origin of the unstable and non-productive 'false' *early* complex. Compared to the *early* complex with RNC_{FtsQ}, which adopts a pseudo-symmetric V-shaped SRP-FtsY NG-domain orientation, we observe in the RNC_{EspP} 'false' *early* complex a flexible, asymmetric heterodimer structure arrangement in which the N-domain of the SRP protein primarily interacts with the NG-domain interface of FtsY (Figures 3A, 3C and 3D). Furthermore, the Ffh NG-domain is displaced towards the M-domain, and the FtsY NG-domain is tilted towards Ffh. This likely results in a weaker interaction with the SRP RNA tetraloop, which is crucial for formation and stabilization of the *early* Ffh-FtsY complex (Bradshaw et al., 2009; Shen and Shan, 2010). Both effects may contribute to the lower stability of the *early* targeting complex formed with RNC_{EspP} (K_d = 311 nM) compared to those formed with a strong SRP cargo (K_d ~40 nM) (Figure 5). The conformational heterogeneity of the Ffh/FtsY NG-domain complex provides additional evidence for the lack of stable molecular interactions in the 'false' *early* complex.

Rearrangement into the stable, quasi-symmetric *closed* complex from this unfavorable and rather unstable NG-domain arrangement(s) would be more difficult, compared to a complex with properly prepositioned NG-domains.

How does the N-terminal extension of EspP disrupt the early targeting complex? The N-terminal extension (EspP 1-25; Figure 1) has a high probability of forming beta strands structures (Peterson et al., 2010). One hypothesis is that this presents a steric block that prevents productive interaction of SRP's M-domain with the signal sequence. This could disrupt the communication between the M- and NG-domains of Ffh and thus lead to less productive interaction of Ffh with FtsY. Alternatively, the steric block from the EspP N-terminal extension could directly interfere with the formation of the NG-domain complex between Ffh and FtsY. The latter possibility is less likely, given that FtsY is 40 Å away from the M-domain where the hydrophobic core of the signal sequence is bound.

The less favourable, non-symmetric NG-domain arrangement observed in the 'false' *early* state is likely responsible for its lower stability and slower rearrangement to the *closed* state observed biochemically. Thus, dissociation of the 'false' *early* complex will likely dominate over the delivery of RNC to the target membrane (Figure 5). Moreover, translation of EspP continues during SRP targeting, and ribosomes with long nascent chains cannot be targeted efficiently via the SRP pathway to the membrane (Raine et al., 2003), imposing a limited time window for successful SRP-dependent targeting (Flanagan et al., 2003; Raine et al., 2003). Incorrect signal sequences like EspP interfere with efficient SRP-FtsY *early* complex formation, and thereby render the targeting reaction to proceed too slowly and unlikely to be completed within this critical

time window, thus resulting in their rejection from the co-translational targeting pathway. Similar observations have been made with RNCs bearing other incorrect signal sequences, which are rejected at steps after the initial SRP binding, in part due to the unstable and unproductive *early* complex.

The SRP is present in all kingdoms of life. Although the mechanisms described here are obtained with prokaryotic SRP, similar mechanisms are likely used by the eukaryotic SRP to reject incorrect substrate proteins. N-terminal extensions that act as 'SRP avoidance' sequences are not unique to bacterial autotransporters like EspP. Several mitochondrial proteins have been reported to contain extensions N-terminal to their targeting pre-sequence. These extensions effectively inhibit the nascent polypeptide from engaging the SRP pathway, and their deletion leads to efficient SRP-dependent targeting to the ER. Presumably, these N-terminal extensions are important for directing the proteins to the mitochondria. Moreover, in a systematic screen of *Saccharomyces cerevisiae* SRP substrates, significant binding of the SRP to nascent chains with neither transmembrane nor signal sequences was detected (del Alamo et al., 2011). Nascent polypeptide-associated complex (NAC), which has overlapping substrate specificity with SRP *in vivo*, was suggested to improve the specificity of SRP in binding the correct cargos (Lauring et al., 1995); however, yeast cells lacking NAC do not suffer from increased protein mistargeting (del Alamo et al., 2011). Given the evolutionary conservation of the SRP and its receptor, it is likely that highly similar surveillance mechanisms using induced fit and proofreading mechanisms exist also in eukaryotes to reject incorrect substrate proteins after initial SRP-RNC recognition.

ACKNOWLEDGMENTS

We thank Tanvir Shaikh for advice with Spider refinement and Pavel Penczek for assistance with SPARX. We thank Dr. Maria Bacia for excellent technical assistance, and the protein expression facility at EMBL Heidelberg as well as the Partnership for Structural Biology in Grenoble for support. The Polara microscope is part of the IBS Structural Biology and Dynamics GIS-IBISA-labeled platform. CS acknowledges support by the Agence Nationale de Recherche (JC09_471873), the region Rhône-Alpes (CIBLE_1976) and the European Research Council by an ERC Starting grant (project 281331). K.K. was supported by a postdoctoral EMBO fellowship. We thank Ishu Saraogi for sharing unpublished results and for critical reading of the manuscript. S.S. is supported by NIH grant R01 GM078024, and the Fellowship for science and engineering from the David and Lucile Packard foundation. A.A. was supported by the NIGMS Ruth L. Kirschstein National Research Service Award (F31GM095294) and the NIH/NRSA Training Grant 5T32GM07616. X.Z. is a Howard Hughes Medical Institute Fellow of the Helen Hay Whitney Foundation.

AUTHOR CONTRIBUTIONS

C.S., I.B, X.Z., and S.S designed experiments; C.S., K.H., O.V.L., A.A. and X.Z. performed sample preparations; A.A. and X.Z. carried out biochemical experiments; K.K., G.S. and M.K. performed the electron microscopy; O.V.L., M.K. and C.S. performed image analysis and model building; C.S., O.V.L., A.A., X.Z., and S.S. prepared the manuscript.

MATERIALS AND METHODS

Preparation of RNC_{EspP}-SRP-FtsY complexes

The plasmid pUC19StrepEspPSecM encodes for a N-terminal triple StrepII-tag, 88 amino acids of the EspP N-terminus with the signal sequence and 33 amino acids of the SecM C-terminus including the stalling sequence (Zhang et al., 2010). pUC19StrepEspPSecM was transcribed and translated *in vitro* using membrane-free cell extract as previously described (Schaffitzel and Ban, 2007). Briefly, the ribosome-nascent chain complexes (RNCs) were purified by sucrose gradient centrifugation and affinity chromatography. After centrifugation, the ribosomal pellet was dissolved in buffer A (50 mM Hepes-KOH, 100 mM KOAc, 8 mM $Mg(OAc)_2$, pH 7.5). To stabilize the SRP-FtsY complex, we used a construct in which full-size FtsY is linked to full-size Ffh via a 31 amino acid linker (corresponding to ~ 117 Å linker) (Estrozi et al., 2011). The single-chain SRP-FtsY construct (scSRP) was purified by affinity purification via the hexahistidine-tag and anion exchange chromatography (MonoQ) as described before (Estrozi et al., 2011). The complexes were reconstituted by incubation of 200 nM RNCs displaying the EspP nascent chain (RNC_{EspP}) with a 10-fold molar excess of scSRP for at least 60 min on ice. The binding of scSRP to RNC_{EspP} under these conditions was confirmed by co-sedimentation experiments through a 0.5 M sucrose cushion in buffer A.

Electron microscopy and image processing of RNC_{EspP}-SRP-FtsY complexes

Lacey carbon grids (Cu 300 mesh, Agar scientific) were glow discharged on both sides for 30 s, and 3 μl sample (200 nM RNCs) was applied on the carbon side. The grids were plunge frozen in liquid ethane using a Mark IV vitrification robot (FEI) after blotting for

1 s at 20ºC and 100% relative humidity. CCD frames were recorded under low-dose conditions on a Tecnai G2 Polara (FEI) operating at 300 kV and a specimen level magnification of 76,000x with a Gatan 4k x 4k CCD camera in a defocus range between -0.7 μm and -5.7 μm with an initial pixel size of 1.875 Å on the object scale.

The contrast transfer function (CTF) was determined and corrected with bctf (Bsoft package (Heymann and Belnap, 2007)). The CCD frames were re-sampled to 3.75 Å/pixel. A total number of 165,820 particles was selected semi-automatically from 1,974 CCD frames using e2boxer (EMAN2) (Tang et al., 2007). The data were classified into four subsets according to ribosomal conformations, using low pass filtered ratcheted and not-ratcheted vacant ribosomes as initial references (EMDB IDs: 1363, 1056 (Valle et al., 2003a; 2003b)), and SRP-FtsY complex presence in SPIDER (Shaikh et al., 2008). We also used maximum likelihood 3D refinement by XMIPP (Scheres et al., 2008) on the complete dataset using a band-pass filtered 50S structure as initial reference to avoid bias in the sorting procedure (Fischer et al., 2010). However, the resulting three structures containing density corresponding to SRP-FtsY ultimately did not refine to the same resolution as with the approach described above. The pool of not-ratcheted RNC_{EspP}–SRP-FtsY complex contained 52,020 particles. Special care was taken not to have an overrepresentation of raw images in some of the class averages used for the reconstruction. Limiting the population of each class to the same number resulted in using 46,945 images for the final reconstruction. Full-size images were used for the last round of refinement. At the end of refinement, the data were split randomly to generate two reconstructions. These two independent reconstructions were then used for calculation of the FSC curve, and the resolution was assessed to be 12 Å by the Fourier

shell correlation with a 0.5 threshold, and 8.3 Å according to the FSC 0.143 criterion (Rosenthal and Henderson, 2003).

Generation of the Quasi-Atomic Model

The crystal structure of the *E. coli* 70S ribosome (Schuwirth et al., 2005) was fitted into the EM map with UCSF Chimera (Pettersen et al., 2004). The atomic model of the *E. coli* SRP-FtsY complex was generated using the crystal structures of the *E. coli* 4.5S RNA (Ataide et al., 2011), of the *Sulfolobus solfataricus* Ffh M-domain with signal sequence (Janda et al., 2010) which fitted our density better (correlation coefficient 0.152) compared to the *Methanococcus jannaschii* M-domain with signal sequence (cc of 0.148), and of the Ffh and FtsY NG-domains (Freymann et al., 1997; Montoya et al., 1997). The domains were placed as rigid bodies into the EM density using UCSF Chimera (Pettersen et al., 2004). The resulting model was energy minimized in CNS Version 1.0 (Brünger et al., 1998). The figures were generated with PyMOL (DeLano Scientific).

Protein Targeting and Translocation Assay

The signal sequences of EspP and variants (Figure 1A) were fused N-terminally to the signal peptidase cleavage site and to the mature region of pre-Prolactin. Their respective targeting efficiencies were determined by a co-translational protein targeting and translocation assay in the presence of SRP, FtsY and endoplasmatic reticulum microsomes, as described previously (Shan et al., 2007). To accurately determine targeting efficiency and to avoid a bottleneck in the translocation step, Prolactin was chosen as a model substrate rather than the EspP protein because its translocation is

highly efficient across the membrane and thus is not rate-limiting for the observed reaction. For the same reason, microsomal membranes were used for this assay because they are more active in *in vitro* translocation compared to *E. coli* membranes. Endogenous SRP and SRP receptor from microsomal membranes have been removed by high salt wash and trypsin digestion. Importantly, *E. coli* SRP and FtsY can mediate protein targeting in this assay as efficiently as the mammalian SRP and SRP receptor (Powers and Walter, 1997).

Fluorescence Measurements

Fluorescence measurements were carried out on a FluoroLog-3-22 spectrofluorometer (Jobin-Yvon) or an SF-2004 stopped-flow apparatus (KinTek). In experiments involving SRP-RNC complexes, saturating concentrations of RNCs (50- or 100-fold above the respective K_d value) were used to ensure that >90% of SRP was bound with cargo. All reactions were carried out at 25 ºC in assay buffer (50 mM KHEPES pH 7.5, 150 mM KOAc, 10 mM $Mg(OAc)_2$, 2 mM DTT and 10% glycerol).

The binding affinities of SRP for RNCs were determined using fluorescence anisotropy as described (Zhang et al., 2010). Equilibrium titrations were carried out with 5-10 nM of fluorescein-labeled Ffh(C421) and varying concentrations of RNC. Observed anisotropy values (A) are fit to equation 1,

$$A = A_0 + (A_1 - A_0)\left\{\frac{[SRP] + [RNC] + K_d - \sqrt{([SRP] + [RNC] + K_d)^2 - 4[SRP][RNC]}}{2[SRP]}\right\}$$

(1)

in which A_0 is the anisotropy value of free SRP, A_1 is the anisotropy value when SRP is bound to cargo, and K_d is the equilibrium dissociation constant of SRP for the RNC.

Equilibrium titrations of the *early* intermediate were carried out using FRET between donor (DACM)-labeled SRP(C235) and acceptor (BODIPY-FL)-labeled FtsY(C487), respectively, as described previously (Zhang et al., 2008; 2011). Rate constants for rearrangement of the *early* intermediate to the *closed* complex were measured using SRP-C235 labeled with acrylodan. An RNC-SRP-FtsY *early* intermediate was preformed in the presence of saturating SRP and FtsY with respect to the K_d value of the *early* intermediate. The reaction was initiated by mixing 500 mM GppNHp with the *early* intermediate. The time course of fluorescence change was fit to single-exponential functions to give the rearrangement rate constants.

Association rate constants for SRP–FtsY *closed* complex formation were determined using FRET as described previously (Zhang et al., 2009). Complex assembly was initiated by mixing SRP with varying amounts of FtsY in the presence of 100 μM GppNHp, and the time course of fluorescence change was monitored, giving the observed rate constants for SRP-FtsY binding (k_{obsd}). Linear fits (eq 2) of the observed rate constants were plotted as a function of FtsY concentration to give the second-order association rate constant, k_{on}.

$$k_{obsd} = k_{on}[\text{FtsY}] + k_{off} \qquad (2)$$

TABLE

Table 1. Interaction parameters of RNC-SRP-FtsY and resulting translocation efficiencies.

	EspP	**EspPΔN**	**EspP-Hydro**	**EspPΔN-Hydro**
RNC-SRP K_d (nM)	13.6 ± 1.2	13.4 ± 0.78	1.0 ± 0.05	1.0 ± 0.3
Early complex K_d (nM)	311 ± 11	58 ± 10	300 ± 4	42 ± 5
Early Complex FRET	0.39 ± 0.02	0.55 ± 0.01	0.51 ± 0.01	0.61 ± 0.02
Early-to-closed rearrangement $k_{e\rightarrow c}$ (s^{-1})	0.04 ± 0.01	0.13 ± 0.01	0.10 ± 0.01	0.18 ± 0.02
Closed complex assembly rate k_{on} x 10^3 ($M^{-1}s^{-1}$)	9.2 ± 1.1	91.2 ± 7.8	15.2 ± 1.2	112 ± 5.3
% Translocation	15.8 ± 1.2	66.7 ± 5.3	22.8 ± 2.0	68.3 ± 1.9

FIGURES

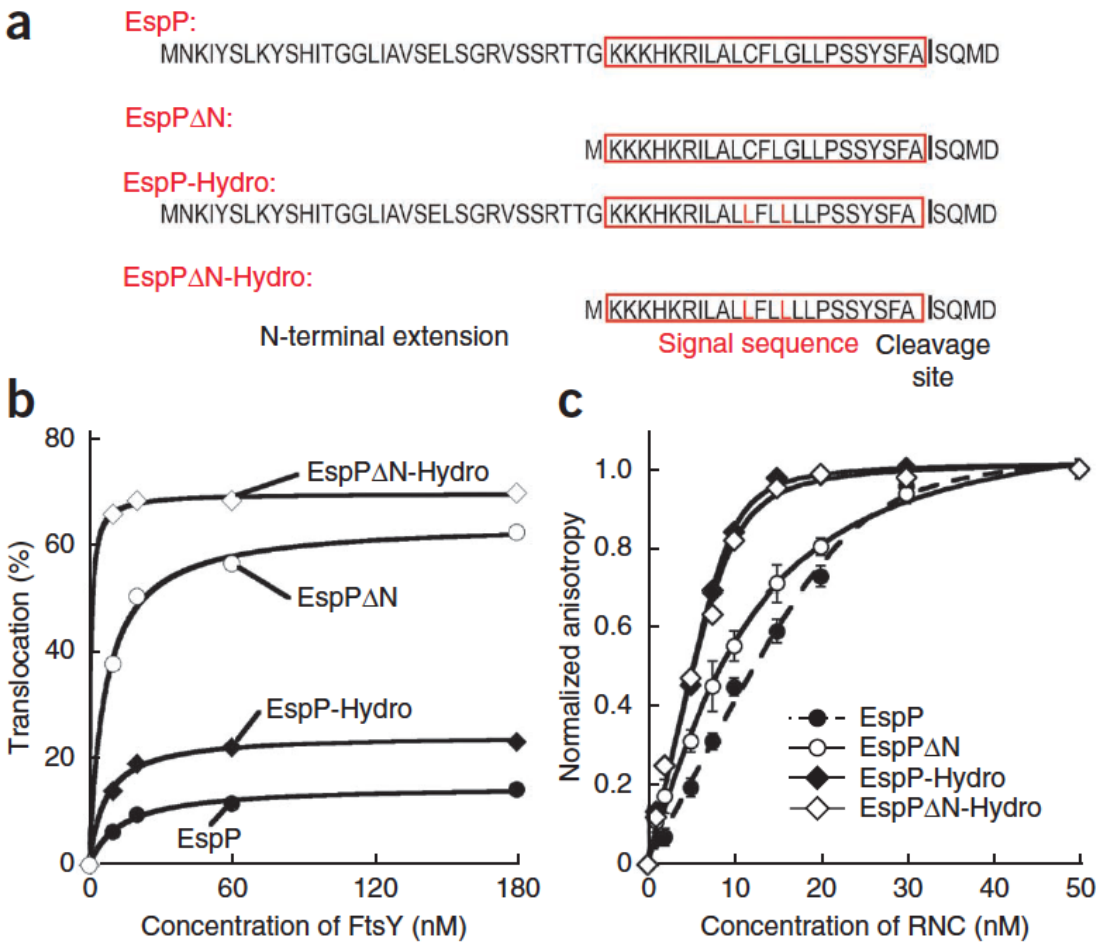

Figure 1. The N-terminal extension of EspP inhibits co-translational protein targeting but does not affect RNC-SRP binding. (A) Signal sequences of EspP and its variants used in this study. The N-terminal extension of the signal sequence and the signal peptide cleavage site are indicated. The classical signal sequence is marked by a red box, and mutations are highlighted by red letters. (B) *In vitro* targeting and translocation efficiency of EspP signal sequence variants fused to prolactin using microsomal membranes. (C) Equilibrium titration of RNC-SRP binding.

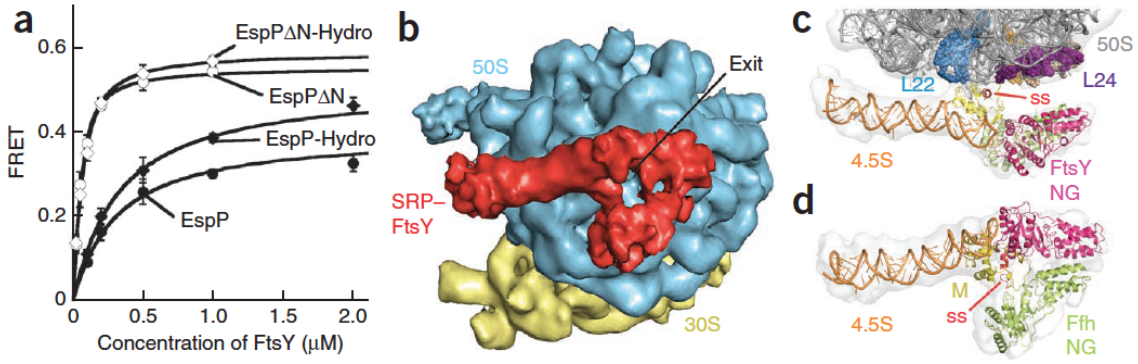

Figure 2. The EspP N-terminal extension leads to a weaker and distorted *early* targeting complex. (A) Equilibrium titration of the SRP•FtsY *early* complex in the presence of RNCs bearing EspP signal sequence variants. 300-500 nM RNCs were used to ensure that most of the SRP is ribosome-bound. (B) Cryo-EM structure of RNC_{EspP}-SRP-FtsY shown with the view into the polypeptide exit tunnel. The large ribosomal subunit (50S) is depicted in blue, the small ribosomal subunit (30S) in yellow and the single chain SRP-FtsY in red. (C, D) EM reconstruction and quasi-atomic model of the RNC_{EspP}-SRP-FtsY *early* complex (C) in a close-up view from the back of the 50S subunit and (D) in a view as in (C). The experimental density is shown in light grey, 4.5S RNA in orange, the EspP signal sequence in red, the Ffh M-domain in yellow, the Ffh NG-domain in greenyellow, the FtsY NG-domain in magenta, the 50S rRNA in dark gray, ribosomal proteins L24 in purple, L22 in skyblue, L29 in wheat and L23 in orange. The density of the ribosome is not shown in (D) for clarity.

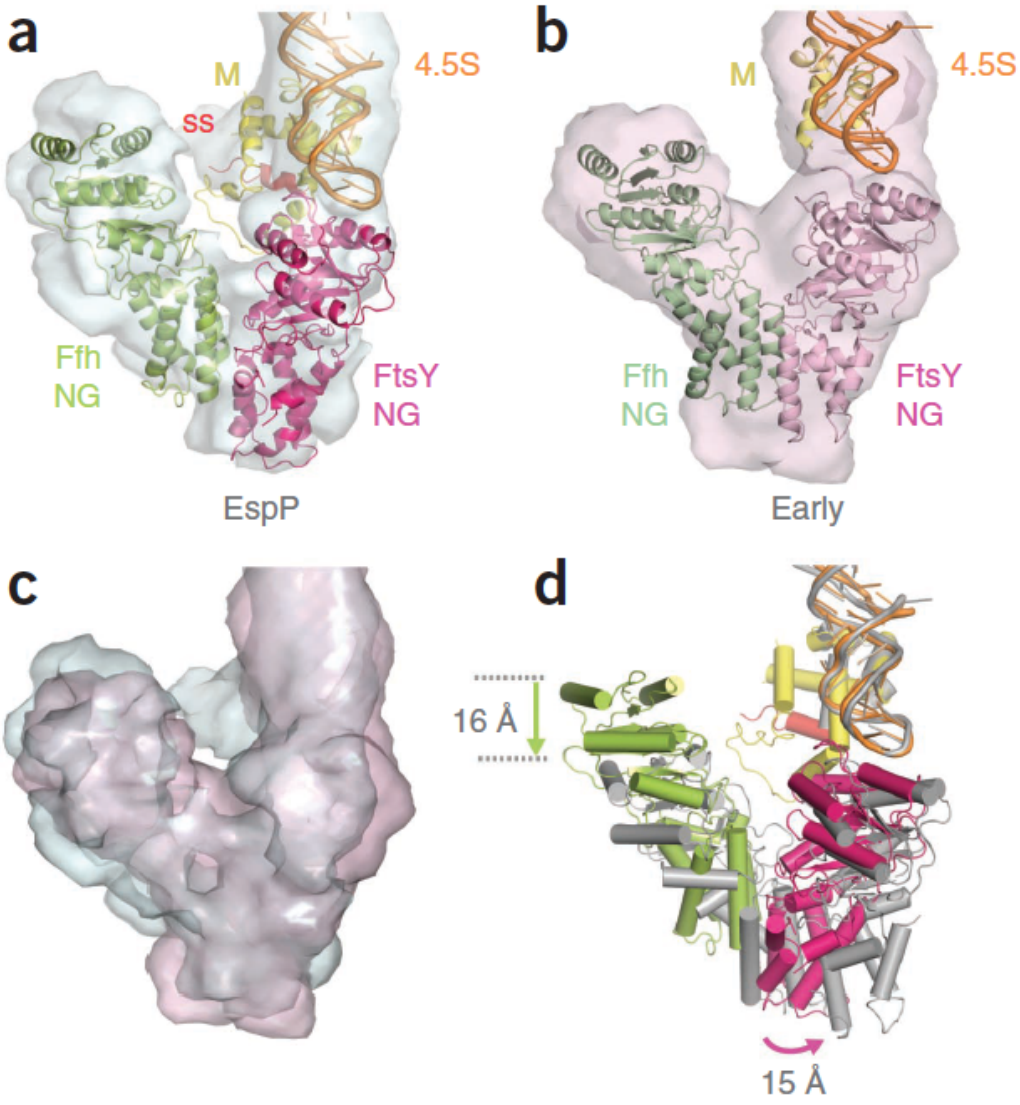

Figure 3. Ffh/FtsY NG-domain arrangement in the 'false' *early* complex formed with EspP compared to the productive *early* complex formed with a correct cargo.

(A) In the RNC_{EspP}•SRP•FtsY 'false' *early* complex, the Ffh/FtsY NG-domains have a weak interface involving the N-domain of Ffh and the NG-domain of FtsY. The experimental density is depicted in pale cyan; unfilled density indicates flexibility in this part. (B) Pseudo-symmetric V-shaped NG-domain arrangement in the *early* targeting complex with RNC_{FtsQ} (Estrozi et al., 2011). The experimental density of this complex is

shown in light pink. (C, D) Overlays of (C) the EM densities of the *early* targeting complexes from (A) & (B), and (D) the corresponding quasi-atomic models. Arrows indicate positional differences of the NG-domains. For the overlays (C, D), the RNA tetraloops of the structures (C) models (D) have been aligned. Color codings of the quasi-atomic models are as in Figure 2.2 except in (D), where the NG-domain complex of the *early* targeting complex with RNC_{FtsQ} is depicted in grey for clarity.

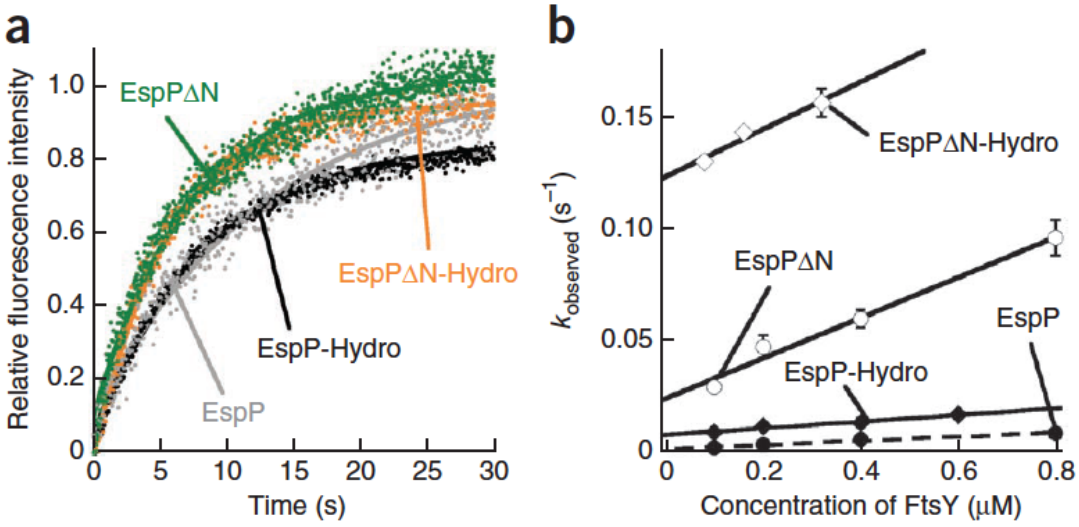

Figure 4. The N-terminal extension leads to a less productive *early* complex and slower assembly of the *closed* SRP-FtsY complex. (A) Kinetics for rearrangement of the *early* to the *closed* complex for EspP and variants. (B) Assembly rates of the *closed* SRP/FtsY complex mediated by RNCs displaying EspP signal sequence variants.

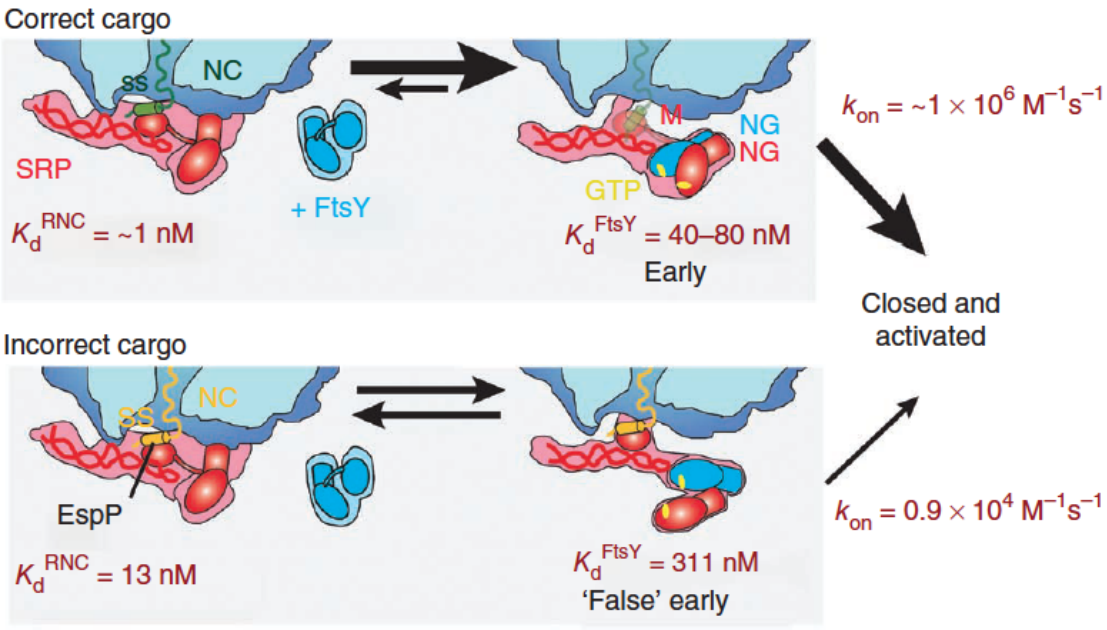

Figure 5. Model of signal sequence surveillance by the SRP and FtsY.

Correct cargo is tightly bound by the SRP. FtsY binding leads to detachment of SRP from the ribosome, and a pseudo-symmetric NG-domain arrangement. EspP has a less hydrophobic signal sequence, leading to a moderate affinity of SRP (13 nM). FtsY has a lower affinity (311 nM) for this SRP-RNC_{EspP} complex and forms a less favourable, distorted and flexible Ffh/FtsY NG-domain heterodimer. The EspP 'false' *early* targeting complex NG-domains are loosely associated and rearrange inefficiently into the *closed/activated* state leading to premature FtsY dissociation rather than successful completion of the targeting reaction.

SUPPLEMENTARY FIGURES

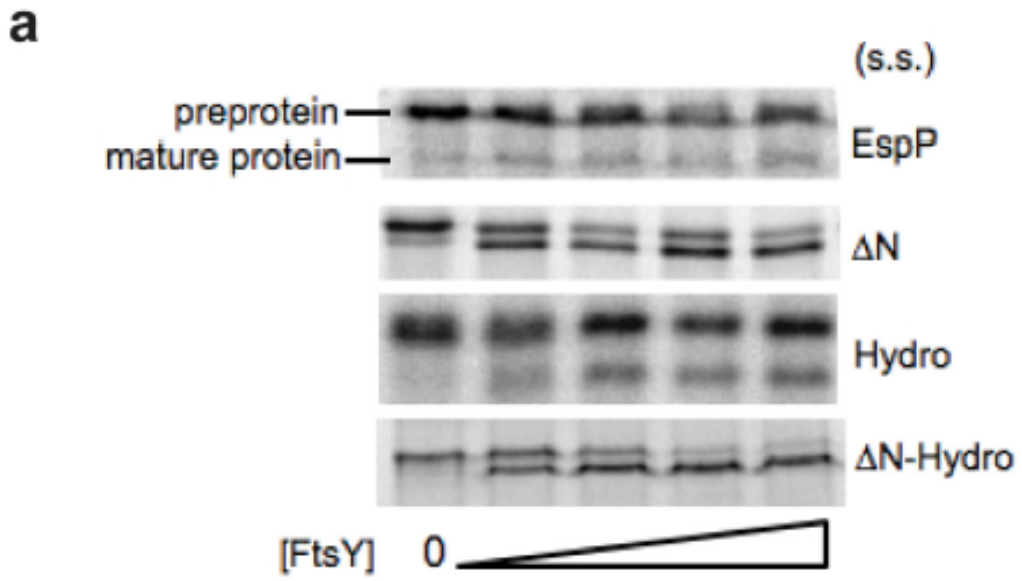

Supplementary Figure 1: In vitro translocation of EspP signal sequence variants and SRP binding to ribosomal complexes. (A) In vitro co-translational targeting and translocation through microsomal membranes. The EspP signal sequence variants were fused N-terminally to the signal peptidase cleavage site and to the mature region of pre-Prolactin. Translocation of the preprotein leads to cleavage of the signal sequence.

CHAPTER III

Molecular interplay with a co-translational chaperone improves the fidelity of SRP-dependent protein targeting

This chapter contains unpublished work done with Jae Ho Lee and Ishu Saraogi.

ABSTRACT

The ribosome exit site is a crowded environment where numerous protein biogenesis factors contact the nascent polypeptide to influence its folding, localization, and quality control. Timely and accurate partitioning of the nascent polypeptide into the proper biogenesis pathway is essential for accurate protein biogenesis. Here we probe, at energetic and molecular detail, how accurate sorting of the nascent protein occurs between the major co-translational chaperone trigger factor (TF) and Signal Recognition Particle (SRP) that mediates co-translational protein targeting to membranes. We show that TF regulates SRP function at three distinct stages, including cargo binding, recruitment to the SRP receptor, and rejection of nascent polypeptides beyond a critical length. Collectively, these regulations enhance the fidelity of SRP in substrate selection. Our results reveal the rich mechanisms of molecular interplay at the ribosome exit site, and provide a conceptual framework to understand how nascent proteins are sorted among the myriad of biogenesis machineries in this crowded environment.

INTRODUCTION

Proper biogenesis of newly synthesized proteins is a pre-requisite for the maintenance of a functional proteome. Accumulating data indicate that this process begins at the ribosome exit site, wherein no less than eleven protein biogenesis machineries interact and can gain access to the nascent polypeptide. This includes chaperones (Fedyukina and Cavagnero, 2011) such as trigger factor (TF) (Lill et al., 1988), Hsp70 and the nascent-polypeptide-associated-complex (del Alamo et al., 2011; Powers and Walter, 1996); modification enzymes (Kramer et al., 2009) such as N-acetyl transferase, methionine aminopeptidase and arginyl transferase; targeting and translocation machineries such as signal recognition particle (SRP), the SecYEG (or Sec61p) translocase, and even possibly SecA (Huber et al., 2011), and the ribosome-bound quality control complex (Gautschi et al., 2001). Engagement of these factors with the nascent polypeptide chain influences its folding, assembly, localization, processing, and quality control. Within seconds to minutes after the nascent polypeptide emerges from the ribosomal exit tunnel, it must engage the correct set of factors and thus commit to the proper biogenesis pathway. How this is accomplished in the crowded environment at the ribosome exit site is an emerging question at the heart of accurate protein biogenesis. In this work, we address these questions by deciphering how nascent proteins are sorted between two major biogenesis machineries in bacteria, SRP and TF.

SRP is a universally conserved machinery responsible for the co-translational targeting of proteins to their proper membrane destinations (Akopian et al., 2013). SRP recognizes ribosome-nascent chain complexes (termed RNC or cargo) carrying strong signal sequences and delivers them to translocation machineries on the target membrane.

SRP binds RNC via two interactions: a helical N-domain in the SRP54 protein (called Ffh in bacteria) binds the ribosomal protein L23, and a methionine-rich M-domain binds hydrophobic signal sequences on nascent membrane and secretory proteins as they emerge from the translating ribosome. Both Ffh and the SRP receptor (called FtsY in bacteria) also contain a conserved NG-domain, comprised of a GTPase G-domain and the N-domain, whose direct interaction mediates the delivery of cargo to the target membrane.

Delivery of cargo to the membrane is mediated by the assembly of the SRP and FtsY GTPases. Kinetic and biophysical analyses (Zhang et al., 2008; 2009) showed that this is a two-step process in which Ffh and FtsY first associate via their N-domains to form a transient *early* intermediate, which can form with or without GTP (Zhang et al., 2008; 2011). GTP-dependent rearrangements then bring the G-domains of both proteins into close contact, giving a stable *closed* complex (Egea et al., 2004; Focia et al., 2004). Rearrangement to the *closed* complex also exposes a membrane binding helix of FtsY and allows it to associate more strongly with the target membrane. Importantly, these rearrangements during SRP-FtsY assembly contribute extensively to the accuracy of substrate selection by SRP. Previous work showed that the initial recognition of RNC by SRP is insufficient to reject incorrect cargos bearing weak signal sequences. Instead, a correct cargo strongly stabilizes the otherwise labile *early* intermediate and thus accelerates formation of the SRP•FtsY *closed* complex over 10^3-fold, whereas an incorrect cargo cannot. This enables rapid delivery of the correct cargos to the target membrane, and provides kinetic discrimination against the incorrect cargos.

TF is a major and highly abundant co-translational chaperone in bacteria with an estimated cellular concentration of 50 –80 μM (Lill et al., 1988). Due to their binding affinity of ~1 μM, virtually every ribosome in the cell is bound to TF (Maier et al., 2003). Like SRP, TF contacts the ribosome via the L23 protein (Ferbitz et al., 2004; Kramer et al., 2002) at the nascent polypeptide exit site. This is carried out through a conserved ribosome-binding loop in its N-terminal domain. Also analogous to SRP, the interaction of TF with RNCs is strongly enhanced by hydrophobic sequences on the emerging nascent polypeptide (Lakshmipathy et al., 2007; Merz et al., 2008; Rutkowska et al., 2008). TF's interface with these nascent chains is facilitated by a large inner surface that hovers over the ribosome exit site (Ferbitz et al., 2004; Lakshmipathy et al., 2007; Merz et al., 2008). This cradle-like feature is formed by its N-terminal and C-terminal domains and is primarily hydrophobic, marked by a few polar and charged residues. Despite these similarities with SRP, TF has a distinct set of substrate proteins: it is reported to facilitate the productive folding of cytosolic proteins (Deuerling et al., 1999; Lakshmipathy et al., 2007; Merz et al., 2008) and to interact with secretory proteins that enter the post-translational Sec pathway (Beck et al., 2000; Eisner et al., 2006; Lee and Bernstein, 2002).

SRP and TF represent two distinct biogenesis pathways that a nascent protein must commit to. This raises intriguing questions: How do these two factors, which have overlapping substrate preferences, compete, collaborate, or otherwise interplay with one another at the ribosome exit site? How are nascent proteins sorted between them and committed to the correct biogenesis pathway in a timely and accurate manner? Extensive past work done to address this question has led to different (and sometimes contradictory)

models, including: (i) TF and SRP compete for binding RNC (Eisner et al., 2006; Ullers et al., 2006; 2003); (ii) TF and SRP can co-bind the RNC (Buskiewicz et al., 2004; Raine et al., 2004); (iii) the SRP receptor FtsY helps reject TF from SRP-bound ribosomes (Buskiewicz et al., 2004); and (iv) they have different preferences for nascent chain length, with SRP preferentially binding short nascent chains and TF preferentially occupying longer nascent chains (Oh et al., 2011; Rutkowska et al., 2008; Siegel and Walter, 1988). However, some of these observations could be the outcome of the molecular sorting process between TF and SRP, rather than the mechanism that give rise to them. More importantly, most of these studies have focused on the initial binding of SRP or TF to the nascent polypeptide, which, as exemplified by the studies on SRP, may not represent the commitment step at which nascent proteins are selected into their respective biogenesis pathways.

In this work, we used high-resolution biochemical and biophysical analyses to investigate, at energetic and molecular level of detail, the molecular interplay between TF and SRP at the ribosome exit site and the regulation of the SRP pathway through this interplay. We show that TF regulates the function of SRP via three distinct mechanisms, which together enhance the ability of the SRP pathway to reject borderline substrates that belong to the Sec pathway. Our results establish a comprehensive and cohesive model that explains previous observations, delineates the rich interplay between protein biogenesis factors at the ribosome exit site, and provides a conceptual foundation to understand how timely and accurate selection of substrates are achieved in this crowded environment.

RESULTS

Anti-cooperative binding of SRP and TF to ribosome•nascent chain complexes.

To understand the molecular interplay between TF and SRP, we first asked how TF affects cargo recognition by the SRP as the nascent polypeptide begins to emerge from the ribosome exit tunnel. To this end, we used amber suppression technology to incorporate a fluorescent non-natural amino acid, 7-hydroxycoumaryl ethylglycine (Cm), into the nascent polypeptide two residues downstream of the signal sequence (Figure 1A) (Saraogi et al., 2011). When paired with SRP labeled with BODIPY-FL at residue 421 in the Ffh M-domain, efficient Förster resonance energy transfer (FRET) was observed (Saraogi et al., 2011), providing a highly specific and sensitive assay to report on the interaction of SRP with the nascent polypeptide on RNC. To test whether TF helps enhance the specificity of SRP, we used a range of substrates with varying dependences on SRP (Figure 1B). FtsQ, a bona-fide SRP substrate, uses an integral transmembrane domain as the signal sequence. 3A7L contains an engineered signal sequence, which is significantly less hydrophobic than FtsQ and just sufficient to mediate SRP-dependent targeting (Zhang et al., 2010). As incorrect cargos, we used EspP and phoA, which are preferentially targeted by the post-translational Sec pathway (Peterson et al., 2006). For all the experiments in Figures 1-5, we purified homogeneous stalled RNCs with 80-85 amino acids between the start of signal sequence and the peptidyl transferase center of the ribosome. This mimics the stage at which the signal sequence emerges from the ribosome exit tunnel and is optimal for recognition by SRP (Siegel and Walter, 1988; Walter and Blobel, 1981b).

There has been extensive debate on whether TF and SRP compete with one another for binding RNCs (Figure S1A), or whether they can co-bind the same RNC (Figure S1B) (Buskiewicz et al., 2004; Eisner et al., 2006; Raine et al., 2004; Ullers et al., 2003; 2006).Well-established theoretical treatments and kinetic simulations show that these alternative models can be distinguished by quantitatively analyzing the effect of TF on SRP-RNC binding using our conformation-sensitive FRET assay. If binding of TF and SRP to RNCs is mutually exclusive, then TF will deplete the free RNCs available to bind the SRP, necessitating higher SRP concentrations for reaching saturation (Figure S1A). However, when SRP is allowed to bind RNC at saturating concentrations, TF would not be able to affect the conformation, and hence the FRET value of the RNC•SRP complex (Figure S1A). In contrast, if TF altered the FRET value of the RNC•SRP complex, this could only be explained by a model in which TF and SRP co-bind the same RNC and 'nudge' each other at the ribosome exit site (Figure S1B). This could either strengthen (cooperative) or weaken (anti-cooperative) SRP binding at the RNC; the latter model is depicted in Figure S1B.

To test and distinguish between these models, we carried out equilibrium titrations to determine how TF affects RNC-SRP binding. With all four substrates, increasing amounts of TF induces two significant changes: (i) increasingly higher SRP concentrations are required to reach saturation; and (ii) successive reductions in the FRET end point when the RNC•SRP complex is formed at saturating concentrations (Figures 1C, D and S1C, D). These results provide strong evidence for anti-cooperative binding between TF and SRP to the RNC, but are incompatible with models in which their binding to RNC are mutually exclusive (cf. Figure S1A). In addition, the effect of

TF on the observed RNC-SRP binding affinity (app K_d^{SRP}) is saturable (Figure S1E). This is also consistent with predictions from a model in which TF and SRP co-bind the RNC to form a ternary complex, but is incompatible with models in which their binding is mutually exclusive (Figure S1F).

If TF weakens the affinity of RNC for SRP, then reciprocally, SRP would weaken the affinity of TF for the RNC. To test this prediction, we developed a FRET assay to measure RNC-TF interaction. We labeled TF with BODIPY-FL at an engineered cysteine (C377) which, when paired with Cm-labeled RNC, induced efficient FRET (Figures 2A & B). Equilibrium titrations using this FRET assay showed that TF binds tightly to all the RNCs tested, with K_d^{TF} values ranging from 2.5 – 8.4 nM (Figures 2C, D and S2A, B, blue lines; Figure 2E, grey bars). SRP induces two changes to RNC-TF binding: (i) a modest weakening of the binding affinity between TF and RNC; and (ii) a reduced FRET end point at saturating TF concentrations when the RNC•TF complex is formed (Figures. 2C, D and S2A, B). This provides corroborative evidence for anti-cooperative binding between SRP and TF at the RNC (Figure S1B).

The extent to which TF and SRP weaken the affinity of one another for RNC shows a modest correlation with the strength of the signal sequence: 15–25 fold for RNC_{FtsQ} and RNC_{3A7L}, SRP substrates that contain more hydrophobic signal anchor or signal sequences, and 4–10 fold for RNC_{EspP} and RNC_{phoA}, Sec substrates whose signal sequences are less hydrophobic (Figures 1E, 2E, S1E and S2C). As the cellular TF concentration (>50 μM), which is over 10,000-fold higher than the weakest RNC-TF affinity observed here, the effect from SRP has negligible consequences on the occupancy of TF on the RNCs. On the other hand, SRP is far less abundant, ~400 nM

(Figure 1E, dashed red line). In the presence of TF, the K_d values for SRP binding to RNC_{EspP} and RNC_{phoA} begin to approach the cellular SRP concentration. Thus, TF could influence SRP occupancy on these RNCs (see more discussion below).

Collectively, the results in this section show that TF and SRP can bind to the same RNC, on which they alter the binding energetics and conformation of one another. This mode of interplay has negligible consequences for the occupancy of TF on the RNCs, but allows TF to preferentially lower the occupancy of SRP on RNCs bearing the Sec substrates. Nevertheless, all the RNC-SRP dissociation constants are still below the cellular SRP concentration in the presence of TF (Figure 2E). Thus at cellular concentrations, significant amounts of RNC•SRP•TF ternary complexes accumulate for both the SRP and Sec pathway substrates.

TF slows the recruitment of SRP receptor to incorrect cargos.

In the next step of the SRP pathway, efficient recruitment of the SRP receptor FtsY to RNC•SRP complexes is essential for the rapid delivery of cargo to the target membrane. Kinetic regulation of this process plays a key role in the ability of the SRP pathway to discriminate against incorrect substrates (Zhang et al., 2010). We asked whether TF increases substrate discrimination by the SRP during this process.

Previous work showed that stable SRP-FtsY assembly is a two-step process in which a transient *early* intermediate is initially formed followed by a GTP-dependent rearrangement to form a stable, *closed* complex. The stability of the *early* intermediate directly correlates with the rate at which the *closed* complex is formed, and represents a

major commitment step for the correct cargos (Zhang et al., 2009; 2010). We therefore tested how TF affects formation of the *early* targeting complex.

To this end, we assembled ternary RNC•SRP•TF complexes using saturating concentrations of the respective RNC and TF, as established by the results in Figures 1 and 2. As the *early* intermediate can form with or without GTP but its subsequent rearrangement is strictly GTP-dependent, we isolated the *early* intermediate by leaving out GTP analogs during complex assembly with FtsY (Zhang et al., 2008; 2009). Formation of the SRP•FtsY complex was monitored using FRET between DACM-labeled at SRP C153 and BODIPY-labeled at FtsY C345 (Figure 3A) (Zhang et al., 2008; 2009). Equilibrium titrations using this assay showed that, with a bona-fide SRP substrate such as RNC_{FtsQ}, a highly stabilized SRP•FtsY *early* complex is formed, and TF has negligible effects on its stability or FRET efficiency (Figure 3B). As the signal sequence becomes weaker, the RNC•SRP•FtsY *early* complex becomes less stable, as reported previously (Zhang et al., 2010). Importantly, TF further weakens the *early* complex, and this effect is more substantial as the signal sequence becomes weaker (Figures 3C-3E; summarized in Figure 3F). Furthermore, TF lowers the FRET endpoint when the *early* targeting complex is formed at saturating FtsY concentrations, and this effect also becomes more significant as the signal sequence becomes weaker (Figures 3B-3E). This indicates that TF alters the conformation of SRP•FtsY *early* complexes formed with weaker SRP substrates, such that the G-domains of SRP and FtsY (where the FRET probes are located) are positioned further apart.

If TF induces the formation of a weaker and distorted *early* targeting complex for RNCs bearing weaker signal sequences, then the rate of assembling the stable *closed*

SRP•FtsY complex for these substrates will be significantly slowed by TF. To test this hypothesis, we compared the kinetics of SRP-FtsY *closed* complex assembly between pre-formed RNC•SRP and RNC•SRP•TF complexes. Complex assembly was measured using the same FRET assay but in the presence of GMPPNP, which allows the *early* intermediate to proceed to the *closed* complex (Figure 4A). With strong SRP substrates such as FtsQ, complex formation is rapid and unaffected by TF (Figures 4B, F). With a weaker substrate, 3A7L, TF slows SRP-SR *closed* complex assembly 3-fold (Figures 4C, F). With Sec-substrates such as EspP and phoA, TF slows down *closed* complex assembly more substantially, 10-12 fold (Figures 4D-4F). Together these results show that, although SRP can strongly discriminate between correct and incorrect cargos via the kinetics of FtsY recruitment, TF enhances this discrimination by an additional order of magnitude (Figure 4F).

TF more effectively displaces SRP from the RNC as the nascent chain elongates

It has been a long-standing observation that, as the nascent polypeptide elongates beyond a critical length of ~130 amino acids, SRP loses its ability to target the RNCs (Siegel and Walter, 1988). This imposes a limited time window for the SRP and FtsY to complete the targeting reaction, especially in bacteria where translation elongation occurs rapidly and SRP does not pause translation. However, the molecular basis underlying this phenomenon has been unclear and controversial. To address this question, we prepared RNCs bearing longer nascent chains, with 130-135 amino acids from the N-terminus of the signal sequence to the peptidyl transferase center. Using the FRET assays described above, we tested whether and how a longer nascent chain length affects cargo recognition

by the SRP (K_d^{SRP}) and the assembly of a *closed* RNC•SRP•SR complex (k_{on}; Figure 5A). Intriguingly, for all the substrates tested, a longer nascent chain length exerted only modest effects: it weakens RNC-SRP binding affinity by ≤4-fold, and slows SRP-FtsY closed complex assembly by 2–3 fold (Table 1). These effects are statistically significant, but insufficient to account for the rejection of RNCs from the SRP pathway once the nascent chain exceeds the critical length.

We asked whether TF could contribute to this rejection. We first tested how TF affects the binding of SRP to RNCs. Analogous to observations with shorter nascent chains, we observed anti-cooperative binding between TF and SRP to RNCs with a nascent chain length of 130-135 amino acids (Figures 5B and E). Significantly, TF exerts a much larger weakening effect on the binding of SRP to RNCs with longer nascent chains than those with shorter chain lengths (Figures 5C and F): the affinity of SRP for RNC_{FtsQ} is weakened to ≥ 31 nM and that for RNC_{3A7L}, to ≥ 210 nM. As the signal sequence becomes weaker, a much lower concentration of TF was needed to antagonize SRP binding to RNCs with long nascent chains (Figures 5F).

We next tested whether TF also more effectively prevents the targeting of long chain-RNCs to the membrane through SRP-FtsY assembly. With RNC_{FtsQ}, which contains a strongly hydrophobic transmembrane domain, SRP-FtsY *closed* complex assembly remains rapid at the longer chain length and is not significantly affected by TF (Figure 5D). With RNC_{3A7L}, which contains a weaker signal sequence comparable to those in SRP-dependent secretory proteins, TF further slows the assembly of the targeting complex by six-fold (Figure 5G).

Collectively, the results in this section show that at longer nascent chain lengths, TF becomes more effective in inhibiting SRP functions in both binding the RNC and recruitment of SRP receptor. Together, these allosteric inhibitions from TF could contribute significantly to the rejection of RNC from the SRP pathway once the nascent chain reaches a critical length.

TF enhances the specificity of SRP-dependent protein targeting

The results from the biophysical measurements above strongly suggest that TF will enhance the discrimination of SRP against borderline substrates with sub-optimal signal sequences, such as EspP and phoA. To test this hypothesis, we determined the effect of TF on the targeting efficiency of proteins with the different signal sequences. We used a well-established heterologous assay in which an established SRP substrate, preprolactin (pPL), or various signal sequences fused to prolactin (PL) are translated in a wheat germ extract devoid of endogenous SRP, SRP regulators and TF (Powers and Walter, 1997; Shan et al., 2007). The ability of *E. coli* SRP and FtsY to mediate the co-translational targeting of pPL or pPL variants to microsomal membranes is tested using cleavage of signal sequence as a readout for successful targeting and translocation (Figure 6). The bacterial SRP and FtsY mediate pPL targeting as efficiently as their mammalian homologues despite the heterologous nature of this assay (Powers and Walter, 1997); this highlights the remarkable conservation of the SRP pathway and allows us to test insights from biophysical studies of bacterial SRP and FtsY in a complete and functional targeting reaction.

In agreement with previous observations, pPL and 3A7L-pPL are efficiently targeted and translocated in this assay (Figures 6A and 6B), whereas the borderline substrates such as EspP and phoA retained ~20-25% targeting (Figure 6C and D). Importantly, the presence of TF substantially inhibited the targeting of EspP and phoA, reducing their targeting levels to ~5-10%, whereas TF has negligible effects on the targeting and translocation of pPL and 3A7L-PL (Figure 6A and B). This provides direct evidence that the complex interplay between SRP and TF contribute to enhancing the specificity of co-translational protein targeting.

DISCUSSION

The ribosome is replete with numerous protein biogenesis factors at its exit site. These include a wide array of chaperones, post-translational modification enzymes and targeting machineries. The proper timing and accurate decision-making by RNCs are required to ensure that it enters the correct biogenesis pathway. However, many questions remain, as the molecular mechanisms by which such decisions are carried out have been unclear. In this work we endeavored to gain insight into this problem and explored the molecular interplay between the SRP and TF. Using quantitative fluorescence assays, results reveal an elegant multitude of mechanisms by which TF and SRP influence one another. This interplay allows the SRP to be more discriminatory against 'incorrect cargo' and thus, overall, enhances the selectivity of this co-translational targeting pathway.

TF regulates SRP at three distinct stages (Figure 7). First, TF can reduce the occupancy of SRP on RNCs (Figure 7, Step 1). A mathematical calculation based on the RNC-SRP affinities determined here and a cellular SRP concentration of 400 nM shows that, without TF present, there is <5% difference in the fraction of RNC bound by SRP between strong (FtsQ and 3A7L) and weak (phoA) signal sequences (Figure S3A, light grey bars; see also Zhang et al, Science 2010). In contrast, TF reduces the occupancy of SRP on RNC_{ftsQ}, RNC_{3A7L}, RNC_{EspP} to ~90%, but those RNC_{phoA} to 75% (Figure S3B, light grey bars). This is because the cellular SRP concentration far exceeds the intrinsic value of K_d^{SRP} for all the RNCs but in the presence of TF, the RNC-SRP binding affinity (Figure S1B, $K_{d,2}^{SRP}$) begins to approach the cellular SRP concentration for the Sec- but not SRP-dependent substrates.

Second, TF enhances the selectivity of SRP for RNCs by antagonizing SRP's interaction with its receptor, FtsY, during the targeting reaction specifically for non-SRP substrates (Figure 7, Step 2). Once SRP successfully engages the RNC, it must efficiently assemble with its receptor, FtsY, in order to deliver the cargo to the target membrane in a prompt manner. This step represents a crucial checkpoint in this targeting scheme; only 'correct cargo' can kinetically stabilize the SRP-FtsY association reaction (Zhang, et al., 2008). For example, the assembly rate of these two GTPases is 120-, 300- and 2000-fold faster in the presence of RNC_{FtsQ} than RNC_{3A7L}, RNC_{phoA} and RNC_{EspP}, respectively (Figure 4, Zhang et al., 2010). Using these observed rate constants, mathematical modeling shows that >99% of RNC_{FtsQ} and RNC_{3A7L} are retained (Figure S3A). However, ~96% and 59% of RNC_{phoA} and RNC_{EspP} still remain in the SRP pathway, despite being categorized as non-SRP substrates (Figure S3A, dark grey bars). Intriguingly, the presence of TF allows SRP to be more discriminatory at this stage of protein targeting. TF effectively reduced the complex assembly rates of SRP and FtsY when SRP is bound to RNCs bearing weaker signal sequences (RNC_{phoA} and RNC_{EspP}) but not for RNCs bearing strong signal sequences (RNC_{FtsQ} and RNC_{3A7L}; Figure 4F). Considering these observed rate constants obtained in the presence of TF, the amount of RNC_{phoA} and RNC_{EspP} that remains in the SRP pathway have been significantly lowered to 42% and 9.2%, respectively (Figure S3B, dark grey bars) and begins to approach the amounts we observe *in vitro* (Figure 6).

In the third regulatory event, TF further helps SRP reject the wrong substrates when the nascent chain is elongated beyond a critical length (Figure 7, Step 3). Evidence from this work shows that TF imposes this 'timer' in two ways. First, TF further reduces

the occupancy of SRP on RNCs with longer nascent chains (Figure 5C, F), thus allowing incorrect cargo to be rejected at an earlier targeting stage. Second, TF has a stronger decelerating effect on the SRP•FtsY *closed* complex assembly rates for RNCs bearing weak signal sequences and not for RNCs with a strong signal sequence (Figure 5D, G).

It has been shown previously that the mathematical simulations carried out in Figure S3A and B can be directly correlated with the overall targeting efficiencies of SRP for cargo with various signal sequences (Zhang, et al., 2010). Indeed, when the experimentally determined targeting efficiencies (Figure 6) were compared to the predictions based on our kinetic and thermodynamic measurements, there was a very high correlation, with and without TF (Figure S3C, D). This suggests that our model (Figure 7) is indeed a faithful recapitulation of how substrate selection by the SRP is enhanced by the presence of TF. Thus, the results herein establish a comprehensive and cohesive model that explains previous observations, delineates the rich interplay between protein biogenesis factors at the ribosome exit site, and provides a conceptual foundation to understand how timely and accurate selection of substrates are achieved in this crowded environment.

Table 1. Summary of the effect of nascent chain length on SRP-RNC binding affinities and SRP-FtsY closed complex assembly rates.

RNC	K_d^{SRP} (nM)		k_{on}^{FtsY} (10^6 $M^{-1}s^{-1}$)	
	80mer	130mer	80mer	130mer
FtsQ	1.1	3.3	18.5	13.5
3A7L	2.8	10.5	0.145	0.064
phoA	17.2	12.7	0.0635	N.D.

FIGURES

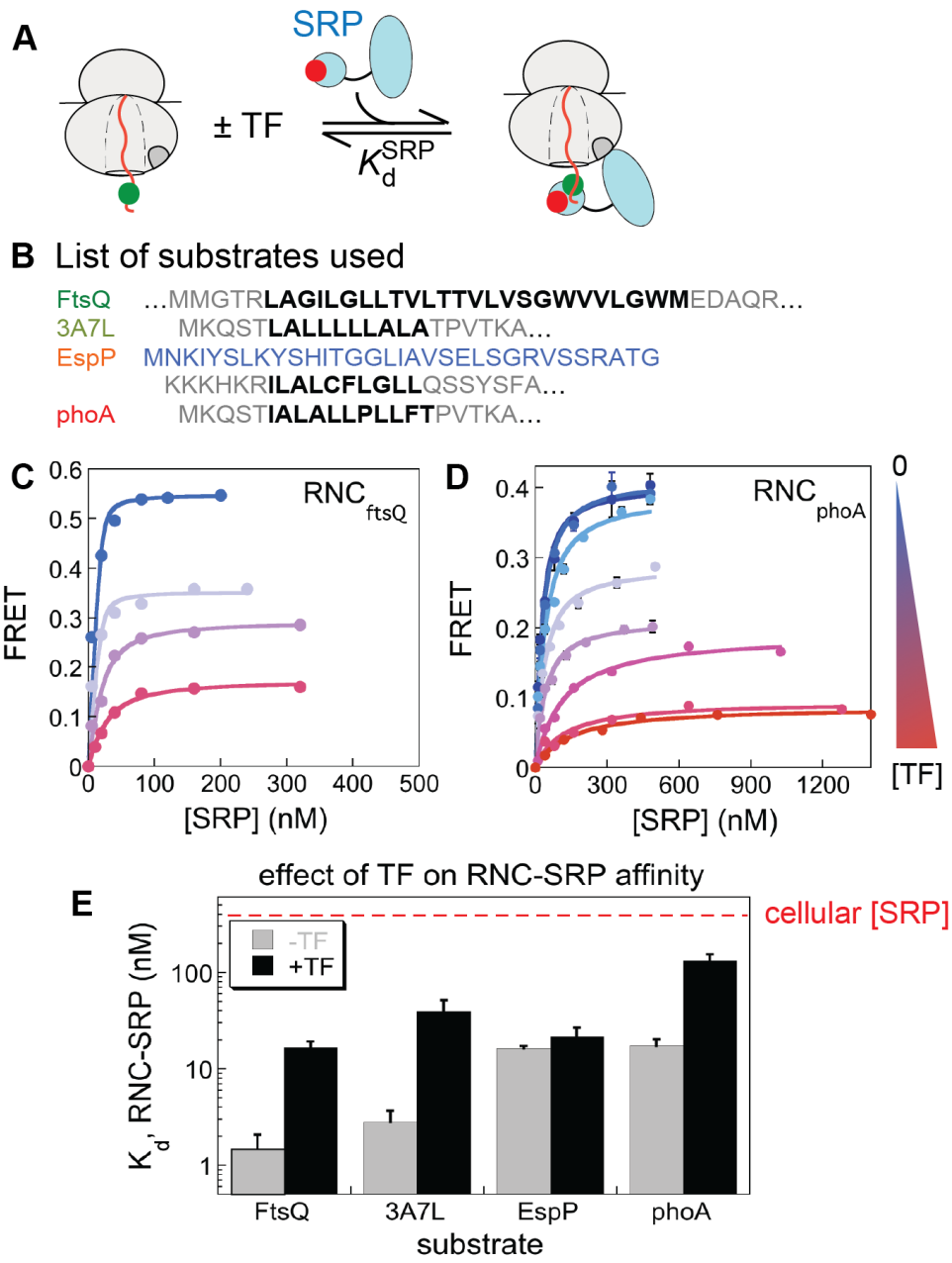

Figure 1. TF binds to SRP-occupied RNCs and weakens SRP binding. (A) Schematic depiction of the FRET assay to measure RNC-SRP binding. Green dot denotes Cm (donor), red dot denotes BODIPY-FL (acceptor). (B) N-terminal sequences of the different substrate used in this study. Bold highlights the hydrophobic core of the signal sequences. (C, D) Equilibrium titrations for RNC-SRP binding in the presence increasing

TF (indicated as increasing shades of red). The data were fit to Equation 2 and yields the following parameters. (C) Apparent K_d values for RNC_{FtsQ} binding of 1.1, 1.5, 9.2 and 16.6 nM, and FRET end points of 0.54, 0.35, 0.29 and 0.17, respectively, with 0, 1, 5 and 30 μM TF present. (D) Apparent K_d values for RNC_{phoA} binding of 17.2, 21.1, 30.3, 28.3, 31.5, 104.5, 106.3 and 131.9 nM and FRET end points of 0.40, 0.41, 0.39, 0.29, 0.21, 0.19, 0.09 and 0.08, respectively, with 0, 0.1, 0.2, 0.5, 1, 2, 5 and 10 μM TF present. (E) Summary of the effect of TF on apparent RNC-SRP binding affinity with the different substrates.

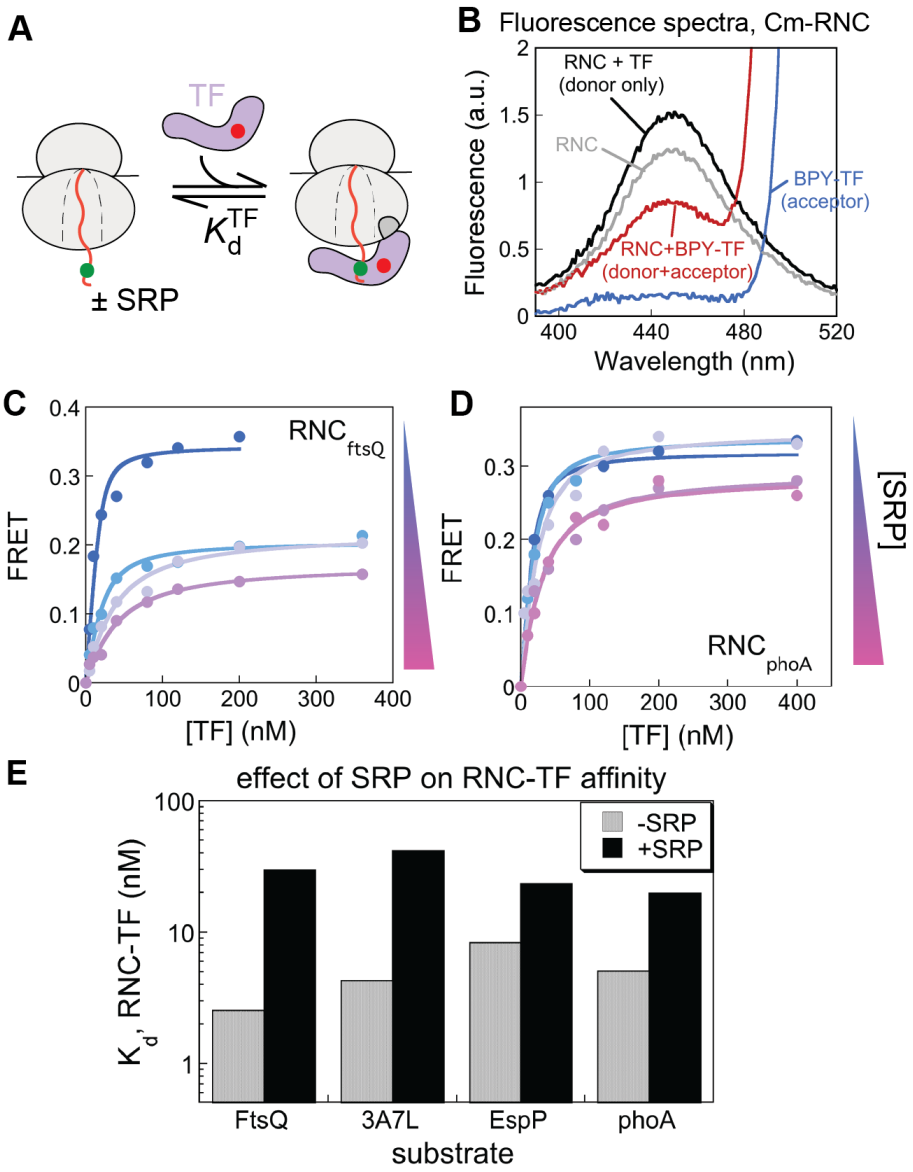

Figure 2. SRP binds TF-occupied RNCs and weakens the binding of TF. (A) Scheme depicting the FRET assay to measure TF binding to RNC. Green dot denotes Cm (donor), red dot denotes BODIPY (acceptor). (B) Fluorescence emission spectra for Cm-labeled RNC (grey), BODIPY-labeled TF (BDY-TF, blue), and Cm-RNC in the presence of unlabeled TF (black) or BDY-TF (red). (C-D) Equilibrium titrations for RNC-TF binding in the presence increasing SRP (indicated as increasing shades of red). The data were fit to Equation 2 and yields the following parameters. (C) Apparent K_d values for TF-

RNC_{FtsQ} binding of 2.6, 9.2, 26 and 30 nM, and FRET end points of 0.34, 0.21, 0.22 and 0.17, respectively, with 0, 100, 200 and 400 nM SRP present. (D) Apparent K_d values for RNC_{phoA} binding of 5.1, 7.6, 13.1, 20.9 and 19.5 nM, and FRET end points of 0.32, 0.33, 0.35, 0.29 and 0.29, respectively, with 0, 100, 200, 400 and 800 nM SRP present. (E) Summary of the effect of SRP on the apparent RNC-TF binding affinity for the different substrates.

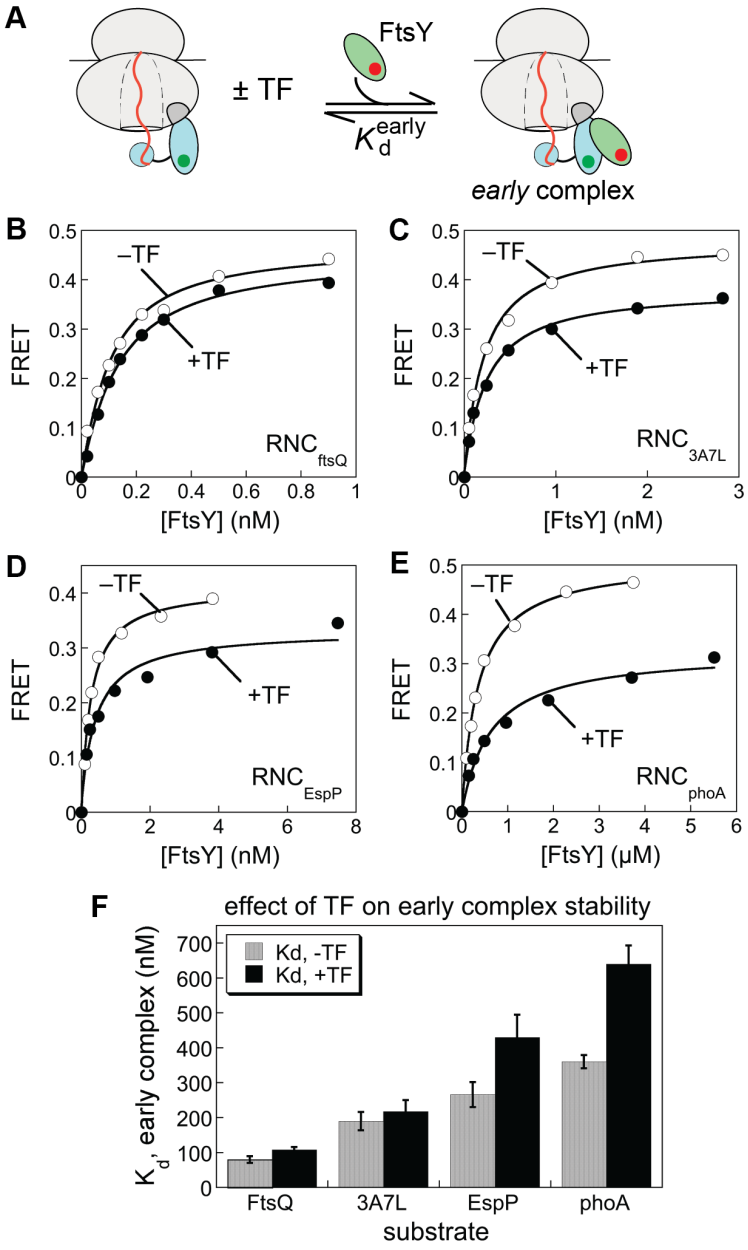

Figure 3. TF induces formation of a weaker and distorted RNC•SRP•FtsY *early* complex. (A) Scheme depicting the FRET assay for measuring the formation of the *early* complex. (B-E) Equilibrium titrations for formation of the *early* targeting complex without (open circles) or with (closed circles) 20 μM TF present for SRP loaded with 450 nM RNC_{FtsQ} (B), 400 nM RNC_{3A7L} (C), 600 nM RNC_{EspP} (D) and 1 μM RNC_{phoA} (E). The data were fit to Equation 3 and yielded the following parameters. Part B, K_d values of

80 and 108 nM and FRET ends points of 0.47 and 0.45, respectively, with and without TF. Part C, K_d values of 191 and 218 nM and FRET ends points of 0.47 and 0.37, respectively, with and without TF. Part D, K_d values of 266 and 428 nM and FRET ends points of 0.42 and 0.32, respectively, with and without TF. Part E, K_d values of 358 and 640 nM and FRET ends points of 0.51 and 0.33, respectively, with and without TF. (F) Summary of the effects of TF on the stability of the *early* complex formed with the different substrates.

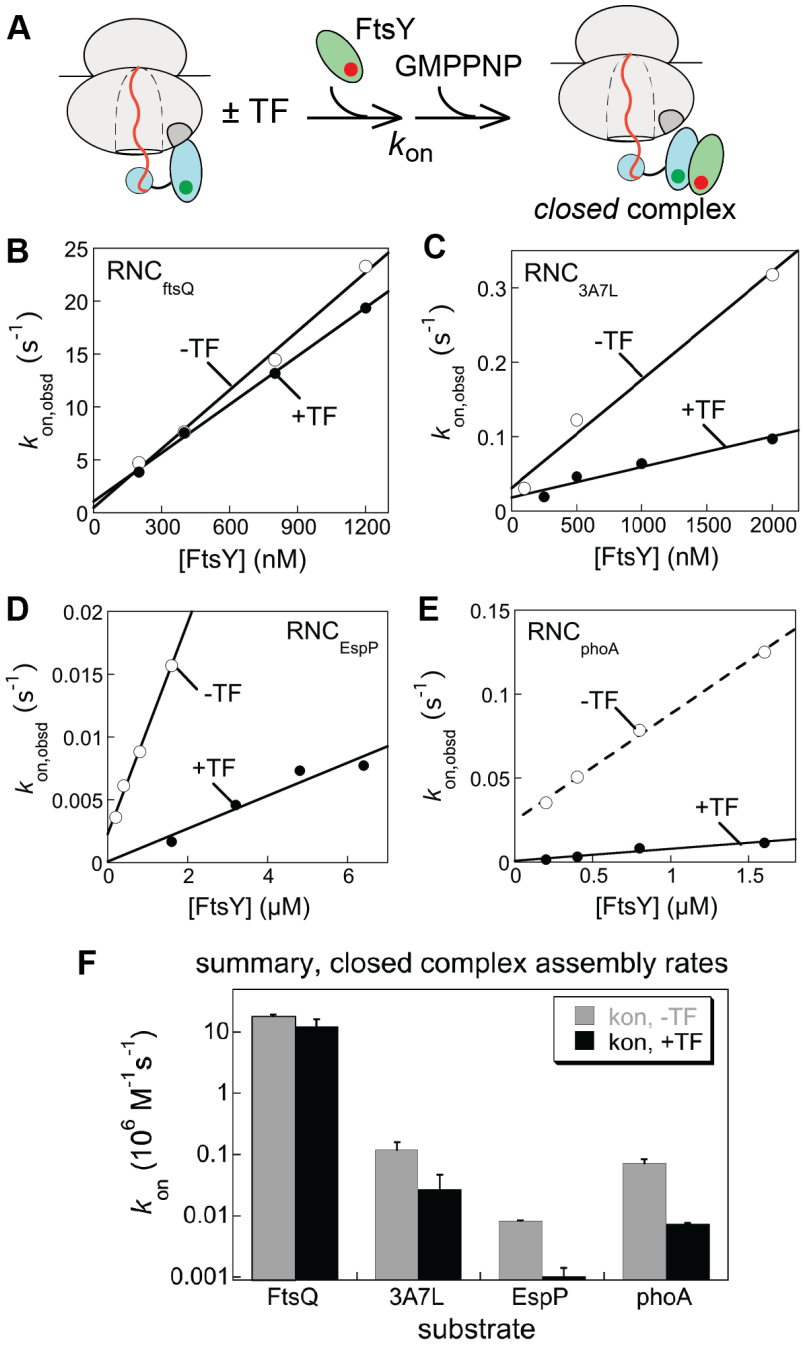

Figure 4. TF selectively slows SRP-FtsY *closed* complex assembly with the incorrect cargos. (A) Scheme for the FRET assay to measure the kinetics of SRP-FtsY *closed* complex assembly (k_{on}). (B-E) Association rate constants for SRP-FtsY *closed* complex assembly in the presence and absence of 20 μM TF, for SRP loaded with 800 nM RNC_{FtsQ} (B), 350 nM RNC_{3A7L} (C), 500 nM RNC_{EspP} (D) and 600 nM RNC_{phoA} (E). The

data were fit to Equation 4 and yields the following values of k_{on}: part B, 18.5×10^6 and 16.2×10^6 $M^{-1}s^{-1}$ with and without TF present, respectively; part C, 1.45×10^5 and 0.41×10^5 $M^{-1}s^{-1}$ with and without TF present, respectively; part D, 8.4×10^3 and 1.3×10^3 $M^{-1}s^{-1}$ with and without TF present, respectively; part E, 6.3×10^4 and 0.71×10^4 $M^{-1}s^{-1}$ with and without TF present, respectively. (F) Summary of the effect of TF on the rate of SRP-FtsY *closed* complex assembly with different substrates.

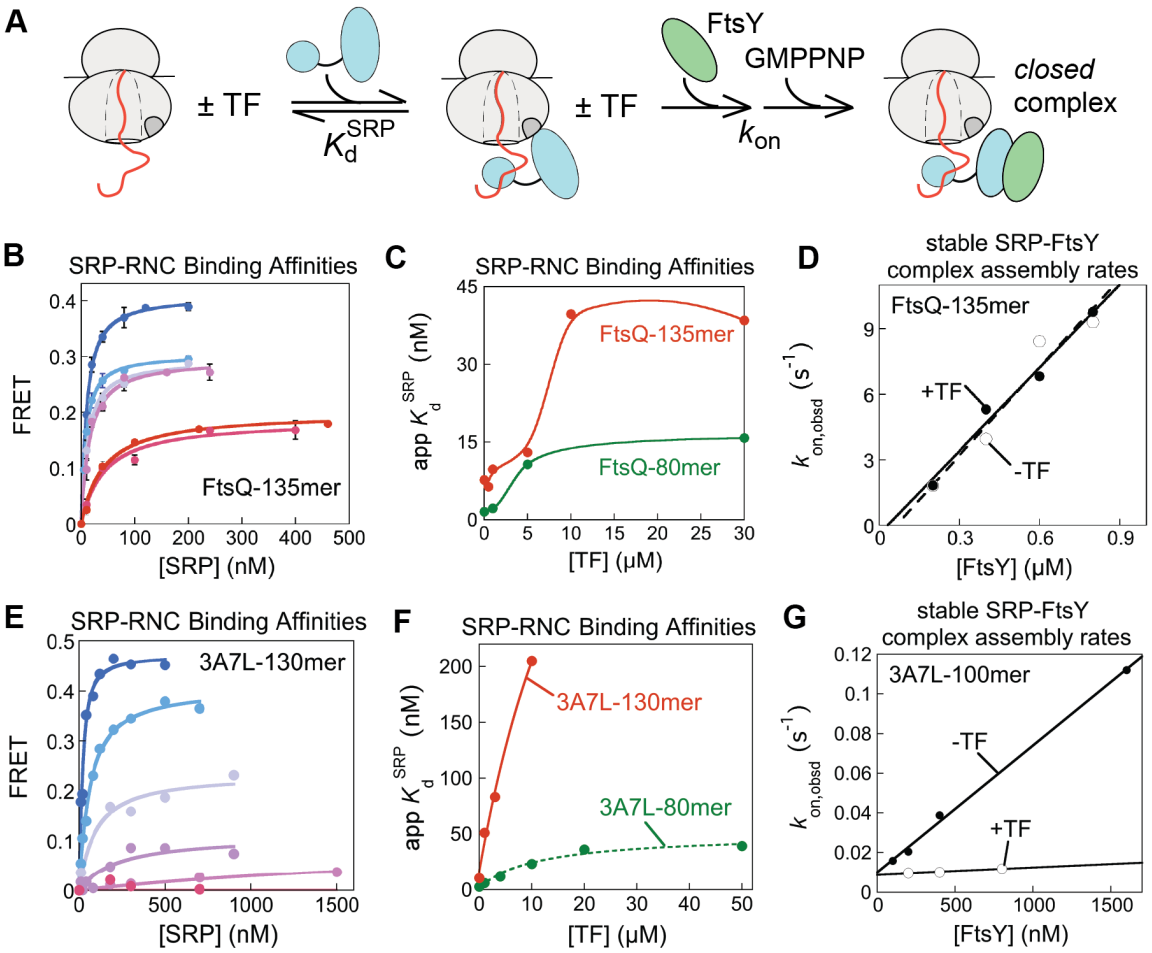

Figure 5. TF more effectively inhibits SRP at longer nascent chain length. (A) Scheme depicting the two steps examined in this figure, binding of SRP to RNC and assembly of the *closed* targeting complex. (B, D) Effect of TF on the apparent binding affinity of SRP to RNC_{ftsQ} (part B) or FtsQ3A7L (part D) when the nascent chain is 85 amino acids (green dashed lines) or 130-135 amino acids long (read lines). (C, E) Effect of TF on the assembly of *closed* targeting complex with RNC_{FtsQ} (part C) or RNC3A7L (part E) when the nascent protein is 130-135 residues long.

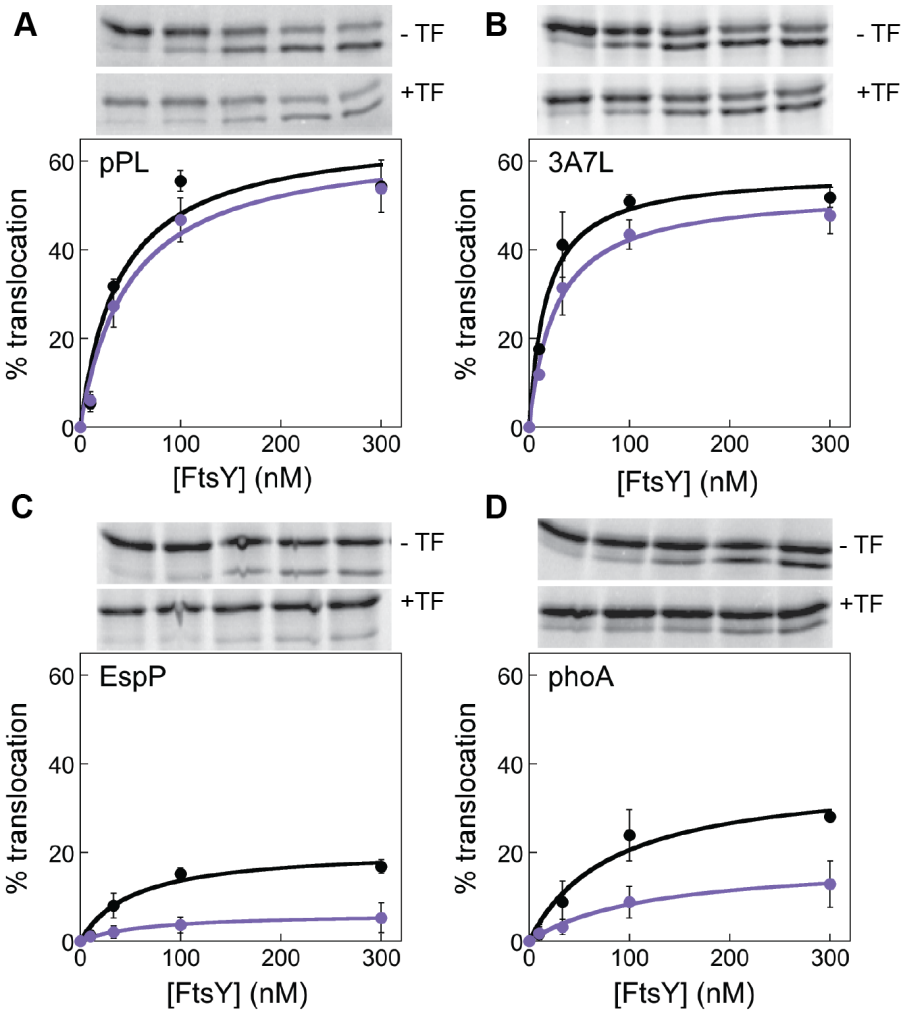

Figure 6. TF enhances specificity of SRP-dependent targeting to ER microsomal membranes. (A-D) Translocation of pPL (part A), 3A7L-PL (part B), EspP-PL (part C) and phoA-PL (part D) by SRP and SR in the absence (black) and presence of TF (purple). In each panel, a representative gel is shown on the top, with quantification of the gel on the bottom.

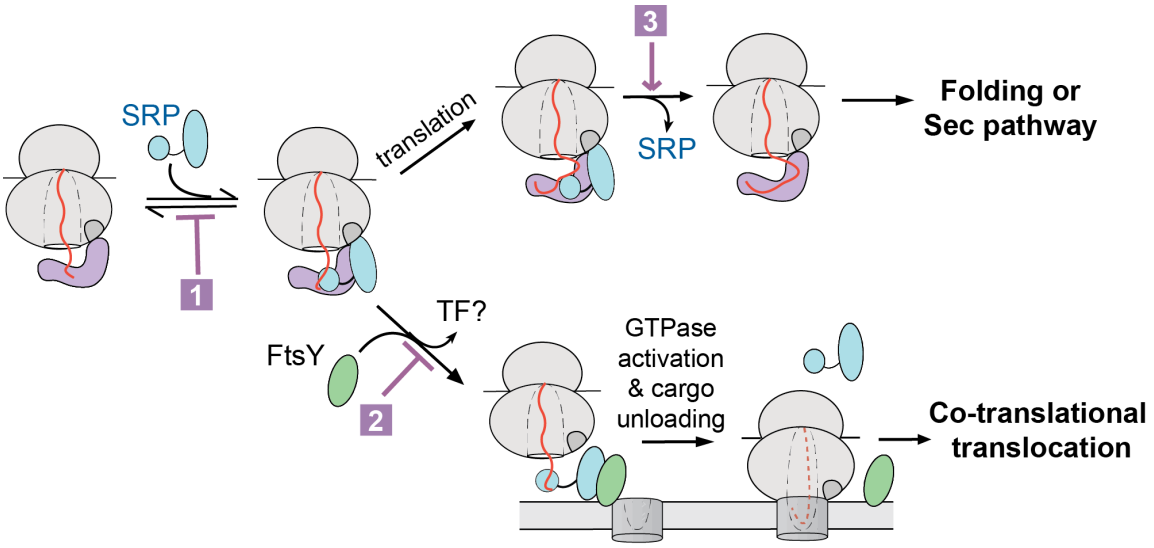

Figure 7. Model describing the molecular mechanism of substrate partitioning into the SRP or TF pathway. TF regulates SRP at three steps: (1) SRP binding to RNC; (2) targeting of RNC to the membrane via SRP-FtsY assembly; and (3) removal of SRP from ribosomes when the nascent polypeptide exceeds a critical length.

SUPPLEMENTARY FIGURES

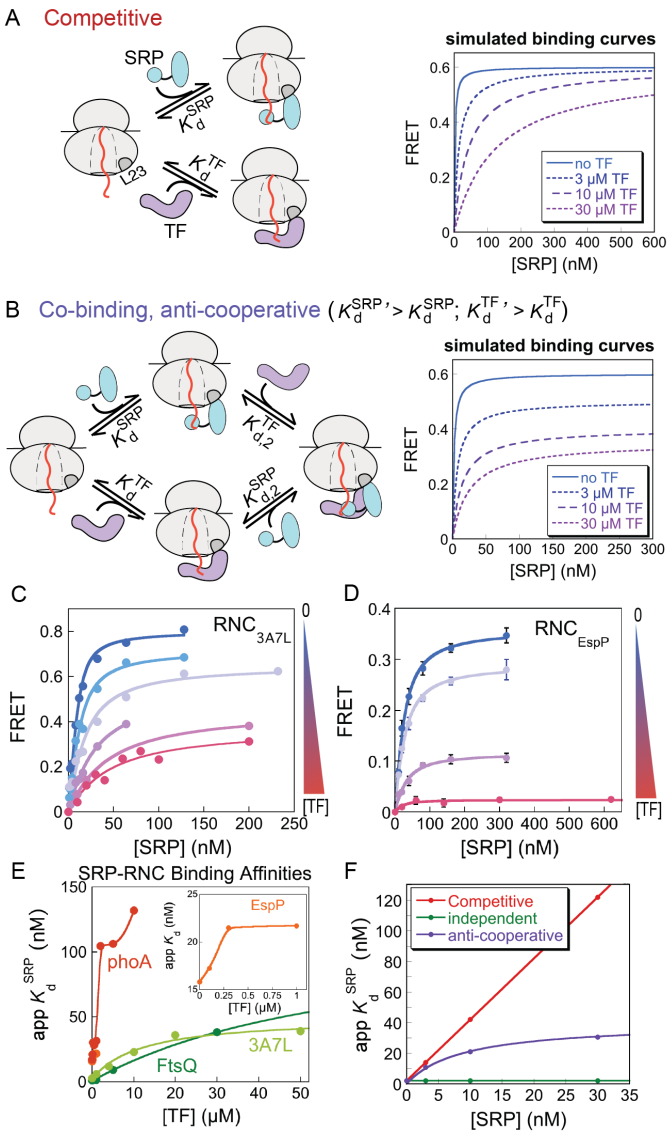

Figure S1. Experimental setup to distinguish different models of how TF affects SRP binding to RNC. (A-B) Depiction of models in which SRP and TF binding to RNC are strictly competitive (A) or anti-cooperative (B) with one another (left panels), and simulation of the effect of TF on RNC-SRP binding curves predicted by each model (right panels). Simulations used a K_d value for RNC-SRP binding of 2 nM, a K_d value for RNC-TF binding of 0.5 μM, and for model (B), a 20-fold weakening effect of TF on

SRP-RNC binding ($K_{d,2}^{SRP} = 20\ K_d^{SRP}$). (C-D) Equilibrium titrations for RNC-SRP binding in the presence increasing TF (indicated as increasing shades of red). The data were fit to Equation 2 and yields the following parameters. (C) Apparent K_d values for RNC_{3A7L} binding of 2.8, 6.0, 12.1, 23.4, 36.4 and 39.3 nM, and FRET end points of 0.80, 0.72, 0.65, 0.55, 0.45 and 0.37, respectively, with 0, 1, 4, 10, 20 and 50 µM TF present. (D) Apparent K_d values for RNC_{EspP} binding of 15.8, 17.2, 21.5, and 21.7, and FRET end points of 0.36, 0.29, 0.12 and 0.02 respectively, with 0, 0.1, 0.3 and 1 µM TF present. (E) Summary of the effect of TF on the apparent RNC-SRP binding affinity for the different substrates. (F) Simulated effect of TF on the apparent RNC-SRP binding affinity, as predicted by models in which SRP and TF binding are strictly competitive (red), anti-cooperative (purple), or independent (green) of one another. The data for the competitive and anti-cooperative models are from the simulation results in Figure S1A-B.

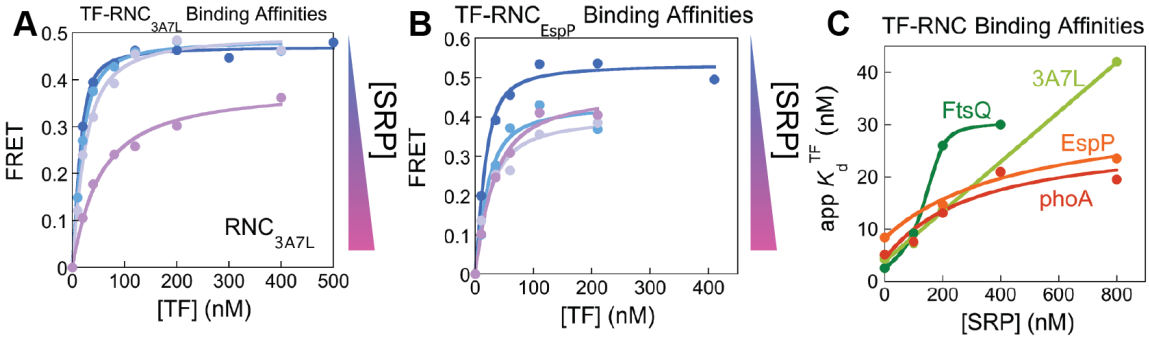

Figure S2. SRP weakens the binding of TF to different RNCs, related to Figure 2. (A) Apparent K_d values for RNC_{3A7L} binding of 4.3, 7.3, 13.6 and 42 nM, and FRET end points of 0.47, 0.49, 0.50 and 0.39, respectively, with 0, 100, 200 and 800 nM SRP present. (B) Apparent K_d values for RNC_{EspP} binding of 6.2, 10.5, 14.7 and 21 nM, and FRET end points of 0.54, 0.43, 0.40 and 0.47, respectively, with 0, 200, 400 and 800 nM SRP present.

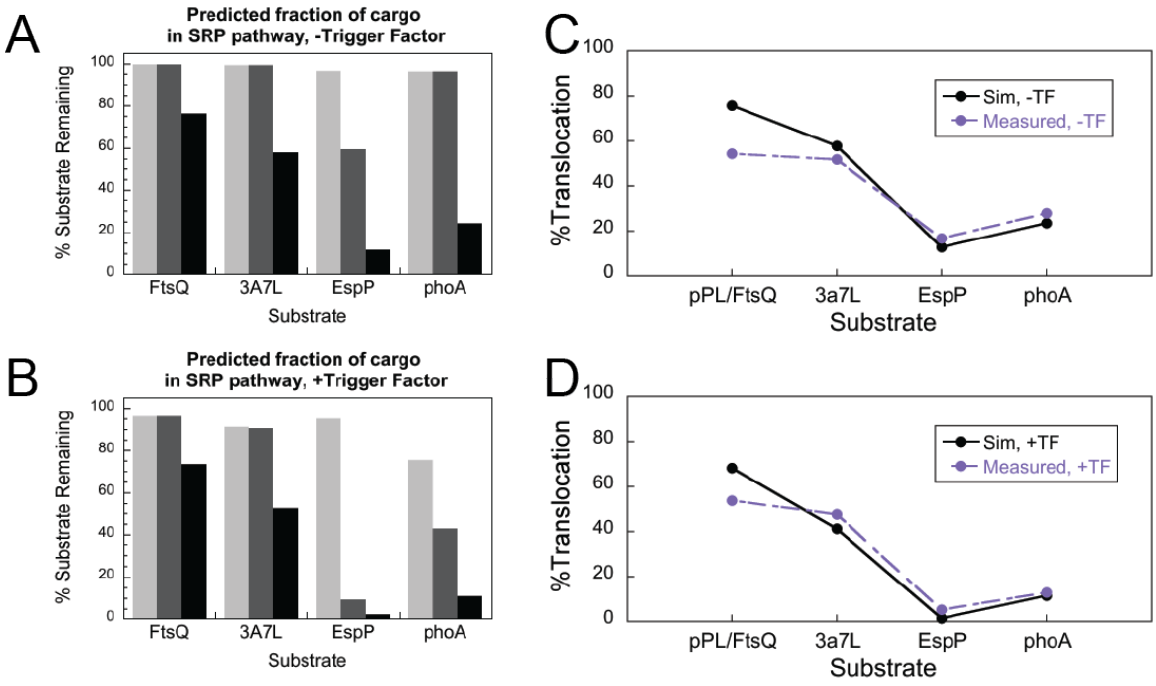

Figure S3. Mathematical simulations of SRP pathway occupancy of various RNCs at distinct checkpoints within the targeting pathway. (A-B) Predicted fraction of cargos retained in the SRP pathway during each checkpoint without TF (A) and with TF (B). Light grey bars represent the amount of cargo retained at the RNC binding stage; dark grey bars show remaining percentage of substrates after the *closed* SRP-FtsY complex assembly step; and, black bars showsoccupancy through kinetic proofreading via GTP hydrolysis. (C-D) Comparison of predicted and experimentally determined amounts of substrate remaining in the SRP targeting pathway without TF (C) and with TF (D). The values plotted are obtained from Figures S3A and B (black bars) and Figure 6.

MATERIALS AND METHODS

Materials

The *E. coli* Ffh, FtsY, 4.5S RNA and Trigger Factor were expressed and purified using established protocols (Kramer et al., 2004; Peluso et al., 2001). Single cysteine mutations were introduced via Quikchange mutagenesis (Stratagene) and were purified using the same procedures as wild-type protein. Ffh (C153) was labeled with N-(7-dimethylamino-4-methylcoumarin-3yl)-maleimide (DACM) and FtsY (C345), Ffh (C421) and TF (C377) were labeled with BODIPY-FL-N-(2-aminoethyl)-maleimide (Invitrogen). For the single molecule studies, 4.5S RNA was labeled with Cy3 as previously described (Shen et al., 2012) and TF (C377) was labeled with Atto647N using maleimide chemistry. After the labeling reaction, proteins were purified free of unconjugated dyes via gel filtration chromatography using Sephadex G-25 resin (Sigma) (Zhang et al., 2008). Labeling efficiencies were usually >95%. RNCs were prepared and purified as described (Saraogi et al., 2011).

Fluorescence measurements

All fluorescence measurements were carried out on a FluoroLog-3-22 spectrofluorometer (Jobin-Yvon) or an SF-2004 stopped-flow apparatus (KinTek) in assay buffer (50 mM KHEPES pH 7.5, 150 mM KOAc, 10 mM $Mg(OAc)_2$ and 2 mM DTT). All reactions were carried out at 25 ºC unless otherwise stated.

The binding affinities of SRP for RNCs were determined via equilibrium titrations as previously described (Saraogi, et al., 2011). In this approach, FRET measurements were carried out between 20 nM Cm-labeled RNCs (donor) and varying concentrations of BODIPY-FL labeled Ffh (C421). These steady state measurements were carried out in

the absence or presence of increasing amounts of TF. The observed FRET efficiency values (E) were calculated from Equation 1, in which F_{DA} and F_D are fluorescence intensities of the donor measured in the presence and absence of acceptor, respectively. These E values were plotted against SRP concentration and the data were fit to Equation 2,

$$E = 1 - \frac{F_{DA}}{F_D} \qquad (1)$$

$$E = E_{max}\left\{\frac{[RNC]+[SRP]+K_d-\sqrt{([RNC]+[SRP]+K_d)^2-4[RNC][SRP]}}{2[RNC]}\right\} \qquad (2)$$

where E_{max} is maximum FRET efficiency at saturating SRP concentrations and K_d is the equilibrium dissociation constant of SRP for the RNC.

To determine the equilibrium binding affinities of TF for the RNCs, in the presence or absence of SRP, equilibrium titrations were carried out using a similar FRET approach described above. The equilibrium binding affinity, $K_{d,}$ of TF for the various RNCs were measured by titrating increasing quantities of BODIPY-FL labeled TF(C377) into 20 nM Cm-labeled RNCs. To determine the K_d of TF for the various RNCs, the FRET efficiencies (E) were calculated (Equation 1) and plotted against TF concentration. The data were fit to Equation 2 except the term [SRP] was replaced by [TF].

The equilibrium stability of the SRP-FtsY *early* intermediate and the association rate constants for the SRP-FtsY *closed* complex were determined using FRET between donor (DACM) and acceptor (BODIPY-FL)-labeled SRP(C153) and FtsY(C345), respectively, as described previously (Zhang et al., 2008). In these experiments, SRP was loaded with different RNCs, with concentrations 5- to 100-fold above their respective K_d for SRP±TF were used to ensure 80-99% occupancy of SRP by the cargo.

For the *early* complex, equilibrium titrations were carried out using 50 nM RNC-bound, donor-labeled SRP and increasing amounts of acceptor-labeled FtsY in the absence of GTP or any GTP analogue. The titrations were carried out with 0 or 10-20 μM TF. FRET efficiency was calculated as described and plotted as a function of FtsY concentration. The data were fit to Equation 3,

$$\mathrm{E} = E_{max} \times \frac{[\mathrm{FtsY}]}{\mathrm{K_d} + [\mathrm{FtsY}]} \qquad (3)$$

where E_{max} is the FRET value at saturating amounts of FtsY, and K_d is the equilibrium dissociation constant of the *early* intermediate.

The SRP-FtsY *closed* complex assembly rates were determined by mixing 50 nM RNC-bound SRP with varying amounts of FtsY in the presence of 100 μM GppNHp, and the change of fluorescence signal was monitored over time. These time courses were carried out with 0 or 10-20 μM TF and were fit using a single exponential equation to get the observed rate constant, k_{obsd}. To obtain the second-order rate constant, k_{on}, the observed rate constants were plotted against [FtsY] and were fit to Equation 4, in which k_{on} and k_{off} are the rate constants for *closed* complex assembly and disassembly, respectively.

$$k_{obsd} = k_{on}\,[\mathrm{FtsY}] + k_{off} \qquad (4)$$

Co-translational protein targeting and translocation assay

The protein targeting efficiency of SRP, with or without TF, was determined by a co-translational translocation assay using ^{35}S-methionine-labeled preprolactin (pPL) as a substrate, as described previously (Shan et al., 2007). The signal sequences of 3A7L, EspP and phoA were fused to the mature region of prolactin (PL). Reactions were carried out using 345 nM SRP, 0 μM or 16 μM TF, varying concentrations of FtsY, and 1.5

equivalent of trypsin-digested, EDTA and salt-washed ER microsomal membranes (TEKRM). Reactions were analyzed by SDS-PAGE followed by autoradiography.

ACKNOWLEDGEMENTS

This work was supported by National Institutes of Health (NIH) grant GM078024 S.-O.S and the NIH Ruth L Kirschtein National Research Service Award F31 GM095294 to A.R.A.

REFERENCES

Akopian, D., Shen, K., Zhang, X., and Shan, S.-O. (2013). Signal recognition particle: an essential protein-targeting machine. Annu. Rev. Biochem. *82*, 693–721.

Angelini, S., Deitermann, S., and Koch, H.-G. (2005). FtsY, the bacterial signal-recognition particle receptor, interacts functionally and physically with the SecYEG translocon. EMBO Rep. *6*, 476–481.

Ataide, S.F., Schmitz, N., Shen, K., Ke, A., Shan, S.-O., Doudna, J.A., and Ban, N. (2011). The crystal structure of the signal recognition particle in complex with its receptor. Science *331*, 881–886.

Batey, R.T., Rambo, R.P., Lucast, L., Rha, B., and Doudna, J.A. (2000). Crystal structure of the ribonucleoprotein core of the signal recognition particle. Science *287*, 1232–1239.

Batey, R.T., Sagar, M.B., and Doudna, J.A. (2001). Structural and energetic analysis of RNA recognition by a universally conserved protein from the signal recognition particle. J. Mol. Biol. *307*, 229–246.

Beck, K., Wu, L.F., Brunner, J., and Müller, M. (2000). Discrimination between SRP- and SecA/SecB-dependent substrates involves selective recognition of nascent chains by SRP and trigger factor. Embo J. *19*, 134–143.

Bernstein, H.D. (1998). Protein targeting: getting into the groove. Curr. Biol. *8*, R715–R718.

Bradshaw, N., and Walter, P. (2007). The signal recognition particle (SRP) RNA links conformational changes in the SRP to protein targeting. Mol. Biol. Cell *18*, 2728–2734.

Bradshaw, N., Neher, S.B., Booth, D.S., and Walter, P. (2009). Signal sequences activate the catalytic switch of SRP RNA. Science *323*, 127–130.

Braig, D., Mircheva, M., Sachelaru, I., van der Sluis, E.O., Sturm, L., Beckmann, R., and Koch, H.-G. (2011). Signal sequence-independent SRP-SR complex formation at the membrane suggests an alternative targeting pathway within the SRP cycle. Mol. Biol. Cell *22*, 2309–2323.

Brünger, A.T., Adams, P.D., Clore, G.M., DeLano, W.L., Gros, P., Grosse-Kunstleve, R.W., Jiang, J.S., Kuszewski, J., Nilges, M., Pannu, N.S., et al. (1998). Crystallography & NMR system: A new software suite for macromolecular structure determination. Acta Crystallogr. D Biol. Crystallogr. *54*, 905–921.

Buskiewicz, I., Deuerling, E., Gu, S.-Q., Jöckel, J., Rodnina, M.V., Bukau, B., and Wintermeyer, W. (2004). Trigger factor binds to ribosome-signal-recognition particle (SRP) complexes and is excluded by binding of the SRP receptor. Proc. Natl. Acad. Sci. U.S.a. *101*, 7902–7906.

Cleverley, R.M., Zheng, N., and Gierasch, L.M. (2001). The cost of exposing a hydrophobic loop and implications for the functional role of 4.5 S RNA in the Escherichia coli signal recognition particle. J. Biol. Chem. *276*, 19327–19331.

Connolly, T., Rapiejko, P.J., and Gilmore, R. (1991). Requirement of GTP hydrolysis for dissociation of the signal recognition particle from its receptor. Science *252*, 1171–1173.

Datsenko, K.A., and Wanner, B.L. (2000). One-step inactivation of chromosomal genes in Escherichia coli K-12 using PCR products. Proc. Natl. Acad. Sci. U.S.a. *97*, 6640–6645.

Datta, S., Costantino, N., and Court, D.L. (2006). A set of recombineering plasmids for gram-negative bacteria. Gene *379*, 109–115.

del Alamo, M., Hogan, D.J., Pechmann, S., Albanèse, V., Brown, P.O., and Frydman, J. (2011). Defining the specificity of cotranslationally acting chaperones by systematic analysis of mRNAs associated with ribosome-nascent chain complexes. PLoS Biol. *9*, e1001100.

Deuerling, E., Schulze-Specking, A., Tomoyasu, T., Mogk, A., and Bukau, B. (1999). Trigger factor and DnaK cooperate in folding of newly synthesized proteins. Nature *400*, 693–696.

Doudna, J.A., and Batey, R.T. (2004). Structural insights into the signal recognition particle. Annu. Rev. Biochem. *73*, 539–557.

Egea, P.F., Shan, S.-O., Napetschnig, J., Savage, D.F., Walter, P., and Stroud, R.M. (2004). Substrate twinning activates the signal recognition particle and its receptor. Nature *427*, 215–221.

Eisner, G., Moser, M., Schäfer, U., Beck, K., and Muller, M. (2006). Alternate recruitment of signal recognition particle and trigger factor to the signal sequence of a growing nascent polypeptide. J. Biol. Chem. *281*, 7172–7179.

Estrozi, L.F., Boehringer, D., Shan, S.-O., Ban, N., and Schaffitzel, C. (2011). Cryo-EM structure of the E. coli translating ribosome in complex with SRP and its receptor. Nat. Struct. Mol. Biol. *18*, 88–90.

Fedyukina, D.V., and Cavagnero, S. (2011). Protein folding at the exit tunnel. Annu Rev Biophys *40*, 337–359.

Ferbitz, L., Maier, T., Patzelt, H., Bukau, B., Deuerling, E., and Ban, N. (2004). Trigger factor in complex with the ribosome forms a molecular cradle for nascent proteins. Nature *431*, 590–596.

Fischer, N., Konevega, A.L., Wintermeyer, W., Rodnina, M.V., and Stark, H. (2010). Ribosome dynamics and tRNA movement by time-resolved electron cryomicroscopy. Nature *466*, 329–333.

Flanagan, J.J., Chen, J.-C., Miao, Y., Shao, Y., Lin, J., Bock, P.E., and Johnson, A.E. (2003). Signal recognition particle binds to ribosome-bound signal sequences with fluorescence-detected subnanomolar affinity that does not diminish as the nascent chain lengthens. J. Biol. Chem. *278*, 18628–18637.

Focia, P.J., Shepotinovskaya, I.V., Seidler, J.A., and Freymann, D.M. (2004). Heterodimeric GTPase core of the SRP targeting complex. Science *303*, 373–377.

Freymann, D.M., Keenan, R.J., Stroud, R.M., and Walter, P. (1997). Structure of the conserved GTPase domain of the signal recognition particle. Nature *385*, 361–364.

Gautschi, M., Lilie, H., Fünfschilling, U., Mun, A., Ross, S., Lithgow, T., Rücknagel, P., and Rospert, S. (2001). RAC, a stable ribosome-associated complex in yeast formed by the DnaK-DnaJ homologs Ssz1p and zuotin. Proc. Natl. Acad. Sci. U.S.a. *98*, 3762–3767.

Gilmore, R., Blobel, G., and Walter, P. (1982a). Protein translocation across the endoplasmic reticulum. I. Detection in the microsomal membrane of a receptor for the signal recognition particle. J. Cell Biol. *95*, 463–469.

Gilmore, R., Walter, P., and Blobel, G. (1982b). Protein translocation across the endoplasmic reticulum. II. Isolation and characterization of the signal recognition particle receptor. J. Cell Biol. *95*, 470–477.

Hainzl, T., Huang, S., Meriläinen, G., Brännström, K., and Sauer-Eriksson, A.E. (2011). Structural basis of signal-sequence recognition by the signal recognition particle. Nat. Struct. Mol. Biol. *18*, 389–391.

Halic, M., and Beckmann, R. (2005). The signal recognition particle and its interactions during protein targeting. Curr. Opin. Struct. Biol. *15*, 116–125.

Halic, M., Becker, T., Pool, M.R., Spahn, C.M.T., Grassucci, R.A., Frank, J., and Beckmann, R. (2004). Structure of the signal recognition particle interacting with the elongation-arrested ribosome. Nature *427*, 808–814.

Halic, M., Blau, M., Becker, T., Mielke, T., Pool, M.R., Wild, K., Sinning, I., and Beckmann, R. (2006). Following the signal sequence from ribosomal tunnel exit to signal recognition particle. Nature *444*, 507–511.

Heymann, J.B., and Belnap, D.M. (2007). Bsoft: image processing and molecular modeling for electron microscopy. J. Struct. Biol. *157*, 3–18.

Holtkamp, W., Lee, S., Bornemann, T., Senyushkina, T., Rodnina, M.V., and Wintermeyer, W. (2012). Dynamic switch of the signal recognition particle from scanning to targeting. Nat. Struct. Mol. Biol. *19*, 1332–1337.

Huber, D., Rajagopalan, N., Preissler, S., Rocco, M.A., Merz, F., Kramer, G., and Bukau, B. (2011). SecA interacts with ribosomes in order to facilitate posttranslational translocation in bacteria. Mol. Cell *41*, 343–353.

Janda, C.Y., Li, J., Oubridge, C., Hernández, H., Robinson, C.V., and Nagai, K. (2010). Recognition of a signal peptide by the signal recognition particle. Nature *465*, 507–510.

Keenan, R.J., Freymann, D.M., Walter, P., and Stroud, R.M. (1998). Crystal structure of the signal sequence binding subunit of the signal recognition particle. Cell *94*, 181–191.

Kramer, G., Rutkowska, A., Wegrzyn, R.D., Patzelt, H., Kurz, T.A., Merz, F., Rauch, T., Vorderwülbecke, S., Deuerling, E., and Bukau, B. (2004). Functional dissection of Escherichia coli trigger factor: unraveling the function of individual domains. J. Bacteriol. *186*, 3777–3784.

Kramer, G., Boehringer, D., Ban, N., and Bukau, B. (2009). The ribosome as a platform for co-translational processing, folding and targeting of newly synthesized proteins. Nat. Struct. Mol. Biol. *16*, 589–597.

Kramer, G., Rauch, T., Rist, W., Vorderwülbecke, S., Patzelt, H., Schulze-Specking, A., Ban, N., Deuerling, E., and Bukau, B. (2002). L23 protein functions as a chaperone docking site on the ribosome. Nature *419*, 171–174.

Lakshmipathy, S.K., Tomic, S., Kaiser, C.M., Chang, H.-C., Genevaux, P., Georgopoulos, C., Barral, J.M., Johnson, A.E., Hartl, F.U., and Etchells, S.A. (2007). Identification of nascent chain interaction sites on trigger factor. J. Biol. Chem. *282*, 12186–12193.

Lam, V.Q., Akopian, D., Rome, M., Henningsen, D., and Shan, S.-O. (2010). Lipid activation of the signal recognition particle receptor provides spatial coordination of protein targeting. J. Cell Biol. *190*, 623–635.

Lauring, B., Kreibich, G., and Weidmann, M. (1995). The intrinsic ability of ribosomes to bind to endoplasmic reticulum membranes is regulated by signal recognition particle and nascent-polypeptide-associated complex. Proc. Natl. Acad. Sci. U.S.a. *92*, 9435–9439.

Lee, H.C., and Bernstein, H.D. (2001). The targeting pathway of Escherichia coli presecretory and integral membrane proteins is specified by the hydrophobicity of the targeting signal. Proc. Natl. Acad. Sci. U.S.a. *98*, 3471–3476.

Lee, H.C., and Bernstein, H.D. (2002). Trigger factor retards protein export in Escherichia coli. J. Biol. Chem. *277*, 43527–43535.

Lill, R., Crooke, E., Guthrie, B., and Wickner, W. (1988). The “trigger factor cycle” includes ribosomes, presecretory proteins, and the plasma membrane. Cell *54*, 1013–1018.

Maier, R., Eckert, B., Scholz, C., Lilie, H., and Schmid, F.-X. (2003). Interaction of trigger factor with the ribosome. J. Mol. Biol. *326*, 585–592.

Merz, F., Boehringer, D., Schaffitzel, C., Preissler, S., Hoffmann, A., Maier, T.,

Rutkowska, A., Lozza, J., Ban, N., Bukau, B., et al. (2008). Molecular mechanism and structure of Trigger Factor bound to the translating ribosome. Embo J. *27*, 1622–1632.

Montoya, G., Svensson, C., Luirink, J., and Sinning, I. (1997). Crystal structure of the NG domain from the signal-recognition particle receptor FtsY. Nature *385*, 365–368.

Morgan-Kiss, R.M., Wadler, C., and Cronan, J.E. (2002). Long-term and homogeneous regulation of the Escherichia coli araBAD promoter by use of a lactose transporter of relaxed specificity. Proc. Natl. Acad. Sci. U.S.a. *99*, 7373–7377.

Oh, E., Becker, A.H., Sandikci, A., Huber, D., Chaba, R., Gloge, F., Nichols, R.J., Typas, A., Gross, C.A., Kramer, G., et al. (2011). Selective ribosome profiling reveals the cotranslational chaperone action of trigger factor in vivo. Cell *147*, 1295–1308.

Peluso, P., Herschlag, D., Nock, S., Freymann, D.M., Johnson, A.E., and Walter, P. (2000). Role of 4.5S RNA in assembly of the bacterial signal recognition particle with its receptor. Science *288*, 1640–1643.

Peluso, P., Shan, S.O., Nock, S., Herschlag, D., and Walter, P. (2001). Role of SRP RNA in the GTPase cycles of Ffh and FtsY. Biochemistry *40*, 15224–15233.

Peterson, J.M., and Phillips, G.J. (2008). Characterization of conserved bases in 4.5S RNA of Escherichia coli by construction of new F' factors. J. Bacteriol. *190*, 7709–7718.

Peterson, J.H., Szabady, R.L., and Bernstein, H.D. (2006). An unusual signal peptide extension inhibits the binding of bacterial presecretory proteins to the signal recognition particle, trigger factor, and the SecYEG complex. J. Biol. Chem. *281*, 9038–9048.

Peterson, J.H., Woolhead, C.A., and Bernstein, H.D. (2010). The conformation of a nascent polypeptide inside the ribosome tunnel affects protein targeting and protein folding. Mol. Microbiol. *78*, 203–217.

Pettersen, E.F., Goddard, T.D., Huang, C.C., Couch, G.S., Greenblatt, D.M., Meng, E.C., and Ferrin, T.E. (2004). UCSF Chimera--a visualization system for exploratory research and analysis. J Comput Chem *25*, 1605–1612.

Phillips, G.J. (1999). New cloning vectors with temperature-sensitive replication. Plasmid *41*, 78–81.

Phillips, G.J., and Silhavy, T.J. (1992). The E. coli ffh gene is necessary for viability and efficient protein export. Nature *359*, 744–746.

Pool, M.R., Stumm, J., Fulga, T.A., Sinning, I., and Dobberstein, B. (2002). Distinct modes of signal recognition particle interaction with the ribosome. Science *297*, 1345–1348.

Powers, T., and Walter, P. (1996). The nascent polypeptide-associated complex modulates interactions between the signal recognition particle and the ribosome. Curr.

Biol. *6*, 331–338.

Powers, T., and Walter, P. (1997). Co-translational protein targeting catalyzed by the Escherichia coli signal recognition particle and its receptor. Embo J. *16*, 4880–4886.

Raine, A., Ivanova, N., Wikberg, J.E.S., and Ehrenberg, M. (2004). Simultaneous binding of trigger factor and signal recognition particle to the E. coli ribosome. Biochimie *86*, 495–500.

Raine, A., Ullers, R., Pavlov, M., Luirink, J., Wikberg, J.E.S., and Ehrenberg, M. (2003). Targeting and insertion of heterologous membrane proteins in E. coli. Biochimie *85*, 659–668.

Rosendal, K.R., Wild, K., Montoya, G., and Sinning, I. (2003). Crystal structure of the complete core of archaeal signal recognition particle and implications for interdomain communication. Proc. Natl. Acad. Sci. U.S.a. *100*, 14701–14706.

Rosenthal, P.B., and Henderson, R. (2003). Optimal determination of particle orientation, absolute hand, and contrast loss in single-particle electron cryomicroscopy. J. Mol. Biol. *333*, 721–745.

Rutkowska, A., Mayer, M.P., Hoffmann, A., Merz, F., Zachmann-Brand, B., Schaffitzel, C., Ban, N., Deuerling, E., and Bukau, B. (2008). Dynamics of trigger factor interaction with translating ribosomes. J. Biol. Chem. *283*, 4124–4132.

Saraogi, I., and Shan, S.-O. (2011). Molecular mechanism of co-translational protein targeting by the signal recognition particle. Traffic *12*, 535–542.

Saraogi, I., Zhang, D., Chandrasekaran, S., and Shan, S.-O. (2011). Site-specific fluorescent labeling of nascent proteins on the translating ribosome. J. Am. Chem. Soc. *133*, 14936–14939.

Schaffitzel, C., and Ban, N. (2007). Generation of ribosome nascent chain complexes for structural and functional studies. J. Struct. Biol. *158*, 463–471.

Schaffitzel, C., Oswald, M., Berger, I., Ishikawa, T., Abrahams, J.P., Koerten, H.K., Koning, R.I., and Ban, N. (2006). Structure of the E. coli signal recognition particle bound to a translating ribosome. Nature *444*, 503–506.

Scheres, S.H.W., Núñez-Ramírez, R., Sorzano, C.O.S., Carazo, J.M., and Marabini, R. (2008). Image processing for electron microscopy single-particle analysis using XMIPP. Nat Protoc *3*, 977–990.

Schuwirth, B.S., Borovinskaya, M.A., Hau, C.W., Zhang, W., Vila-Sanjurjo, A., Holton, J.M., and Cate, J.H.D. (2005). Structures of the bacterial ribosome at 3.5 A resolution. Science *310*, 827–834.

Shaikh, T.R., Gao, H., Baxter, W.T., Asturias, F.J., Boisset, N., Leith, A., and Frank, J.

(2008). SPIDER image processing for single-particle reconstruction of biological macromolecules from electron micrographs. Nat Protoc *3*, 1941–1974.

Shan, S.-O., Chandrasekar, S., and Walter, P. (2007). Conformational changes in the GTPase modules of the signal reception particle and its receptor drive initiation of protein translocation. J. Cell Biol. *178*, 611–620.

Shen, K., and Shan, S.-O. (2010). Transient tether between the SRP RNA and SRP receptor ensures efficient cargo delivery during cotranslational protein targeting. Proc. Natl. Acad. Sci. U.S.a. *107*, 7698–7703.

Shen, K., Arslan, S., Akopian, D., Ha, T., and Shan, S.-O. (2012). Activated GTPase movement on an RNA scaffold drives co-translational protein targeting. Nature *492*, 271–275.

Shen, K., Zhang, X., and Shan, S.-O. (2011). Synergistic actions between the SRP RNA and translating ribosome allow efficient delivery of the correct cargos during cotranslational protein targeting. Rna *17*, 892–902.

Siegel, V., and Walter, P. (1988). The affinity of signal recognition particle for presecretory proteins is dependent on nascent chain length. Embo J. *7*, 1769–1775.

Siu, F.Y., Spanggord, R.J., and Doudna, J.A. (2007). SRP RNA provides the physiologically essential GTPase activation function in cotranslational protein targeting. Rna *13*, 240–250.

Szabady, R.L., Peterson, J.H., Skillman, K.M., and Bernstein, H.D. (2005). An unusual signal peptide facilitates late steps in the biogenesis of a bacterial autotransporter. Proc. Natl. Acad. Sci. U.S.a. *102*, 221–226.

Tang, G., Peng, L., Baldwin, P.R., Mann, D.S., Jiang, W., Rees, I., and Ludtke, S.J. (2007). EMAN2: an extensible image processing suite for electron microscopy. J. Struct. Biol. *157*, 38–46.

Thompson, J.D., Higgins, D.G., and Gibson, T.J. (1994). CLUSTAL W: improving the sensitivity of progressive multiple sequence alignment through sequence weighting, position-specific gap penalties and weight matrix choice. Nucleic Acids Res. *22*, 4673–4680.

Tian, H., Boyd, D., and Beckwith, J. (2000). A mutant hunt for defects in membrane protein assembly yields mutations affecting the bacterial signal recognition particle and Sec machinery. Proc. Natl. Acad. Sci. U.S.a. *97*, 4730–4735.

Ullers, R.S., Houben, E.N.G., Brunner, J., Oudega, B., Harms, N., and Luirink, J. (2006). Sequence-specific interactions of nascent Escherichia coli polypeptides with trigger factor and signal recognition particle. J. Biol. Chem. *281*, 13999–14005.

Ullers, R.S., Houben, E.N.G., Raine, A., Hagen-Jongman, ten, C.M., Ehrenberg, M.,

Brunner, J., Oudega, B., Harms, N., and Luirink, J. (2003). Interplay of signal recognition particle and trigger factor at L23 near the nascent chain exit site on the Escherichia coli ribosome. J. Cell Biol. *161*, 679–684.

Valent, Q.A., Kendall, D.A., High, S., Kusters, R., Oudega, B., and Luirink, J. (1995). Early events in preprotein recognition in E. coli: interaction of SRP and trigger factor with nascent polypeptides. Embo J. *14*, 5494–5505.

Valle, M., Zavialov, A., Li, W., Stagg, S.M., Sengupta, J., Nielsen, R.C., Nissen, P., Harvey, S.C., Ehrenberg, M., and Frank, J. (2003a). Incorporation of aminoacyl-tRNA into the ribosome as seen by cryo-electron microscopy. Nat. Struct. Biol. *10*, 899–906.

Valle, M., Zavialov, A., Sengupta, J., Rawat, U., Ehrenberg, M., and Frank, J. (2003b). Locking and unlocking of ribosomal motions. Cell *114*, 123–134.

Walter, P., and Blobel, G. (1981a). Translocation of proteins across the endoplasmic reticulum. II. Signal recognition protein (SRP) mediates the selective binding to microsomal membranes of in-vitro-assembled polysomes synthesizing secretory protein. J. Cell Biol. *91*, 551–556.

Walter, P., and Blobel, G. (1981b). Translocation of proteins across the endoplasmic reticulum III. Signal recognition protein (SRP) causes signal sequence-dependent and site-specific arrest of chain elongation that is released by microsomal membranes. J. Cell Biol. *91*, 557–561.

Weiche, B., Bürk, J., Angelini, S., Schiltz, E., Thumfart, J.O., and Koch, H.-G. (2008). A cleavable N-terminal membrane anchor is involved in membrane binding of the Escherichia coli SRP receptor. J. Mol. Biol. *377*, 761–773.

Zhang, X., Kung, S., and Shan, S.-O. (2008). Demonstration of a multistep mechanism for assembly of the SRP x SRP receptor complex: implications for the catalytic role of SRP RNA. J. Mol. Biol. *381*, 581–593.

Zhang, X., Lam, V.Q., Mou, Y., Kimura, T., Chung, J., Chandrasekar, S., Winkler, J.R., Mayo, S.L., and Shan, S.-O. (2011). Direct visualization reveals dynamics of a transient intermediate during protein assembly. Proc. Natl. Acad. Sci. U.S.a. *108*, 6450–6455.

Zhang, X., Rashid, R., Wang, K., and Shan, S.-O. (2010). Sequential checkpoints govern substrate selection during cotranslational protein targeting. Science *328*, 757–760.

Zhang, X., Schaffitzel, C., Ban, N., and Shan, S.-O. (2009). Multiple conformational switches in a GTPase complex control co-translational protein targeting. Proc. Natl. Acad. Sci. U.S.a. *106*, 1754–1759.

Zheng, N., and Gierasch, L.M. (1997). Domain interactions in E. coli SRP: stabilization of M domain by RNA is required for effective signal sequence modulation of NG domain. Mol. Cell *1*, 79–87.